PB84-220318

Effect of Underground Coal Gasification on Groundwater

New Mexico Univ., Albuquerque

Prepared for

Industrial Environmental Research Lab.
Cincinnati, OH

Jul 84

U.S. Department of Commerce
National Technical Information Service
NTIS

TECHNICAL REPORT DATA
(Please read Instructions on the reverse before completing)

1. REPORT NO. EPA-600/2-84-123	2.
3. RECIPIENT'S ACCESSION NO. PB84 220318	
4. TITLE AND SUBTITLE The Effect of Underground Coal Gasification on Groundwater	5. REPORT DATE July 1984
	6. PERFORMING ORGANIZATION CODE
7. AUTHOR(S) Edward A. Walters and Thomas M. Niemczyk	8. PERFORMING ORGANIZATION REPORT NO.
9. PERFORMING ORGANIZATION NAME AND ADDRESS University of New Mexico Department of Chemistry Albuquerque, NM 87131	10. PROGRAM ELEMENT NO. INE825
	11. CONTRACT/GRANT NO. R806303
12. SPONSORING AGENCY NAME AND ADDRESS Environmental Protection Agency Office of Research and Development 26 W. St. Clair Street Cincinnati, Ohio 45268	13. TYPE OF REPORT AND PERIOD COVERED Project Report/Summary
	14. SPONSORING AGENCY CODE EPA/600/12

15. SUPPLEMENTARY NOTES

16. ABSTRACT

The potential effect of underground coal gasification on groundwater has been examined in a laboratory study. The study was directed at Fruitland Formation subbituminous coal of the San Juan Basin and at the groundwater found in this coal seam. Two wells were drilled into the coal seam at a potential UCG test site. Groundwater samples and core samples of overburden, underburden and coal were analyzed to establish baseline characteristics. A number of static leaching and sorption studies were performed on the overburden, underburden, and coal. Ash was prepared at several different temperatures and leaching characteristics were examined.

Cations of the trace elements Be, Al, Cr, Mn, Fe, Co, Ni, Cu, Zn, Cd, Hg and Pb and the anions F^-, AsO_4^{-3}, SeO_3^{-2} and MoO_4^{-2} were selected for coal sorption studies. Distribution coefficients for sorption on coal were determined for the cations and anions under conditions reasonably similar to those in the groundwater of the San Juan Basin. The effect of humic acid on the sorptive characteristics of coal was studied.

17. KEY WORDS AND DOCUMENT ANALYSIS

a. DESCRIPTORS	b. IDENTIFIERS/OPEN ENDED TERMS	c. COSATI Field/Group

18. DISTRIBUTION STATEMENT Release Unlimited	19. SECURITY CLASS (This Report) Unclassified	21. NO. OF PAGES 117
	20. SECURITY CLASS (This page) Unclassified	22. PRICE

EPA Form 2220-1 (Rev. 4-77) PREVIOUS EDITION IS OBSOLETE

PB84-220318

EPA-600/2-84-123
July 1984

THE EFFECT OF UNDERGROUND COAL GASIFICATION ON GROUNDWATER

by

Edward A. Walters and Thomas M. Niemczyk
Department of Chemistry
University of New Mexico
Albuquerque, NM 87131

Research Grant No. R806303

Project Officer:

Patricia S. Fair
Energy Pollution Control Division
Industrial Environmental Research Laboratory
Cincinnati, OH 45268

INDUSTRIAL ENVIRONMENTAL RESEARCH LABORATORY
OFFICE OF RESEARCH AND DEVELOPMENT
U.S. ENVIRONMENTAL PROTECTION AGENCY
CINCINNATI, OHIO 45268

REPRODUCED BY
NATIONAL TECHNICAL
INFORMATION SERVICE
U.S. DEPARTMENT OF COMMERCE
SPRINGFIELD, VA. 22161

NOTICE

This document has been reviewed in accordance with U.S. Environmental Protection Agency policy and approved for publication. Mention of trade names or commercial products does not constitute endorsement or recommendation for use.

FOREWORD

When energy and material resources are extracted, processed, converted, and used, the related pollutional impacts on our environment and even on our health often require that new and increasingly more efficient pollution control methods be used. The Industrial Environmental Research Laboratory - Cincinnati (IERL-Ci) assists in developing and demonstrating new and improved methodologies that will meet these needs both efficiently and economically.

This report deals with the possibility of groundwater contamination in the San Juan Basin as a result of Underground Coal Gasification (UCG). Baseline characteristics of the groundwater, coal and rock at a prospective UCG site are recorded. The sorptive characteristics of metal ions and organics on the rock, clay and coal are examined as well as the solubility and rates of solution of metals and organics from the residue of a UCG burn. Further information on this subject may be obtained from the Oil Shale and Energy Mining Branch, Energy Pollution Control Division.

David G. Stephen
Director
Industrial Environmental Research Laboratory
Cincinnati

ABSTRACT

The potential effect of underground coal gasification (UCG) on groundwater has been examined in a combined field and laboratory study. The study was directed at Fruitland Formation subbituminous coal of the San Juan Basin and at the groundwater found in this coal seam. A field site for a possible UCG test was selected and two wells were drilled into the coal seam which lies about 500 ft. below the surface. Groundwater samples were collected and used to establish baseline features. Core samples of overburden, underburden and coal were used for baseline characterization of the minerals.

A number of static leaching and sorption studies were performed. Overburden was leached by both acidic and basic water. This material acts as a strong buffer, holding the water at a high pH. The amounts of Cl^- and F^- leached from overburden are about 10 ppm and show little dependence on the pH of the leaching solution.

Ash was generated at several different temperatures. The results of leaching studies of these ashes are reported. The amount of ash dissolved depends upon the ionic strength of the leaching solution in addition to pH. Predominant species dissolved are calcium, aluminum, sulfate, hydroxide and carbonate. Indications are that solubility of the ash decreases with increasing ashing temperature.

Adsorption capacity experiments were conducted in an effort to determine the extent to which mineral matter in Fruitland Formation coal contributes to sorption. Results from the study indicate that coal minerals account for about 95% of the sorptive capacity of metal ions while the carbonaceous matter accounts for only about 5%. This sorption appears to be largely ion exchange with the K^+ and Ca^{+2} cations found on the local clay minerals. Distribution coefficients, K_d, for sorption on coal were determined for the cations and anions under conditions reasonably similar to those in the groundwater of the San Juan Basin. The effect of the natural chelating agent humic acid was generally found to be minimal. Numerical values for the K_d are reported as a function of initial concentration in solution and the data are presented graphically as isotherms. The isotherms indicate multilayer adsorption as initial ion concentration increases and generally fit a modified Langmuir equation well.

Phenol adsorption by clay, raw coal and demineralized coal was studied. It was found that phenol adsorbs strongly to the carbonaceous matter and only slightly to the minerals.

The analytical problem of silicon determination in complex matrices by graphite furnace atomic absorption spectrocopy techniques has been studied and improved methods are reported here.

CONTENTS

Foreword iii

Abstract iv

Figures vi

Tables viii

Acknowledgement x

1. Introduction 1

2. Conclusions 2

3. Recommendations 3

4. Baseline Studies 4

    Site 4
    Groundwater 6
    Overburden and Underburden 11

5. Leachate Studies 17

    Overburden 17
    Underburden 18
    Ash 25

6. Distribution Coefficients (Overburden and Underburden) 35

    Procedure 35
    Discussion 36

7. Sorption Studies on Coal 45

    Sorption Capacities 45
    Distribution Coefficients 48

8. Adsorption of Organics 88

9. Analytical Methods Development 91

    Lead Analysis 91
    Silicon Determination 91
    Temperature Effects in Nonflame AAS 97

References 103

FIGURES

Number		Page
1	Deep sample collection device	8
2	The amount of manganese dissolved from Kirtland shale as a function of final pH, σ = 0.33	21
3	The amount of aluminum dissolved from Kirtland shale as a function of final pH, σ = 0.33	22
4	The amount of magnesium dissolved from Kirtland shale as a function of final pH, σ = 0.12	23
5	Total dissolved solids from Pictured Cliffs sandstone as a function of initial pH	27
6	Major cationic constituents of Fruitland ash leachate	29
7	Trace metal constituents of Fruitland ash leachate	31
8	K_d for Cd^{+2} on Pictured Cliffs sandstone as a function of initial concentration of Cd^{+2}.	38
9	K_d for Cd^{+2} on Kirtland shale as a function of initial concentration of Cd^{+2}	39
10	The amount of Cd^{+2} adsorbed per gram of rock as a function of the concentration of Cd^{+2} remaining in solution	41
11	The amount of Cd^{+2} adsorbed per gram of rock as a function of initial concentration (all particle sizes, for both underburden and overburden, lie very close together. Thus each represents 6 points)	43
12	K_d for Mg^{+2} on Kirtland shale as a function of pH	44
13	Sorption isotherm of manganese	59
14	Sorption isotherm of iron	60
15	Sorption isotherm of zinc	61
16	Sorption isotherm of cadmium	62

FIGURES (CONT'D)

Number		Page
17	Sorption isotherm of aluminum	63
18	Sorption isotherm of chromium	64
19	Sorption isotherm of cobalt	65
20	Sorption isotherm of nickel	66
21	Sorption isotherm of copper	67
22	Sorption isotherm of mercury	68
23	Sorption isotherm of lead	69
24	Sorption isotherm of beryllium	70
25	Sorption isotherm of fluoride	71
26	Sorption isotherm of selenite	72
27	Sorption isotherm of molybdate	73
28	K_d of aluminum vs. coal particle size	82
29	K_d of manganese vs. coal particle size	83
30	K_d of iron vs. coal particle size	84
31	K_d of zinc vs. coal particle size	85
32	K_d of the sum of ions vs. coal particle size	86
33	Effect of tungstate treated tube on the measured absorbance for Si	93
34	Absorbance vs. time profiles for Si when atomized from PG and NPG surfaces	94
35	Working curve for Si from peak height measurements	95
36	Working curve for Si from integrated absorbance	96
37	Schematic diagram of the optical pyrometer	100
38	Pyrometer response for various filters	101
39	Pyrometer response for the low temperature pair of diodes	102

TABLES

Number		Page
1	Baseline results of water samples collected from wells GT-1 and GT-2	12
2	Physical properties of the over- and underburden from the GT-1 core	13
3	Major components found in Kirtland shale (overburden), a parting, and Pictured Cliffs sandstone (underburden) and respective clays	15
4	Trace element composition of Kirtland shale (overburden), a parting, and Pictured Cliffs sandstone (underburden) and their respective clays	16
5	Concentration of cations leached from Kirtland shale as a function of final pH, [conc. (ppm)/wt. clay (g)]	19
6	Results of leachate analyses from Kirtland shale overburden	24
7	Total dissolved solids and concentrations of Cl^-, F^-, CN^- and SO_4^{-2} extracted from Pictured Cliffs sandstone as a function of pH	26
8	Water-ash leachate	32
9	Trace metal ion concentration increases (in ppm) in distilled water leachate of coal ashes prepared at different temperatures	33
10	K_d values for Cd^{+2} on overburden and underburden of different particle sizes	37
11	Quantities of Mg^{+2}, Na^+, and K^+ desorbed from overburden and underburden by Cd^{+2}	40
12	Sorption capacities of raw and acid-washed Fruitland coal	47
13	Background ionic strength of sorption experiment samples	51
14	Experimental values of sorption variables	51
15	Initial cation concentration ranges	53
16	Initial anion and Be^{+2} concentration ranges	53

TABLES (CONT'D)

Number		Page
17	The adsorption of selected cations on Fruitland formation coal	54
18	The adsorption of selected anions on Fruitland formation coal	57
19	Fruendlich and Langmuir constants for cations	78
20	Fruendlich and Langmuir constants for anions	79
21	Sorption capacity of Fruitland formation coal derived from the Langmuir isotherm	80
22	Effect of particle size on adsorption	81
23	Adsorption of phenol on coal and minerals	89
24	Sensitivites obtained for Si when atomized from various surfaces	97

ACKNOWLEDGEMENT

We wish to acknowledge financial assistance for this project from the New Mexico Energy Research and Development Institute under EMD Project #2-68-3118. We are grateful to the Public Service Company of New Mexico and Western Coal Corporation for providing the site for the field studies and funds for drilling the two wells and to the U.S. Geological Survey for initial draw-down tests of the wells and preliminary analysis of the ground-water. Finally, we would like to acknowledge the assistance of Dr. H. E. Nuttall, Department of Chemical and Nuclear Engineering, University of New Mexico, for coordinating the location of the field site and the well drilling operation.

SECTION I

INTRODUCTION

The subbituminous coal of the San Juan Basin of northwestern New Mexico is one of the largest and most accessible coal deposits of the Southwest. The total amount of subbituminous coal in the basin has been estimated to be about 56.8 billion tons of which 5.9 billion tons lie within the limits of strip mining, that is, within 250 feet of the surface. The remainder, some 45 billion tons, are deep deposits which will probably only be tapped by some version of the technique of underground coal conversion. The most attractive underground conversion method at the present time is underground coal gasification (UCG). It has been explored in a number of countries, notably Russia and England, for some decades, and has been tested extensively in this country at several sites in Wyoming. The basic technology is available at this time, though a number of difficult engineering problems remain. The principal consideration in the ultimate viability of the UCG process is one of economics; however, environmental factors as they are currently regulated play a major role in economics. Consequently an answer to the question of the environmental impact of UCG is of great interest from many perspectives.

There are several potentially serious environmental problems: subsidence, air quality (including SO_x, NO_x and particulates), and groundwater contamination. The possibility of groundwater contamination is the most substantial and least understood of the three. At the San Juan Basin site described in this report, the rock formation immediately above the coal seam and the coal itself belong to a confined aquifer for which the water table lies about 130 feet below the ground level. There are no aquifers above this. After a UCG burn water will seep into the burn cavity to dissolve and react with the ash which contains the metals from the coal and rock and the organics produced by UCG. This process may generate a highly contaminated groundwater containing a large number of compounds, some of which are deleterious. If this contaminated water becomes a supply for either livestock or humans, the consequences could be serious indeed.

The project described in this report is directed at assessing the possibility of groundwater contamination in the San Juan Basin as a result of UCG. The approach is to establish baseline characteristics of groundwater, coal and rock at a prospective UCG site in the San Juan Basin; to determine solubility and rates of solution of metals and organics from the residue of a UCG burn; and to determine sorptive characteristics of metal ions and organics on the rock, clay and coal.

SECTION 2

CONCLUSIONS

From many points of view northwest New Mexico represents a very good site for an underground coal gasification (UCG) project. The proximity of major power plants and a power distribution network, as well as extremely large, deep coal deposits make such a project attractive. The environment of the locale is high desert and therefore characterized by low human and animal populations and sparse vegetation. Background studies indicate the groundwater is brackish. The combination of these factors allow one to project a minimum environmental impact of such a site.

Static leaching of overburden and underburden indicates that pH is a very important variable, with large quantities of rock dissolving at very high and very low pH. Baseline studies show that the groundwater is strongly alkaline and the most abundant dissolved anion is sulfate. Trace metal measurements indicate that only at low pH values are significant amounts extracted. The distribution coefficients determined here for several metals were found to be functions of initial concentration of metal and particle size and when presented as isotherms the data fit the Freundlich equation.

Sorption studies on coal indicate that the inorganic matter in the coal accounts for approximately 95% of the adsorption of trace metals. The amounts of metals adsorbed onto the coal and the distribution function for the process have been measured in the presence of humic acid. The results indicate that the affinity of humic acid for the trace metals studies is: $Fe^{+2} > Al^{+3} > Pb^{+2} > Cr^{+3} > Ni^{+2} > Mn^{+2} > Cd^{+2} > Be^{+2}$. By fitting the sorption results to a Langmuir isotherm the sorption capacity of Fruitland Formation coal was found to be 1.5 g/kg for cations and 2.7 g/kg for anions.

One of the difficulties encountered in the work presented here was the measurement of trace metals in brackish water samples. Graphite Furnace Atomic Absorption Spectroscopy (GFAA) has been explored as a measurement technique. Many interferences have been noted and some have been studied in detail. The results indicate GFAA is a powerful technique, but its use should be limited to samples of well-known matrix content.

SECTION 3

RECOMMENDATIONS

We report the results of some organic and metal ion sorption experiments but more information is needed in this area. The only organic studied to date has been phenol. This represents a very important class of compounds, but the scope should be broadened. In the metal ion studies some effort should be made to evaluate pH effects, especially under alkaline conditions.

The work characterizing the ash should be completed. Also, adsorption or leaching studies on a char product under conditions similar to those found in UCG should be done.

More data is needed to satisfactorily evaluate the eventual impact of UCG on local groundwater supplies. It is important that good data concerning the identity and movement of all possible pollutants be known. All work reported to date has been in the area of static or batch leaching. It is important that some of this work be repeated in a dynamic mode to verify the distribution and ion exchange constants measured and to establish experimentally the rate of migration of trace metal ions.

Continued effort should be made in the area of analytical measurements. It is important that accurate and precise measurement methods be developed for samples of the type found here in order that results can be accepted with confidence.

Ultimately the best possible test of the data and conclusions drawn from this work would be to actually monitor a field test. This would not only allow an evaluation of the laboratory data but provide a critical assessment of any model used to predict the movement of pollutants in the environment.

SECTION 4

BASELINE STUDIES

The baseline characteristics of the groundwater, coal, overburden and underburden at a prospective UCG site in the San Juan Basin are reported in this section. The field work was done in conjunction with the New Mexico Public Service Company and Western Coal Company.

SITE

Description

A site was selected for studies related to a possible underground coal gasification test based on the following criteria:

a) The site should contain a seam of subbituminous, noncaking coal.

b) The principal coal seam should be at least 10 feet thick located at least 250 feet below the surface. The seam should have a dip of less than 5 to 10 percent.

c) In order to facilitate obtaining permits, the site should be located on State of New Mexico land.

d) There should be reasonable access to the site via existing roads.

e) The site should be located near existing or future power plant sites.

f) The site should be within reasonable distance of power and water utilities.

The area which was chosen for study is located in the SW 1/4 NW 1/2 of Section 36, Township 30 N, Range 15 W, New Mexico. The site is about 10 miles northwest of Farmington, NM; it is about 3 miles north of State Highway 550 and about the same distance east of the San Juan Generating Station which is owned primarily by the Public Service Company of New Mexico. The site is on State of New Mexico land under lease to the Western Coal Company. Western Coal Company has now been taken over by Utah International, another coal company.

Fruitland Formation subbituminous coal lies at a depth of 500 feet at the test site and the seam is 16 feet thick. The overburden is part of the Kirtland Shale Formation and the underburden is Pictured Cliffs sandstone.

The site is located in arid country which has an annual rainfall of 4-6 inches. The immediate area is drained by the San Juan River which runs northwestward into Utah. It eventually joins the Colorado River. The overall climate is moderate in terms of temperature (average temperature at Fruitland, elevation 5,120 feet, for July is 74°F and for January is 30°F) and arid to semiarid in terms of moisture.

The terrain consists of rolling, sandy hills, nearly devoid of vegetation. At a distance of approximately 1 mile to the north a set of brown sandstone bluffs are found. The surface at the site is within a major erosional area containing largely alkaline soils. Animal densities are very low due to sparse vegetative cover.

The study area is centrally located in the northwest New Mexico energy production complex. Two coal mines and over 2000 MW generating capacity are located within 15 miles of the lease. A 345 kV transmission corridor passes through the property and a natural gas cleaning plant is only about two miles away. A natural gas pipeline crosses the eastern extension of the property.

Wells

A two-hole pattern of wells was drilled into the Fruitland formation at the selected UCG test site. Surveyed coordinates of the two wells are:

Well No.	N. Coord.	E. Coord.	Elevation
GT-1	2,100,399.4 ft. 640,203.02 m	342,253.6 ft. 104,319.11 m	5297.3 ft. 1614.62 m
GT-2	2,100,402.7 ft. 640,204.02 m	342,283.8 ft. 104,328.31 m	5296.9 ft. 1614.50 m

The wells were drilled, cored, completed and cased in April, 1978 using funds provided by the Public Service Company of New Mexico. Special care was taken to assure vertical drilling at both holes. Subsequent experience indicates that the wells are in fact very nearly vertical. Cores were taken from both wells (GT-1, 4-inch id, and GT-2, 6-inch id) from about 15 feet above the principal seam to about 15 feet into the Pictured Cliffs sandstone which makes up the underburden.

Hydrology

The hydrology of the San Juan Basin is the subject of a long term project by the U.S. Geological Survey (1). In the vicinity of the UCG site water is found in the Kirtland shale and typically fills wells to within 130 ft. of the surface. It is believed that this water is effectively part of a confined aquifer which very slowly drains in the direction of the San Juan River actually entering the river well downstream through springs and seeps. The aquifer does not refill from the surface, but from exposed sections of Kirtland shale and Fruitland Formation coal at nearby mesas.

Shortly after the wells were drilled a set of draw-down tests were conducted by the USGS. These consisted of slug-type tests in which 26-28 gallons of water were removed from GT-2 with a PVC bailer 4 inches in diameter and 4.3 feet long. After bailing, water recovery rates were determined by measuring the water level at frequent intervals. The raw height-time data were treated by the standard procedure for confined aquifers (2). From this a transmissivity of 0.6 $ft^2 day^{-1}$, a permeability of the shale of 0.01 mdarcies, and a storage coefficient of 10^{-5} were calculated. These results are in good agreement with 0.02 mdarcies obtained from an independent determination (see overburden subsection) of the permeability of Kirtland shale. Very low permeabilities ($\sim$0.1 mdarcies) have also been reported for Pictured Cliffs underburden. On the other hand the permeability of the coal is about 10 mdarcies (3). The water migration rate appears to be 1-2 ft. $yr.^{-1}$, so that little flow occurs through the UCG site. The seams must be dewatered prior to gasification, but it seems that there will be no problem of excessive water. This flow rate also suggests that equilibrium will be established between dissolved ions in the water and any adsorption or ion exchange sites in the rock, clay, or coal. This is a very important conclusion for application of laboratory studies of adsorption and for simulations.

During July 1979 extensive ^{85}Kr tracer-air acceptance experiments were conducted at the UCG site and there are three principal conclusions to be drawn from the results (3). First, because of the low permeability of the overburden and underburden all of the flow occurs through the coal seam. Second, the tests indicate that a proper model for flow through the coal seam must take into account the fact that flow is crack-dominated. It appears that flow through this coal seam may be regarded as cracked-flow with regions of porous media dispersed throughout the system. Third, it is clear that the cracks in the coal seam are anisotropic. In particular, much more air is injected than is withdrawn through the second hole; this means that an indefinitely expanding bubble of air has been formed whose orientation is along the preferred direction of permeability.. This anisotropy seems to be at least 2:1 in a direction nearly normal to the line joining the two wells GT-1 and GT-2. It is clear that simulation of flow will require a complex model; a first attempt at a model has been published (4).

GROUNDWATER

Sample Collection

Preliminary water samples were removed from well GT-1 by bailing techniques by the USGS. Glass containers were used and few precautions were taken to stabilize the samples, so the trace metal, anion and organic analyses are not reliable. These results (5) however indicate that the water is brackish (1000-10,000 pm TDS) and has characteristics similar to groundwater found elsewhere in the Southwest (6).

Much more careful sampling and storing procedures than were used in the preliminary study were used for all data reported here. A deep sampling device was used to remove water samples from the wells near the coal seam. This

device, Figure 1, is similar to those described by Spalding, Exner and Gormly (7). It has an open-ended tube with a plug suspended above it. Water flows through and fills the sampler as it descends. When the appropriate depth is reached the sampler is allowed to stabilize briefly and a stainless steel messenger is dropped down the 140 lb. test braided nylon support line; the messenger trips a trigger which closes the device. The filled sampler is retrieved by means of a hand-operated winch and the sample is transferred to a large plastic beaker. The sampler collects about 1400 ml per trip. Measurements of temperature, specific conductivity and pH were made on each sample immediately after collection. The sample was then filtered and preserved according the APHA standard methods (8). The preserved samples were kept cold in plastic bottles until analyses were performed in the laboratory.

The position of the sampler in the well was determined by passing the support line around a wheel which was connected to a revolutions counter. The device was calibrated and it is believed that the reported depths are reliable to within 2 feet and that the depth reproducibility is approximately 6 inches.

Samples were collected both in the overburden region below the casing and in the region of the coal seam. Both of the wells were partially filled with detritus from sloughing of the sides below the casing, so it was not possible to collect samples in the underburden levels.

Filtration was the primary field problem. The source of the problem was the fine clay-size particles suspended in the deep water samples. This problem was overcome by the use of a plate filter. A filter plate of acrylic plastic was made which receives 147 mm diameter Millipore filters. Cleaned filters with a pore size of 0.45 μm were used. The filter was placed between two sheets of nylon screen and positioned over the bottom plate. This plate has a series of grooves machined in it to permit uniform drainage of the filter. The filtrate was collected from a drain in the center of this plate. The top plate has a set of grooves matching those on the lower plate. This is clamped over the filter and the mixture to be filtered is driven through the system by means of a peristaltic pump. The pump operates on an input voltage of 12 volts, so an automobile battery can be used as a power supply for field work. An additional advantage to this device is that the pump can be reversed briefly to backflush the filter. This serves to open clogged pores so more mixture can be filtered.

Analytical Methods

Standard methods were used for most of the analyses of the samples. Field measurements of pH, conductivity, temperature, chloride, and fluoride were made, while all other analyses were done in the laboratory.

pH

pH was measured on a Corning 610A portable pH meter with a Corning Series 500 combination electrode.

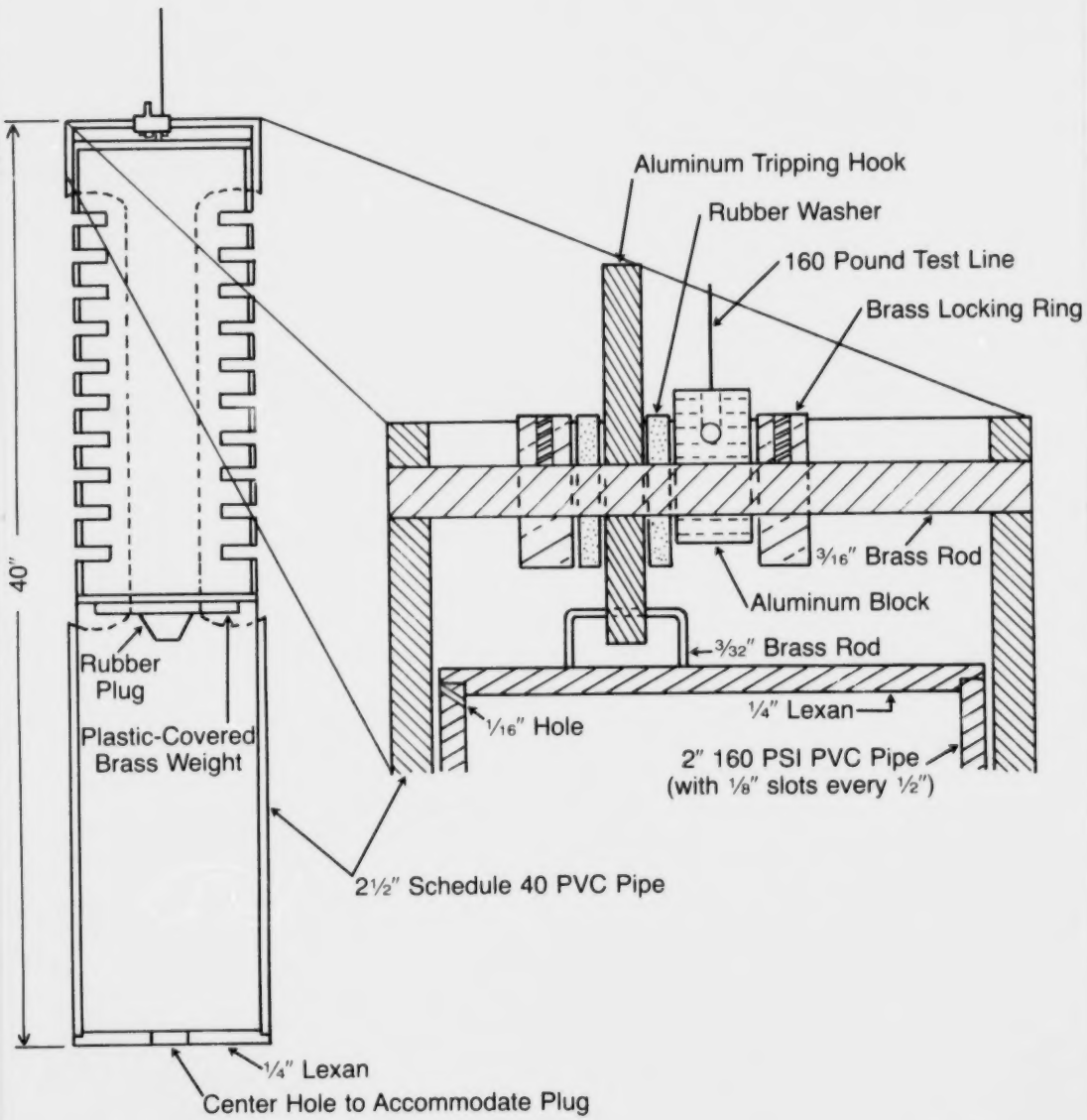

Figure 1. Deep sample collection device.

Specific Conductance

Conductivity was measured on a Barnstead PM-70CB conductivity bridge with a YSI 3401 conductivity cell. Conductance was corrected to 25°C on the basis of the experimentally determined calibration curve.

Chloride

Chloride ion concentration was determined with an Orion 407A Specific Ion Meter, using an Orion 94-17A Specific Ion Electrode, an Orion 90-02 double-junction reference electrode and 0.10 M $NaNO_3$ ionic strength adjustor. Interpretation of results was based on a calibration curve determined from solutions prepared with known NaCl concentrations.

Fluoride

Fluoride ion concentration was determined with an Orion 407A Specific Ion Meter, using an Orion 94-09A Specific Ion Electrode, an Orion 90-01 single-junction reference electrode and TISAB II ionic strength adjustor, in accordance with APHA standard methods (8).

Metals

The metal concentrations were determined using a Varian Techtron AA-6 atomic absorption spectrometer. All general procedures used were those recommended for water and wastewater analysis (8,9). The exact instrument settings for the individual metals (Cu, Zn, Pb, Na, K, Ca, Mg, Sr, Cd, Ni, Co, Cr, Sn, Fe) were those recommended by the instrument manufacturer (10). In all cases the actual analysis procedures conform, except in details specific to the Varian AA-6, to those recommended by the EPA (9). For all the metals the results obtained using direct aspiration of the sample water have been verified by either an extraction procedure using ammonium pyrrolidine dithiocarbamate (APDC), by standard additions, or both.

Alkalinity

The alkalinity of the water was determined by titrating an aliquot of the water with standardized H_2SO_4(8). A mixed bromcresol green-methyl red indicator was used to determine the endpoint. The endpoint corresponded to a pH of 4.5.

Cyanide

The cyanide was determined using a standard colorimetric method (8,9). In the method the CN^- forms CNCl by reaction with chloramine-T which then forms a red-blue dye on the addition of a pyridine-barbituric acid reagent. The absorbance of the dye solution was measured at 578 nm using a Cary 14 spectrophotometer.

Ammonia

The NH_4^+ concentration of the water samples was determined by the Nesslerization method (8,9). The standard procedure was followed and the absorbance at 450 nm was measured using a Spectronic 20 spectrophotometer.

Nitrate

The NO_3^- concentration was determined using the cadmium reduction method (8). The nitrite thus produced was determined by diazotization with sulfanilamide and coupling with N-(1-naphyl)-ethylenediamine to form a colored azo dye. The absorbance of the dye solution was then measured at 543 nm using a Cary 14 spectrophotometer.

Nitrite

The NO_2^- concentration was determined using the diazotization method (8). The dye formed and the spectrophotometric measurements are similar to those used in the NO_3^- method.

Phosphate

The PO_4^{-3} concentration was determined using the standard ascorbic acid method (8). The absorbance of the phosphomolybdic acid produced was measured at 880 nm in a Cary 14 spectrophotometer.

Sulfate

The sulfate concentration was determined by the turbidimetric method (8,9). In this method the SO_4^{-2} ion is precipitated in a hydrochloric acid medium with $BaCl_2$ in such a manner as to form $BaSO_4$ crystals of uniform size. The absorbance of the SO_4^{-2} solution was measured at 420 nm using a Cary 14 spectrophotometer.

Sulfide

The methylene blue method was used for the sulfide determinations (8,9). The absorbance of the methylene blue solution was measured at 625 nm using a Spectronic 20.

Chemical Oxygen Demand

The COD was determined using the dichromate reflux method (8,9).

Total Dissolved Solids

Aliquots of 10.0 ml of the supernatant liquid were transferred by pipet to weighed porcelain crucibles. The liquid was evaporated to dryness in an oven and the crucibles were heated to constant weight at 110°C. The residue remaining was determined from the final weight of the crucible (8,9).

Results

The baseline water samples from the two wells were analyzed in replicate. The results are presented in Table 1.

As anticipated, the principal cations are Na^+, K^+, Ca^{+2}, Sr^{+2} and Mg^{+2}; the major anions are Cl^-, SO_4^{-2} and HCO_3^-. These seven species account for essentially all of the mass observed in the total dissolved solid analyses.

OVERBURDEN AND UNDERBURDEN

Baseline determinations of the nature of Kirtland shale overburden and Pictured Cliffs sandstone underburden were made from rock samples taken from the core from well GT-1. The Kirtland shale was sampled at 493.5 ft. depth and the Pictured Cliffs sandstone was sampled at 519.5 ft. A stringer that appears at about 500 ft. was also sampled.

Analytical Methods

Physical Properties

Sections of overburden and underburden were submitted to Core Laboratories, Inc., Dallas, TX for x-ray diffraction, thin-section, and air permeability and porosity determinations.

Thin-section Petrographic Analysis

Samples sliced from the core of GT-1 were analyzed by Mr. R. Hicks, Geology Department, University of New Mexico. Samples included thin sections of overburden, underburden and a parting or stringer from the Fruitland Formation coal.

Cation Exchange Capacities

The method of Barrett and Wickham (11) was used for the determination of ion exchange capacities of the clay minerals in overburden and underburden. The rock samples were finely ground and equilibrated with a nickel(I) ammine complex; the amount of nickel remaining in solution is determined spectrophotometrically.

Elemental Analysis

The elemental analysis of the rock samples and their clay components was performed by fusing the rock or clay with lithium metaborate, dissolving the sample in water and determining metal ions by atomic absorption spectroscopy. Anhydrous lithium metaborate ($LiBO_2$) was purchased from G. Fredrick Smith, Co. It was recrystallized from hot water before use to give the hydrate $LiBO_2 \cdot 8H_2O$; approximately 100 g dissolved in 1 liter of water. The hot solution was filtered and allowed to stand overnight. Crystals of the hydrate were collected by filtration. They were dehydrated by heating in a furnace at 400°C for several hours; after cooling the crystals were ground into a powder with an alumina mortar and pestle. In a typical experiment (12)

TABLE 1. BASELINE RESULTS OF WATER SAMPLES COLLECTED FROM WELLS GT-1 AND GT-2

Analysis	Units	GT-1		GT-2	
		2/17/79	4/30/79	2/17/79	5/1/79
Cu^{+2}	µg/ℓ	53±1	3.6±0.2	--[a]	1.5±0.2
Zn^{+2}	µg/ℓ	14±2	10.4±0.5	--	10.5±0.5
Pb^{+2}	µg/ℓ	50±1	--	--	--
Na^{+}	mg/ℓ	1380±32	1100±29	--	1045±36
K^{+}	mg/ℓ	14±1	8.8±0.8	--	6.2±0.7
Ca^{+2}	mg/ℓ	1.3±0.1	1.7±0.1	--	1.9±0.1
Mg^{+2}	mg/ℓ	0.42±0.03	0.30±0.04	--	2.05±0.03
Sr^{+2}	mg/ℓ	0.23±0.05	0.35±0.05	--	0.45±0.05
Cd^{+2}	µg/ℓ	14±2	<0.7[b]	--	0.6±0.2
Ni^{+2}	µg/ℓ	<2[b]	<2[b]	--	<2[b]
Co^{+3}	µg/ℓ	20±1	<2[b]	--	<2[b]
Cr^{+3}	µg/ℓ	<7[b]	<7[b]	--	<7[b]
Sn^{+4}	mg/ℓ	<0.4[b]	--	--	--
Fe^{+3}	mg/ℓ	--[a]	1.05±0.02	--	0.11±0.02
Cl^{-}	mg/ℓ	--	1200±150	1150±18	1320±85
SO_4^{-2}	mg/ℓ	--	130±15	810±85	25(1 anal)
S^{-2}	mg/ℓ	--	4±2	25±5	0.18(1 anal)
F^{-}	mg/ℓ	--	2.25±0.04	2.55±0.05	2.60±0.05
PO_4^{-3} as P	mg/ℓ	--	0.10±0.02	0.24±0.02	0.08±0.02
CN^{-}	mg/ℓ	--	3.4±0.2	7.8±1.8	2.5±0.4
NO_3^{-} as N (only 1	µg/ℓ	--	<10[b]	<10[b]	<10[b]
NO_2^{-} as N analysis)	µg/ℓ	--	<2[b]	<2[b]	<2[b]
NH_4^{+} as N	µg/ℓ	--	10±3	--	2.3(1 anal)
Alkalinity	mg/ℓ	--	1200±20	1710±20	1710±20
TDS	mg/ℓ	--	4160±42	3900±26	3900(1 anal)
COD	mg/ℓ		<15[b]	<15[b]	<15[b]
pH	--	9.2±0.1[c]	10.66±0.05[c]	7.82±0.05[c]	9.65±0.05[c]
		--	10.5±0.1[d]	8.2±0.2[d]	9.64±0.05[d]
Water temp.	°C	15.5±0.2[c]	19.7±0.1[c]	15.6±0.2[c]	19.0±0.1[c]
		--	18.9±0.4[d]	18.9±0.2[d]	19.9±0.2[d]
Specific Conductance	mhos/cm	4.8±0.2[c]	6.4±0.1[c]	4.6±0.1[c]	5.5±0.1[c]
		--	6.2±0.2[d]	4.8±0.1[d]	5.7±0.1[d]

a) Blanks indicate the corresponding analysis was not performed on that sample.
b) Result is below detection limit. c) Sample overburden. d) Sample coal seam.

0.1000 g of finely ground (-200 mesh) rock was mixed with 0.5014 g of $LiBO_2$ and transferred to a pre-ignited high-purity graphite crucible. The mixture was fused in a muffle furnace at 950°C for 10 min. The melt was poured into a 250 ml polypropylene Erlenmeyer flask containing 25.0 ml of 3.00% HNO_3 and stirred gently with a Teflon coated magnetic stir bar over a magnetic stirrer until solution was complete, about 30 minutes. The sample was diluted with another 25.0 ml of the 3.00% HNO_3 solution. This solution was analyzed quantitatively for metal ions using the flame atomic absorption spectroscopy techniques described earlier.

The clay components were isolated from the rock samples by flocculation (13).

Results and Discussion

Results of the physical analysis of Kirtland shale overburden and Pictured Cliffs sandstone underburden are collected in Table 2. In both instances it is evident that the rock is composed almost entirely of quartz, feldspar and clay. In both samples clays make up almost 30% of the rock. This number varies quite dramatically with location and we have found many sections of the core with clay-size particles making up more than 60% of the sample. The principal clay minerals are kaolinite and montmorillonite. The large quantity of clay in the overburden is particularly significant for the self-cleaning of groundwater that becomes contaminated as a result of UCG since clays are good, natural ion exchangers. The quantitative basis for this statement is discussed in Section 6. For finely ground samples of overburden and underburden, cation exchange capacities of 2.7 meq/100 g rock and 2.2 meq/100 g rock, respectively, were determined. These values are reasonable for rock containing approximately 30% clay, but it is difficult to be quantitative because of the well-documented variability of cation exchange capacity with method (15).

TABLE 2. PHYSICAL PROPERTIES OF THE OVER- AND UNDERBURDEN FROM THE GT-1 CORE

Sample Property	Kirtland Shale Overburden GT-1 493.5 ft		Pictured Cliffs Sandstone Underburden GT-1 519.5 ft
Permeability (mdarcies)	0.017		0.014
Porosity (percent)	8.1		7.7
Minerals	Whole Rock	Clay (28%)	Whole Rock
Quartz (percent)	47		45
Feldspar	25		26
Kaolinite/Chlorite	17	49	14
Illite/Mica	trace	5	2
Montmorillonite	11	45	13

On the basis of the thin-section petrographic work, the Kirtland shale overburden is a rather simple geological formation. It is an organic-rich claystone which is quite homogeneous. The organic material appears with no preferred orientation in a matrix of clay-size particles. It is a clay-supported matrix. There are small pieces of angular quartz found throughout the matrix. Just how much of the fine particles are actually clay minerals or what kind of clay mineral cannot be determined on the basis of this examination.

Pictured Cliffs sandstone is the generalized term given to the underburden. From the thin-sections taken from this area it is further identified as a claystone-siltstone with no bedding recognizable even at a magnification of 400X. In some instances it is an organic-rich material in which the organic components have no preferred orientation. The biological source material cannot be clearly established though some pieces are probably cross sections of twigs which have been coalified and which have begun to migrate into the surrounding material, which appears to consist of very angular detrital clasts with a cherty cement. Some authigenic clays, mostly likely illite, were observed. Anhedral crystals of pyrite were found in this region as well.

Samples of Kirtland shale (overburden), a shaly parting in the coal seam, and Pictured Cliffs sandstone (underburden) were analyzed for metal ion concentrations by AAS. The clay components were also isolated and analyzed for metals. The major components are listed as oxides in Table 3 and the trace components are listed in Table 4. The composition of all three of these rocks and their clays are quite similar. There are a few significant differences however; Kirtland shale is considerably richer in calcium, iron, zinc and cadmium than Pictured Cliffs sandstone. The presence of calcium and iron in substantial abundance in the Kirtland shale probably indicates the minerals gypsum or anhydrite and pyrite in the sections analyzed. Pyrites can be observed visually in Pictured Cliffs sandstone, so the iron found here is probably also associated with the pyrites. On exposure to air the cores dried with the formation of white needles at the surface of the Kirtland shale portions; analysis of these needles indicated that they were largely gypsum.

TABLE 3. MAJOR COMPONENTS FOUND IN KIRTLAND SHALE (OVERBURDEN), A PARTING, AND PICTURED CLIFFS SANDSTONE (UNDERBURDEN) AND RESPECTIVE CLAYS.

Oxide	Percent Composition					
	Kirtland shale	Kirtland shale clay	Parting	Parting clay	Pictured Cliffs sandstone	Pictured Cliffs sandstone clay
SiO_2	57.1±0.1	55.6±0.1	55.6±0.1	56.2±0.1	63.3±0.1	66.5±0.1
Al_2O_3	19.6±0.2	21.8±0.2	23.4±0.2	25.3±0.2	16.4±0.2	25.7±0.2
Fe_2O_3	3.06±0.05	a	1.18±0.05	a	2.09±0.05	a
FeO	1.82±0.04	a	0.69±0.04	a	1.03±0.04	a
MgO	1.19±0.02	1.5±0.2	0.95±0.02	0.98±0.02	0.66±0.02	1.07±0.02
CaO	0.27±0.03	0.27±0.03	0.29±0.03	0.13±0.03	0.09±0.03	0.05±0.03
Na_2O	1.46±0.05	2.07±0.05	1.70±0.05	2.41±0.05	1.46±0.05	0.96±0.05
K_2O	2.1±0.07	0.97±0.07	1.01±0.07	0.94±0.07	2.49±0.05	0.94±0.07
TiO_2	0.6±0.1	0.5±0.1	0.4±0.1	0.2±0.1	0.7±0.1	0.4±0.1
MnO	0.009±0.005	0.011±0.005	0.003±0.005	0.006±0.005	0.006±0.005	0.008±0.005
SrO	0.021±0.005	0.021±0.005	0.025±0.005	0.024±0.005	0.016±0.005	0.017±0.005
S	<0.01[c]	<0.01[c]	a	<0.01[c]	1.21[b]	a
Total Fe As Fe_2O_3	5.08±0.05	5.47±0.05	1.95±0.05	1.62±0.05	3.22±0.05	2.15±0.05

a) No analysis performed. b) One analysis. c) Below detection limit.

TABLE 4. TRACE ELEMENT COMPOSITION OF KIRTLAND SHALE (OVERBURDEN), A PARTING, AND PICTURED CLIFFS SANDSTONE (UNDERBURDEN) AND THEIR RESPECTIVE CLAYS.

Element	Composition in ppm					
	Kirtland shale	Kirtland shale clay	Parting	Parting clay	Pictured Cliffs sandstone	Pictured Cliffs sandstone clay
Cr	19±2	25±2	13±2	13±2	19±2	55±3
Co	53±4	53±4	35±4	48±4	56±4	49±4
Ni	30±10	10±10	<0.6[a]	3±2	10±2	30±2
Cu	56±8	30±8	25±7	15±7	47±7	35±7
Zn	66±5	87±5	35±5	15±7	13±7	71±7
Cd	24±1	3.9±0.1	3.2±0.1	1.1±0.1	0.2±0.1	0.4±0.1
Ba	151±5	<0.8[a]	300±5	301±5	228±5	76±5
Pd	120±12	120±12	105±6	53±6	140±6	128±6
V	240±22	120±22	<0.9[a]	59±2	120±20	100±20

a) Result is below the detection limit.

SECTION 5

LEACHATE STUDIES

Groundwater passing through an UCG cavity is expected to change in character. It is important to know how this change influences the concentration of solutes from the rock through which it migrates. This section describes leaching experiments on overburden and underburden using simulated groundwater. The major perturbation by UCG is introduction of the chemically modified inorganic components in the ash. Therefore changes in groundwater composition due to leaching of species from the coal ash must be understood. Leaching studies of an ash prepared at 950°C are reported here.

OVERBURDEN

Overburden samples were taken from the GT-1 core 20.5 ft. above the coal seam in the Kirtland Shale Formation. The samples were pulverized and then the leaching characteristics as a function of pH were studied.

Procedure

Cations --

Five-gram samples of Kirtland shale were shaken with sufficient HNO_3 or NaOH to adjust the pH of the solutions to preselected final values. If the desired pH was not obtained with a single addition, more acid or base was added gradually and the mixture was agitated until the final pH was reached. This procedure generally required several days. The mixture was filtered to remove rock and clay and the filtrate was analyzed for metal ion concentrations by AAS using the methods described in Section 4. The metals studied over the pH range of 1 to 10 were manganese, sodium, barium, calcium, chromium, iron, magnesium, zinc, copper, cobalt, nickel, aluminum, lead, cadmium, lithium, and silver.

Anions --

Five-gram samples were allowed to equilibrate through regular agitation with 100 ml of .1 N $NaNO_3$ solutions. Either HNO_3 or NaOH was added to adjust the pH to the initial value desired. The pH of each sample slurry was measured every 3-4 days until a constant value was obtained. The slurry was allowed to separate and aliquots of the clear supernatant liquid were transferred to clean flasks. Conductance, $[Cl^-]$ and $[F^-]$ were determined using the methods described in Section 4.

Results

Cations --

Table 5 summarizes the results of the leaching experiment. For a number of the metals (Mn, Ba, Cr, Cu, Co, Ni, Pb, Cd, and Ag) the amounts in solution at final pH values higher than about 5 were so low that they could not be determined reliably. In each case there is a decrease in the amount of metal in solution from a high value near pH 1 to a much lower value as the pH increases. Manganese is a representative example; its behavior is shown in Figure 2. For metals for which the concentration could be determined over the entire pH range there is the same general decrease in metal ion concentration to a minimum in the vicinity of pH 6-7. In some cases (Fe, Zn, and Al) the concentration increases as the pH approaches pH 10. The most dramatic example of this behavior is exhibited by aluminum as shown in Figure 3. More typical are the results for magnesium, Figure 4, for which the concentration decreases to lower values as pH increases. This experiment offers one explanation for the very low concentrations of a number of metal ions in the strongly basic groundwater taken from wells GT-1 and GT-2 (Section 4) even though fusion tests showed these metals are present in appreciable quantities in Kirtland shale, coal, and Pictured Cliffs sandstone.

Anions --

The $[Cl^-]$, $[F^-]$ and conductance of the leachate from Kirtland shale are listed in Table 6.

The data indicate that the overburden clay has considerable buffer capacity. All but the solutions of very low or very high pH were buffered to a final pH of 8.3 to 8.4. This is compatible with the alkaline character of groundwater (Section 4) and in fact the groundwater basicity may be due to close contact with the Kirtland shale member or with Kirtland shale-like minerals in the coal seam.

The fluoride ion concentrations in the final solutions are very low and show only small variations with pH. The variations are not large enough to detect any trends. The chloride ion concentrations are also very low and show no trend with pH. The low concentrations are probably due to the generally high solubility of fluoride and chloride salts so that the most soluble of these compounds were leached away many years ago.

The conductance of the leachate is significantly higher at the extreme ends of the pH scale. This is an indication that more of the rock is dissolved at very high and low pH's, since conductance increases as ion concentrations increase.

UNDERBURDEN

Underburden samples were taken from the section of core from well GT-1 which reached into the Pictured Cliffs formation. The rock was pulverized

TABLE 5. CONCENTRATION OF CATIONS LEACHED FROM KIRTLAND SHALE AS A FUNCTION OF FINAL pH, [CONC. (ppm)/WT. CLAY (g)].

Cation \ pH	0.35	0.80	1.30	3.20	3.45	3.65	3.80
Ag(± 0.001)	0.004	0.008	0.004	0.0006	a	a	a
Al(± 0.2)	20.1	19.8	15.4	1.2	0.5	0.3	0.2
Ba(± 0.05)	0.85	0.23	0.17	0.17	0.05	0.11	0.28
Ca(± 0.2)	26.5	26.0	26.2	15.7	15.7	12.2	12.5
Cd(± 0.00010)	0.00255	0.00250	0.00220	0.00160	0.00150	0.00125	0.00080
Co(± 0.002)	0.044	0.060	0.052	0.014	0.032	0.018	0.032
Cr(± 0.002)	0.024	0.020	0.018	f	f	f	f
Cu(± 0.002)	0.036	0.039	0.030	0.040	0.036	0.020	0.020
Fe(± 2)	84	81	76	22	16	13	7
Li(± 0.002)	0.039	0.041	0.038	0.019	0.016	0.015	0.013
Mg(± 0.3)	21.0	19.2	15.3	7.2	5.2	4.7	4.0
Mn(± 0.02)	0.43	0.42	0.32	0.16	0.17	0.10	0.11
Na(± 0.2)	13.2	13.3	14.3	13.3	13.4	13.3	12.3
Ni(± 0.002)	0.049	0.072	0.062	0.015	0.037	0.019	0.035
Pb(± 0.002)	0.110	0.099	0.055	0.052	0.038	0.039	0.090
Zn(± 0.02)	0.35	0.35	0.29	0.13	0.13	0.08	0.07

Continued

TABLE 5. (Continued)

Cation \ pH	3.90	4.25	4.75	6.95	7.45	7.70	8.70	9.15	9.95
Ag(± 0.001)	a	a	a	a	a	a	a	a	a
Al(± 0.2)	3.0	1.0	0.1	b	b	0.1	1.0	2.0	1.9
Ba(± 0.05)	0.15	0.05	c	c	c	c	c	c	c
Ca(± 0.2)	7.0	5.0	2.7	1.0	3.0	0.5	0.2	0.1	0.1
Cd(± 0.00010)	d	d	d	d	d	d	d	d	d
Co(± 0.002)	0.012	0.013	0.009	e	e	e	e	e	e
Cr(± 0.002)	f	f	f	f	f	f	f	f	f
Cu(± 0.002)	0.013	0.005	g	g	g	g	g	g	g
Fe(± 2)	5	h	1	i	i	1	2	3	4
Li(± 0.002)	0.011	0.007	0.005	0.002	0.003	0.001	0.001	0.001	0.001
Mg(± 0.3)	4.8	1.7	0.3	0.2	0.2	0.1	0.1	0.1	j
Mn(± 0.02)	0.05	0.04	0.02	k	k	k	k	k	k
Na(± 0.2)	10.3	10.3	11.1	8.4	10.3	8.2	5.8	4.7	4.2
Ni(± 0.002)	0.023	0.023	0.004	ℓ	ℓ	ℓ	ℓ	ℓ	ℓ
Pb(± 0.002)	h	0.015	m	m	m	m	m	m	m
Zn(± 0.02)	0.05	0.03	0.01	<0.005	<0.005	<0.005	0.01	h	0.01

a) <0.003 ppm
b) <0.04 ppm
c) <0.01 ppm
d) <0.0007 ppm
e) <0.007 ppm
f) <0.007 ppm
g) <0.003 ppm
h) Analysis not done at this pH.
i) <0.005 ppm
j) <0.0003 ppm
k) <0.003 ppm
ℓ) <0.002 ppm
m) <0.02 ppm

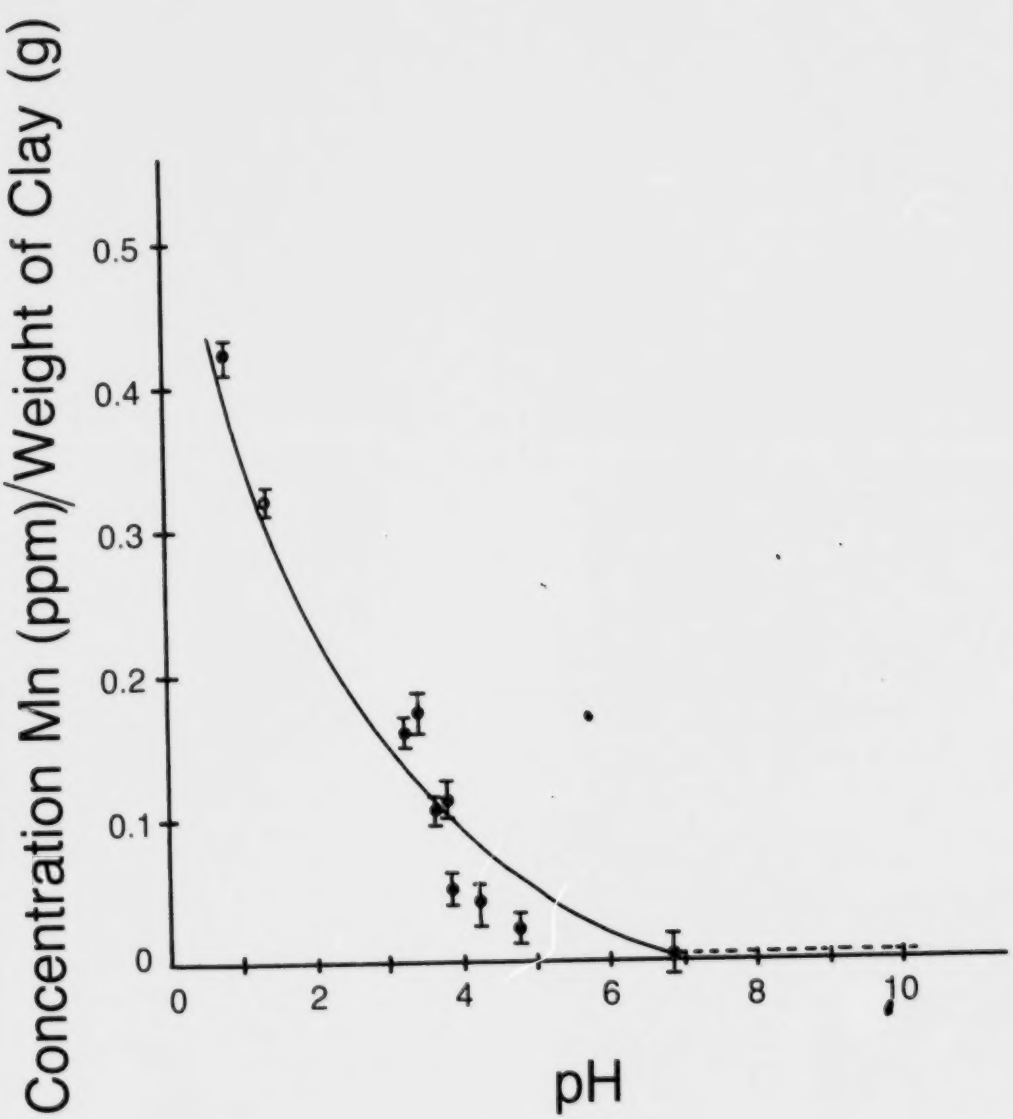

Figure 2. The amount of manganese dissolved from Kirtland shale as a function of final pH, $\sigma = 0.33$.

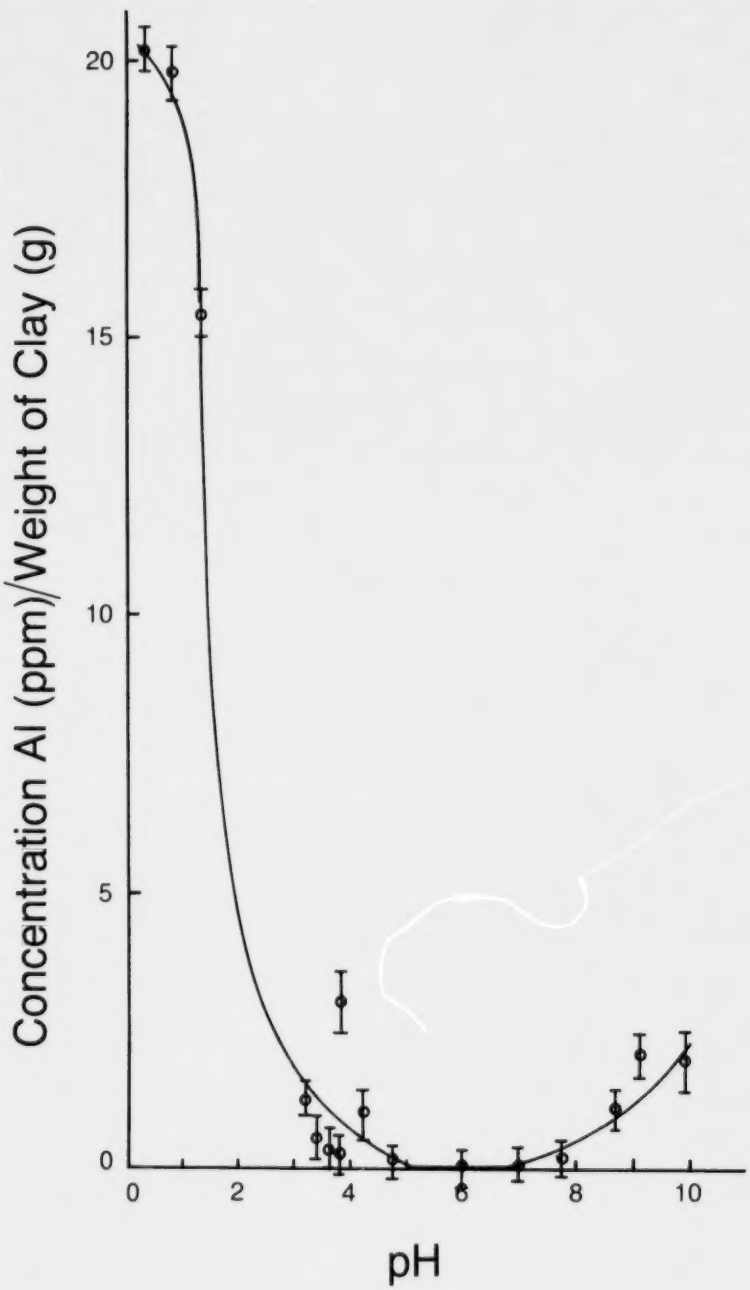

Figure 3. The amount of aluminum dissolved from Kirtland shale as a function of final pH, σ = 0.33.

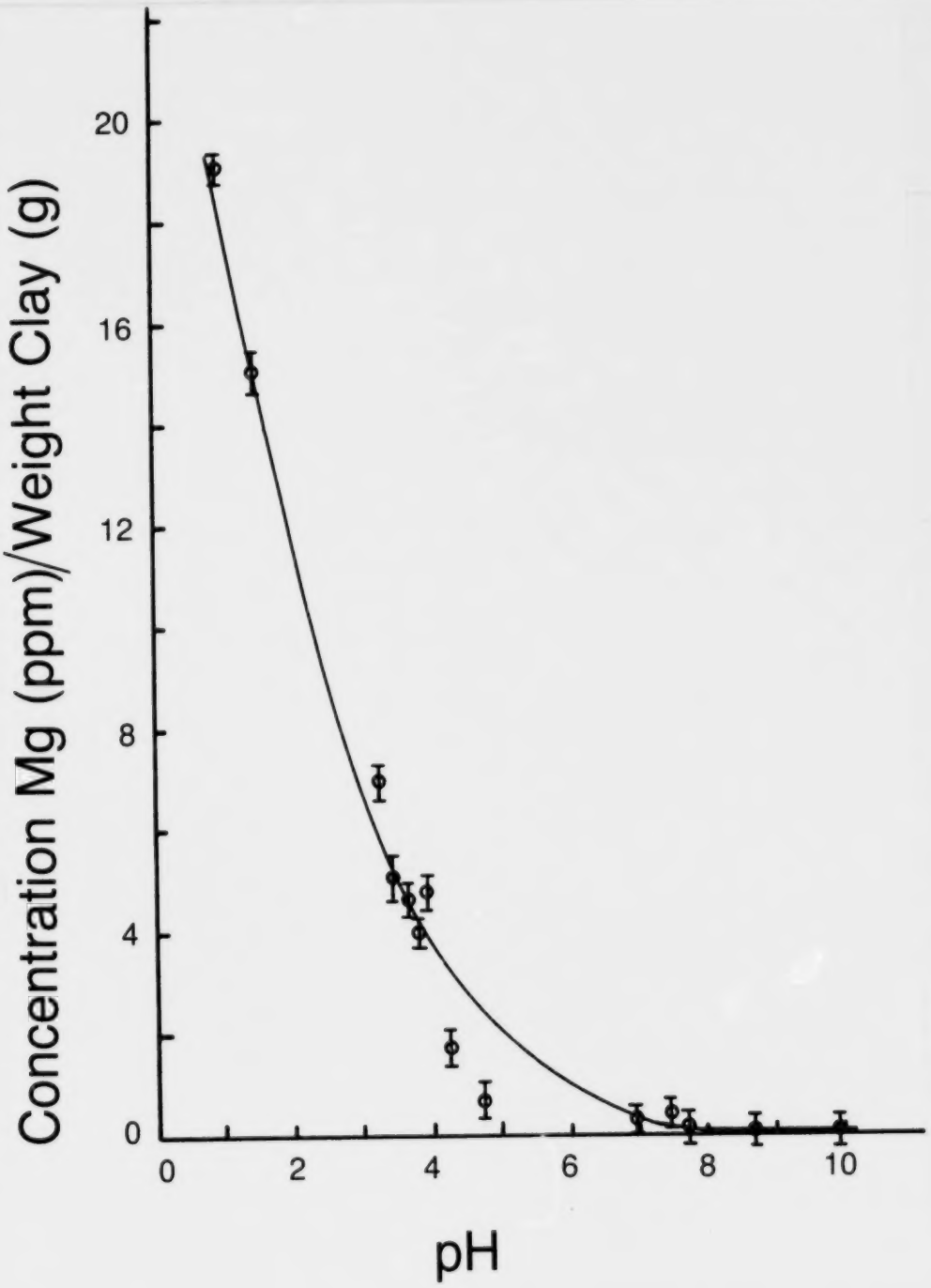

Figure 4. The amount of magnesium dissolved from Kirtland shale as a function of final pH, σ = 0.12.

TABLE 6. RESULTS OF LEACHATE ANALYSES FROM KIRTLAND SHALE OVERBURDEN.

Sample #	Wt. of clay (g)	Initial pH ±0.01	Final pH ±0.01	$[F^-]$ ppm ±0.10	$[Cl^-]$ ppm ±0.33	Conductance ($\times 10^{-3}$mho), ±0.18
1	5.0941	1.19	1.61	0.73	1.56	30.7
2	5.0941	1.19	1.61	0.38	1.70	30.4
3	5.0124	2.35	5.62	0.12	3.15	7.18
4	5.0116	2.35	5.45	0.22	4.90	7.28
5	5.0343	3.30	8.30	0.68	4.58	6.85
6	5.0343	3.30	8.28	0.74	4.20	6.95
7	5.0638	4.40	8.29	1.06	5.60	6.83
8	5.0642	4.40	8.33	0.81	4.54	6.76
9	5.0098	5.25	8.33	0.82	4.54	6.82
10	5.0103	5.25	8.40	1.07	5.50	6.79
11	5.1202	6.13	8.40	0.86	4.54	7.29
12	5.1201	6.13	8 40	0.85	4.00	7.24
13	5.0162	7.24	8.39	0.86	4.70	7.20
14	5.0171	7.24	8.39	0.86	4.10	7.22
15	5.0083	8.12	8.42	0.87	3.83	7.11
16	5.0102	8.12	8.42	0.85	5.60	7.11
17	5.1030	9.29	8.42	0.86	4.20	7.11
18	5.1027	9.29	8.40	0.88	4.20	7.16
19	5.0174	10.43	8.49	0.92	5.80	7.17
20	5.0171	10.43	8.49	0.92	4.85	7.09
21	5.0290	11.15	9.60	0.49	4.85	7.14
22	5.0286	11.15	9.75	0.44	4.85	7.20
23	5.0276	12.41	12.32	0.49	7.60	21.5
24	5.0278	12.41	12.30	0.49	7.60	21.9

and then the leaching characteristics of the anions as a function of pH were studied.

Procedure

Five-gram samples of pulverized underburden (Pictured Cliffs sandstone) were equilibrated with 1000 ml aqueous solutions identical to those used in the overburden leaching experiments over the pH range of 1-12. The initial pH was adjusted by HNO_3 or NaOH stock solutions to the desired value. The solutions were analyzed for the anions Cl^-, F^-, CN^- and SO_4^{-2} and for total dissolved solids (TDS). The analytical methods described in Section 4 were used for all except the CN^- analyses.

Aliquots of the clear supernatant liquid were transferred by pipet to a clean flask where an Orion Model 94-06 cyanide ion electrode and a Model 90-01 single-junction reference electrode were used to determine cyanide ion concentration. The ionic strength was adjusted to 0.10 M with an NaOH solution. Basicity eliminated interference by H^+ and addition of a solution of acetic acid and EDTA removed interferences due to metal ions such as Cd^{+2}, Cu^{+2}, Ni^{+2}, and Zn^{+2}. Cyanide ion concentrations were determined from measured emf values by use of a calibration curve generated from solutions of known NaCN concentration.

Results

Replicate experiments were performed and the results are given in Table 7.

Several interesting conclusions can be drawn from these results. First of all, it is clear that the rock has a strong buffer action which holds the pH of the solutions at about 7.2. This effect may be due to the hydroxyl groups on the clay minerals. The final pH of 7.2 is considerably lower than the pH of the water samples removed from the two wells (Section 4) and it is consistently 1 pH unit lower than the leachate from the overburden material. The reason for this higher acidity is not clear. Second, a plot of TDS vs. initial pH, Figure 5, shows that a large quantity of rock is dissolved in either strongly acidic or strongly basic solutions with a minimum TDS in the vicinity of pH 7. This is consistent with the conductance data from the overburden leachate. Third, by far the most abundant anion is sulfate. The concentrations of chloride, fluoride and cyanide were so low at all pH values that the variations are insignificant. It is also clear that at the extremes of the pH range examined SO_4^{-2} makes up only a small fraction of the total dissolved solids whereas at pH 7 over half of the total dissolved solids are sulfate salts, presumably Na_2SO_4, K_2SO_4, and $CaSO_4$.

ASH

Coal from the Fruitland Formation was used to prepare a series of ash samples to simulate the material which will be left after an underground coal gasification experiment. Both dynamic and batch leaching studies were done. The effect of ashing temperature and leaching media were examined.

TABLE 7. TOTAL DISSOLVED SOLIDS AND CONCENTRATIONS OF Cl^-, F^-, CN^- AND SO_4^{-2} EXTRACTED FROM PICTURED CLIFFS SANDSTONE AS A FUNCTION OF pH.

Initial pH, ±0.01	Final pH, ±0.01	TDS, mg/ℓ, ±200	$[Cl^-]$, mg/ℓ, ±0.045	$[F^-]$, mg/ℓ, ±0.08	$[CN^-]$, mg/ℓ, ±0.007	$[SO_4^{-2}]$, mg/ℓ, ±45
1.05	--	15600	0.75	0.37	0.021	650
2.08	7.14	2600	0.62	0.12	0.028	440
3.03	7.26	1600	0.65	0.18	0.028	460
4.04	--	900	0.64	0.21	0.027	440
5.02	7.22	800	0.64	0.19	0.024	420
6.01	7.24	--	0.62	0.20	0.013	480
7.01	7.12	700	0.62	0.20	--	420
8.01	7.24	--	0.66	0.20	0.012	440
9.02	7.18	700	0.63	0.20	--	440
10.02	7.18	--	0.65	0.20	0.011	400
11.00	7.26	900	0.65	0.21	--	560
12.05	--	1600	0.65	0.39	0.010	430

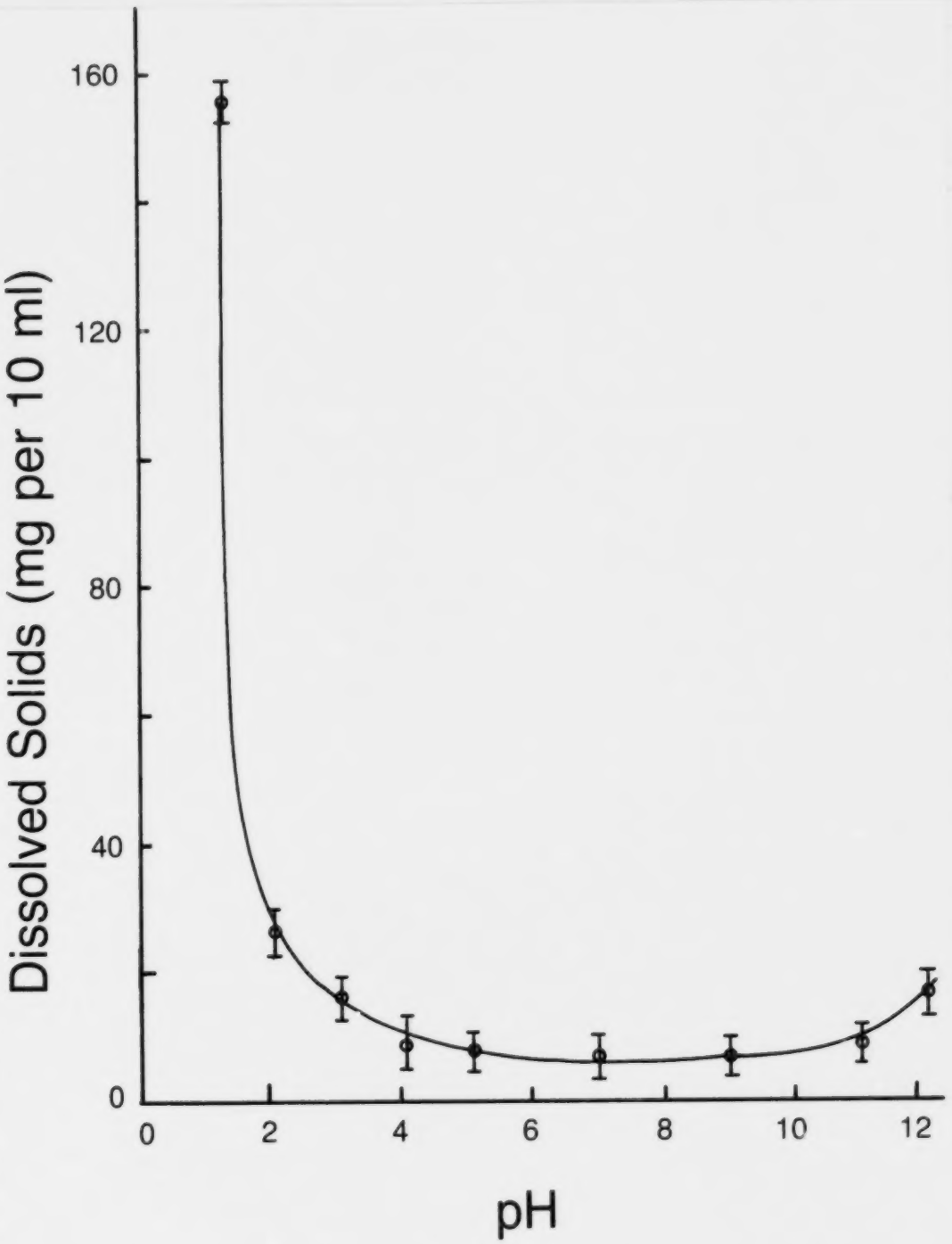

Figure 5. Total dissolved solids from Pictured Cliffs sandstone as a function of initial pH.

Procedure

The ash used in the dynamic studies was prepared using ASTM procedure D-3173 (14). In a typical experiment, a 7.00 g coal sample was placed in a porcelain crucible which was heated to 500°C in a Thermodyne 1500 muffle furnace over a 1-hour period. The temperature was raised to 750°C over the next 1 hour and the sample was held at 750°C until constant weight was obtained. The ash was pulverized and packed into a Pyrex column 25 cm long and 1 cm inside diameter. The column was supported vertically. Both the upper and lower ends of the ash column were held in position by loosely packed glass wool plugs. A distilled-deionized water leachate was gravity-fed through the column from a reservoir at a flow rate of 0.5 ml min^{-1}. The flow was regulated by a valve at the outlet to the column. Samples, 25 ml each, were collected until 1 liter of leachate had passed through the column. The residual ash was collected and dried in an oven at 110°C; 21.4% of the ash dissolved.

Ashes for the batch studies were prepared by ASTM procedure D-3173 (14) except that the final temperatures were 700°C to 1050°C. Replicate 5-g (nominal) ash samples were then pulverized and equilibrated with 200 ml of either distilled-deionized water or simulated well water. The simulated well water contained a weight ratio of 80:64:37:1 of sodium bicarbonate: sodium chloride:sodium sulfate:potassium hydroxide and a total weight of 45.5 g of salt per liter of solution. It approximated the previously characterized groundwater (Section 4) in pH, conductivity and primary ion concentration. The ash samples were allowed to stand in contact with the water and agitated frequently for seven days before the leachates were analyzed. The analytical procedures described in Section 4 were used for all analyses.

Results

The effluent samples from the ash columns were analyzed for specific cations and the results are presented in Figures 6 and 7. The principal cations found were Ca^{+2}, Na^{+}, Mg^{+2}, and K^{+}, while Hg^{+2}, Al^{+3}, and Pb^{+2} were present in rather high concentrations. Appreciable amounts of Fe^{+3}, Zn^{+2}, and Cu^{+2} were also detected.

These results are in agreement with those obtained by Lawrence Livermore National Laboratory (LLNL) in a similar laboratory leaching experiment (15). In the LLNL study the predominant cations released from Felix subbituminous coal ash of Wyoming were Ca^{+2}, K^{+}, Mg^{+2}, Al^{+3}, and Na^{+}. Anionic species detected in the Felix #2 leachate included SO_4^{-2}, OH^{-}, Cl^{-}, and Br^{-}.

Tables 8 and 9 list the results of the batch leaching tests. The results indicate the expected prevalence of calcium, sulfate, and hydroxide-carbonate (alkalinity). The amount of calcium present here and in the actual well waters is about what would be expected for solutions saturated by contact with gypsum and limestone. As can be seen from Tables 8 and 9, aluminum is present in fairly high concentration. This is perhaps surprising but it should be noted that the amount dissolved is a strong function

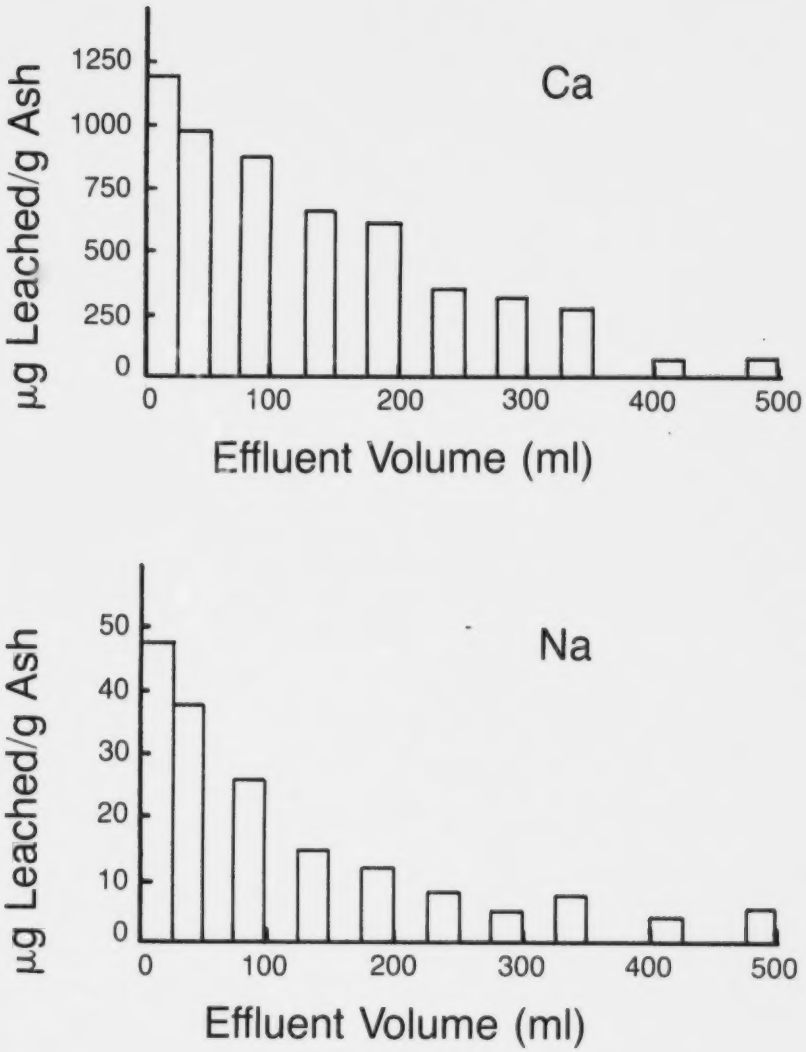

Figure 6. Major cationic constituents of Fruitland ash leachate.

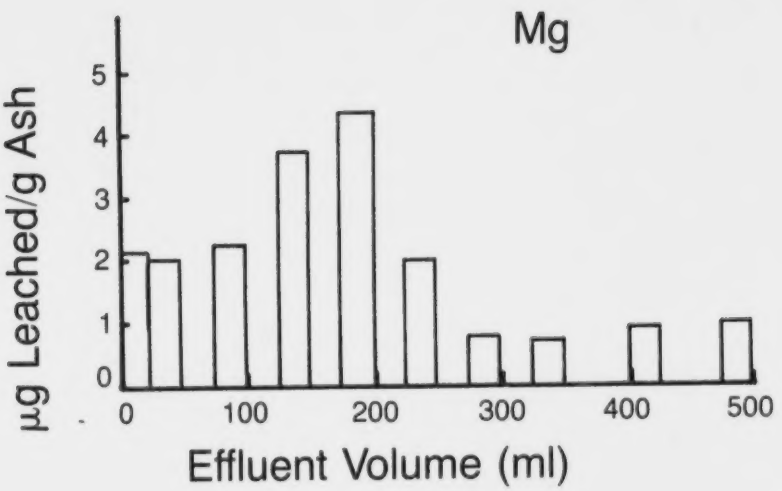

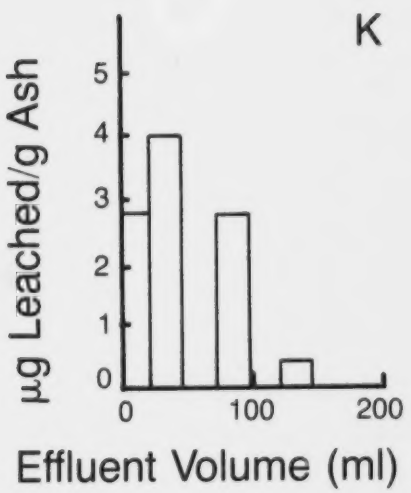

Figure 6. (Continued)

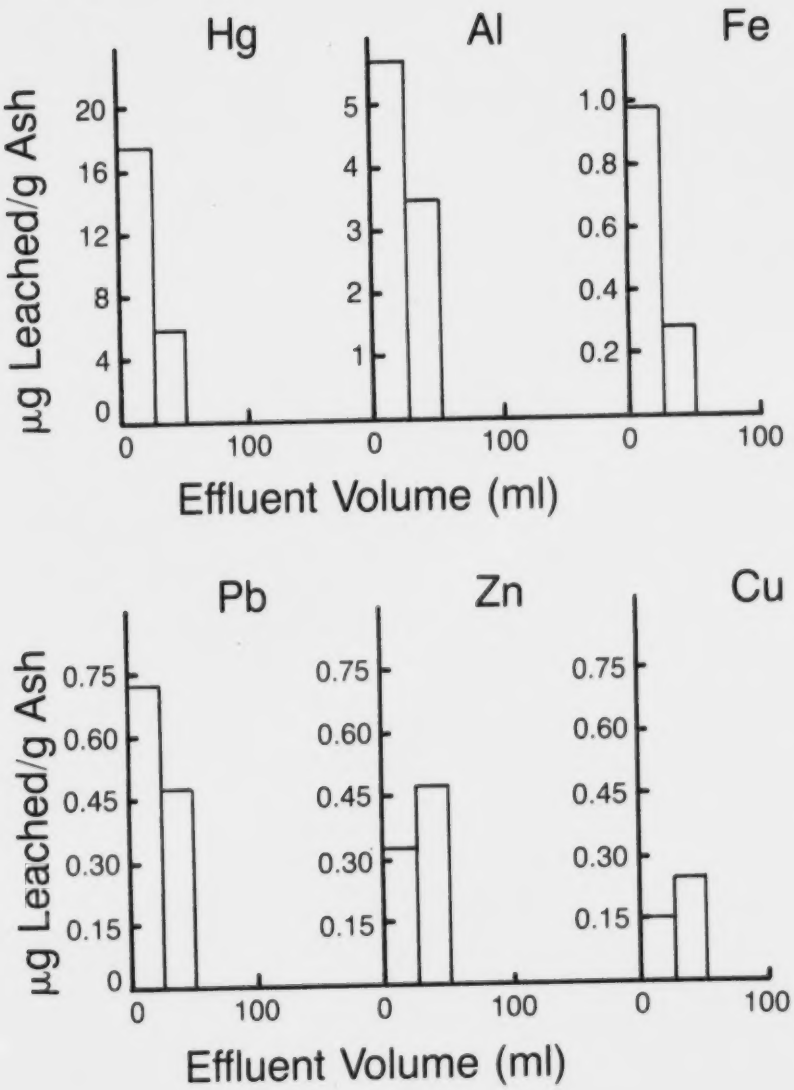

Figure 7. Trace metal constituents of Fruitland ash leachate.

TABLE 8. WATER-ASH LEACHATE.

Measurement	Percent of ash dissolved as that species leach					
	Water leach			Simulated well water leach		
	700[c]	950[c]	1050[c]	700[c]	950[c]	1050[c]
pH	6.41±0.22[d]	9.37±0.06[d]	7.8±1.2[d]	9.45±0.06[d]	9.61±0.06[d]	9.62±0.04[d]
Sulfate	0.98±0.05	0.04±0.05	0.27±0.05	--[a]	--	--
Alkalinity (to pH 4), as mg/ℓ of $CaCO_3$ per gram of ash	--	455±45	--	--	--	--
F^-	<0.002[b]	<0.002[b]	<0.002[b]	<0.002[b]	<0.002[b]	<0.002[b]
Cl^-	<0.001[b]	<0.001[b]	<0.001[b]	<0.001[b]	<0.001[b]	<0.001[b]
Na^+	--	0.011±0.002	--	--	--	--
K^+	--	0.015±0.005	--	--	--	--
Fe^{+2}, Fe^{+3}	--	0.025±0.005	--	--	--	--
Al^{+3}	--	0.22±0.04	--	--	--	--
Mg^{+2}	--	$(7\pm3)\times10^{-5}$	--	--	--	--
Ca^{+2}	--	0.62±0.06	--	--	--	--

a) Blanks indicate that measurements were not made.
b) Below the detection limit.
c) Temperature (°C) at which ash was prepared.
d) pH of leachate.

TABLE 9. TRACE METAL ION CONCENTRATION INCREASES (IN PPM) IN DISTILLED WATER LEACHATE OF COAL ASHES PREPARED AT DIFFERENT TEMPERATURES.

Analyte	Ash Temperatures, °C				
	700	800	900	1000	1050
Al	0.72±0.49	0.25±0.15	0.76±0.91	0.10±0.17	<0.04[a]
B	2.3±1.6	--[b]	1.5±1.5	1.3±0.6	1±3
Cd	0.050±0.015	0.079±0.038	0.015±0.007	0.003±0.001	<0.0007[a]
Co	0.071±0.024	0.043±0.013	0.019±0.008	<0.007[a]	0.025±0.005
Cr	0.003±0.004	<0.002[a]	0.022±0.024	0.014±0.006	0.002±0.005
Cu	0.015±0.012	<0.003[a]	0.015±0.008	<0.003[a]	--
Fe	0.093±0.045	0.041±0.027	0.020±0.017	0.013±0.005	<0.005[a]
Mn	0.006±0.008	0.014±0.006	0.016±0.011	0.014±0.005	<0.003[a]
Ni	<0.002[a]	<0.002[a]	0.005±0.018	0.003±0.015	--
Pb	0.92±0.53	0.63±0.23	0.49±0.45	<0.02[a]	<0.02[a]
Zn	0.013±0.014	0.050±0.011	--	--	--

[a] Below detection limit.
[b] Blanks indicate no analysis was performed.

of ashing temperature. The Ca:Al ratio of 3:1 is lower than the 20:1 ratio found in a LLNL leaching experiment which had a final pH of 10 to 10.5 (16). In the LLNL experiment a tenfold decrease in leachable aluminum at 1100°C when compared with 1000°C was noted (16).

Based on the weight of dried ash before and after leaching, it was also observed that the brine solutions dissolved more of the ash than did the distilled-deionized water. This may be due to ionic strength or pH effects. As with the cations, the amount of sulfate leached showed an inverse relationship to the ashing temperature.

The results presented in Table 9 show a trend of decreasing leachability of metal ions with increasing final ashing temperature for the six metals Al, Cd, Cu, Co, Fe, and Pb. Perhaps because of the low solubility, no clear trend could be observed for the metals B, Cr, Mn and Ni. For most of these species the actual leachate concentrations approached flame AAS detection limits for ash prepared at 1050°C. In a UCG system it may be anticipated that final temperatures in excess of 1000°C in the burn chamber will contribute to a major reduction of metal ions leached into groundwater.

SECTION 6

DISTRIBUTION COEFFICIENTS (Overburden and Underburden)

The rate of migration of an ion is affected by the heterogeneous equilibrium of the ion between the solution and the solid phases. The equilibrium is characterized by a distribution coefficient K_d. This section describes determination of K_d values for the typical cations Cd^{+2} and Mg^{+2} on overburden and underburden. The liquid phase consisted of aqueous solutions of the cations at various pH values.

PROCEDURE

K_d's of Cadmium Ions on Overburden and Underburden (Function of Cd Concentration and Particle Size).

Samples of Kirtland Shale overburden and Pictured Cliff Sandstone underburden were pulverized and sieved through 4-, 7-, 12-, and 100-mesh screens to separate the crushed rocks into three particle size ranges (4.76 mm, 2.83-1.68 mm, and less than 149 μm). Fifty gram samples of overburden and underburden in these known particle size ranges were then equilibrated with 200 ml of aqueous solutions containing a range of $CdCl_2$ concentrations. These mixtures were agitated frequently and the solutions were periodically analyzed for Cd^{+2} using atomic absorption spectroscopy. When no change in Cd^{+2} concentration was observed over a 3 day period, the mixture had reached equilibrium. The concentrations of Cd^{+2}, Na^{+}, K^{+}, and Mg^{+2} in the equilibrium solutions were measured using AAS. The distribution coefficients K_d were calculated from these data for all concentrations and particle sizes. The distribution coefficient K_d for adsorption of a species A is customarily defined as

$$K_d = \frac{\text{(activity of A in the solid phase)}}{\text{(activity of A in the liquid phase)}}$$

where the activities are defined as

$$\text{activity in the solid phase} = \frac{\text{g of A adsorbed}}{\text{g of solid}}$$

$$\text{activity in the liquid phase} = \frac{\text{g of A in solution}}{\text{volume of solution}} .$$

So

$$K_d = \frac{(g \text{ adsorbed})/g \text{ solid}}{(g \text{ in solution})/\text{volume solution}}$$

$$= \frac{(g \text{ adsorbed}) \times \text{volume}}{(g \text{ in solution}) \times \text{wt. sample}}$$

K_d's of Magnesium Ions on Overburden (Function of pH)

Samples of Kirtland Shale overburden were crushed. Fifty gram samples were equilibrated with 200 ml of solutions containing 1000 ppm Mg^{+2} and varying in pH from 2.83 to 4.16.

DISCUSSION

The distribution coefficients for Cd^{+2} on the overburden and underburden as a function of initial Cd^{+2} concentration and rock particle size are listed in Table 10 and shown in Figures 8 and 9. For all of the cases studied K_d values increase with increasing cadmium ion concentration to a maximum in the vicinity of 100 mg/ℓ; this is followed by a rather abrupt decrease. This decrease may be explained in two ways. Either the maximum indicates saturation of surface sites by the Cd^{+2} added from the solution, or ion exchange occurs between the cadmium ions in solution and the abundant metal ions bound to the clay minerals. If the latter alternative is reasonable, the displaced ions should appear in solution. As a result, the solutions were also analyzed for Mg^{+2}, Na^{+}, and K^{+}. The amounts of desorbed Mg^{+2}, Na^{+}, and K^{+} are shown in Table 11. For each concentration range the amount of desorbed cation remains low until the concentration of added Cd^{+2} reaches 1000 mg/ℓ at which point there is an abrupt increase, by a factor of three or more, in the amount of desorbed metal ion.

It is interesting to compare the number of moles of Cd^{+2} adsorbed with the total number of moles of the three cations Mg^{+2}, Na^{+}, and K^{+} released. When the initial concentration of Cd^{+2} is 111 mg ℓ^{-1}, a total of 9.4×10^{-4} mole ℓ^{-1} = 9.5×10^{-4} equivalents ℓ^{-1} of the three cations are found in solution, while an increase in the initial Cd^{+2} concentration by a factor of ten to 1110 mg ℓ^{-1} only increases the total cation concentration by a factor of five to 5.6×10^{-3} mole ℓ^{-1} = 5.7×10^{-3} equivalents. At the same time K_d decreases dramatically. This suggests that ion exchange is the dominant sorption mechanism. As the cadmium ion concentration reaches very high levels the readily accessible ions in the clay matrix become saturated and the amount of ion exchange does not keep up with the increased Cd^{+2} concentration.

It is useful to plot the cadmium adsorption data in two other ways. In the first variation we plot the quantity of cadmium adsorbed per gram of rock (mg Cd^{+2} adsorbed/g rock) as a function of the quantity of cadmium left per milliliter of solution (mg Cd^{+2} in soln/ml soln). The graph is shown in Figure 10. The interesting feature of this graph is the gradual approach to saturation of the rock as the concentration of Cd^{+2} in solution increases. This limit should be the cation exchange capacity of the rock with respect to cadmium. Extrapolation of the graph to the asymptotic limit gives a

TABLE 10. K_d VALUES FOR Cd^{+2} ON OVERBURDEN AND UNDERBURDEN OF DIFFERENT PARTICLE SIZES.

Sample	Particle size	$[Cd^{+2}]_{init.}$ mg/ℓ	Initial pH, ±0.01	Final pH, ±0.01	K_d [a]
Overburden (Kirtland shale)	passed 4.76 mm sieve	0.04	10.36	10.20	130±20
		0.85	10.32	10.18	280±44
		11.1	10.29	10.24	1300±200
		111	9.75	9.67	1800±280
		1110	6.98	6.94	60±10
	2.83-1.68 mm	0.04	10.36	10.27	130±21
		0.85	10.32	10.20	460±72
		11.1	10.31	10.17	1000±160
		111	9.79	9.43	1300±200
		1110	7.10	6.89	70±11
	<149 μm	0.04	10.32	10.04	70±11
		0.85	10.31	10.13	130±21
		11.1	10.27	10.11	250±41
		111	9.65	9.33	400±120
		1110	6.96	6.68	28±4
Underburden (Pictured Cliffs sandstone)	passed 4.76 mm sieve	0.04	8.40	8.22	130[b]
		0.85	8.02	7.10	900±150
		11.1	6.83	6.59	1000±160
		111	6.70	6.12	1200±200
		1110	6.28	5.78	100±15
	2.83-1.68 mm	0.04	10.51	9.80	140[b]
		0.85	10.48	10.14	550±87
		11.1	10.45	10.27	800±120
		111	9.90	9.76	1100±180
		1110	10.30	9.91	110±17
	<149 μm	0.04	10.43	9.90	70±11
		0.85	10.44	10.17	130±21
		11.1	10.40	10.13	170±26
		111	9.81	9.54	300±31
		1110	7.30	7.01	44±7

[a] $K_d = \frac{\text{g adsorbed x volume}}{\text{g in soln x wt. sample}}$

[b] Only one determination made.

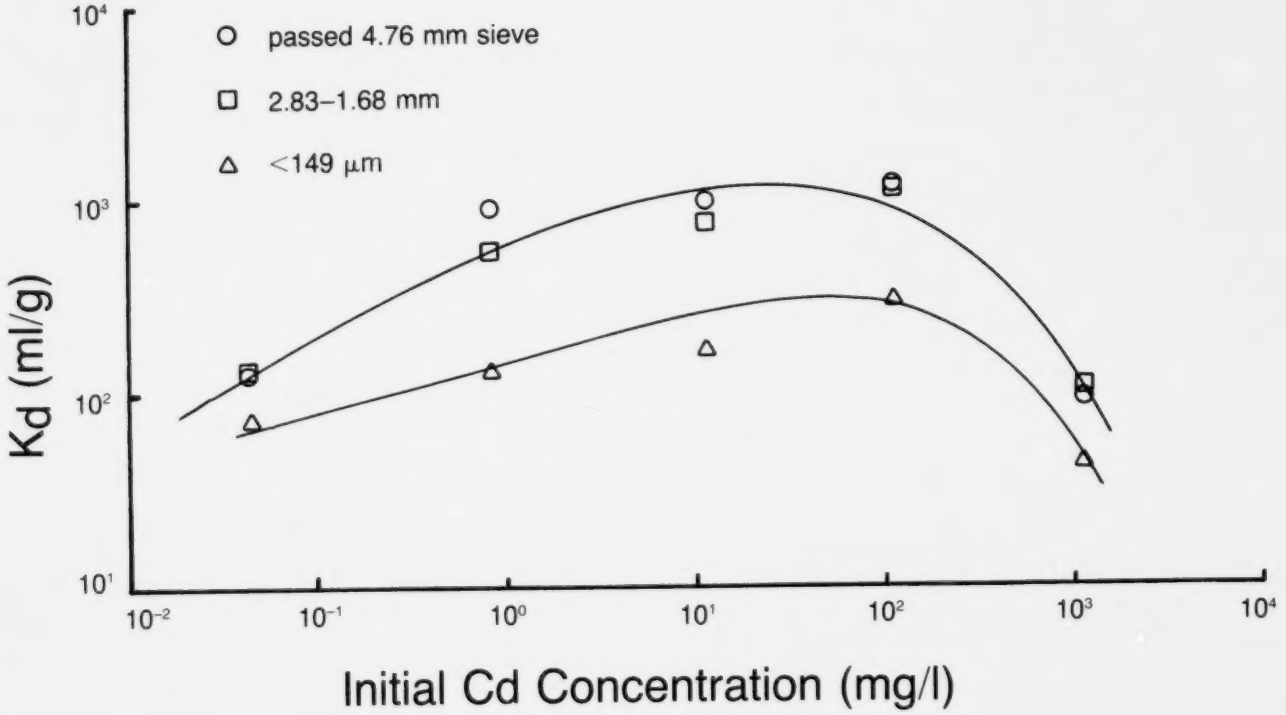

Figure 8. K_d for Cd^{+2} on Pictured Cliffs sandstone as a function of initial concentration of Cd^{+2}.

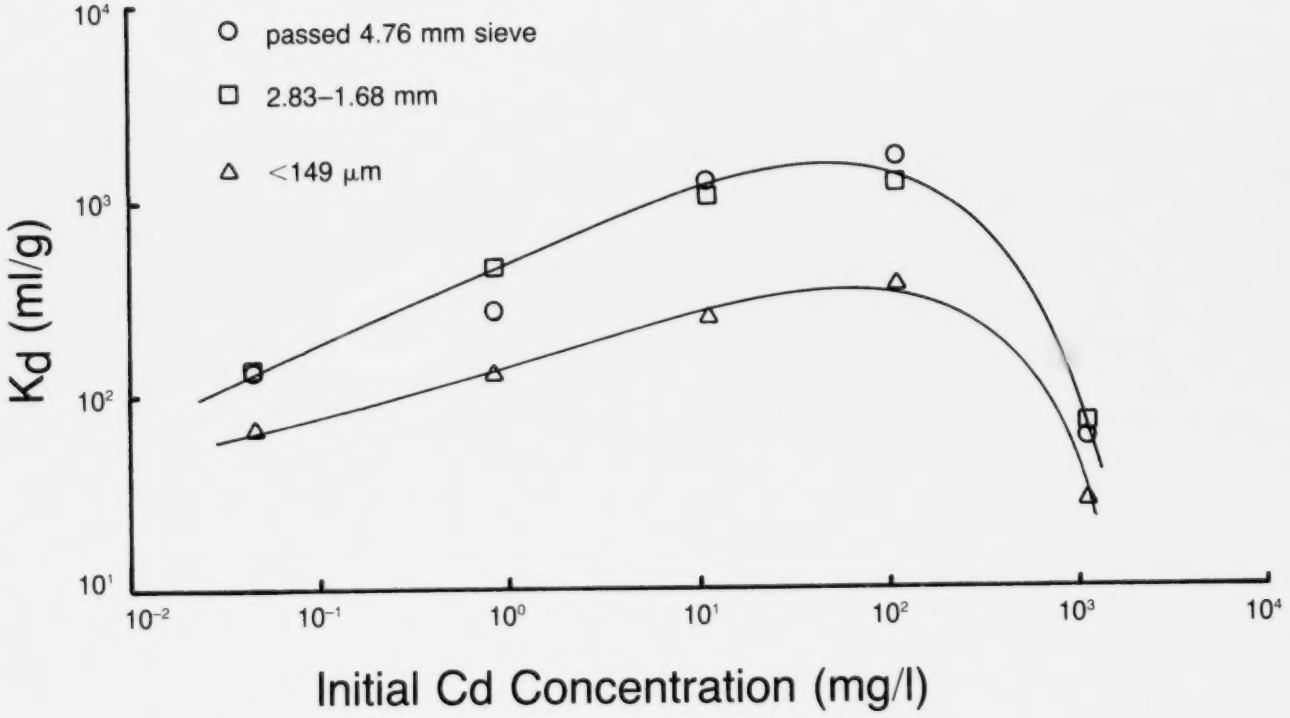

Figure 9. K_d for Cd^{+2} on Kirtland Shale as a function of initial concentration of Cd^{+2}.

TABLE 11. QUANTITIES OF Mg^{+2}, Na^{+}, and K^{+} DESORBED FROM OVERBURDEN AND UNDERBURDEN BY Cd^{+2}.

Sample	Particle size	$[Cd^{+2}]$ mg/ℓ init.	$[Mg^{+2}]$ mg/ℓ, ±0.025	$[Na^{+}]$ mg/ℓ, ±3.7	$[K^{+}]$ mg/ℓ, ±0.75
Overburden (Kirtland shale)	passed 4.76 mm sieve	0.04	0.171	26	5.5
		0.85	0.165	24	4.7
		11.1	0.153	26	4.5
		111	0.144	19	4.2
		1110	1.150	121	12.7
	2.83-1.68 mm	0.04	0.174	31	5.2
		0.85	0.178	28	5.2
		11.1	0.174	25	5.3
		111	0.167	21	5.0
		1110	1.05	118	12.5
	<149 μm	0.04	0.300	31	9.8
		0.85	0.332	26	10.6
		11.1	0.330	27	10.8
		111	0.297	21	10.7
		1110	2.6	74	14.4
Underburden (Pictured Cliffs sandstone)	passed 4.76 mm sieve	0.04	0.168	22	5.2
		0.85	0.150	16	4.4
		11.1	0.160	14	4.5
		111	0.140	16	4.6
		1110	0.367	127	11.6
	2.83-1.68	0.04	0.168	21	4.9
		0.85	0.164	14	4.5
		11.0	0.175	11	5.6
		111	0.144	16	4.7
		1110	0.348	115	11.6
	<149 μm	0.04	0.268	24	9.8
		0.85	0.278	19	10.5
		11.1	0.303	22	12.1
		111	0.264	35	10.6
		1110	0.806	94	14.4

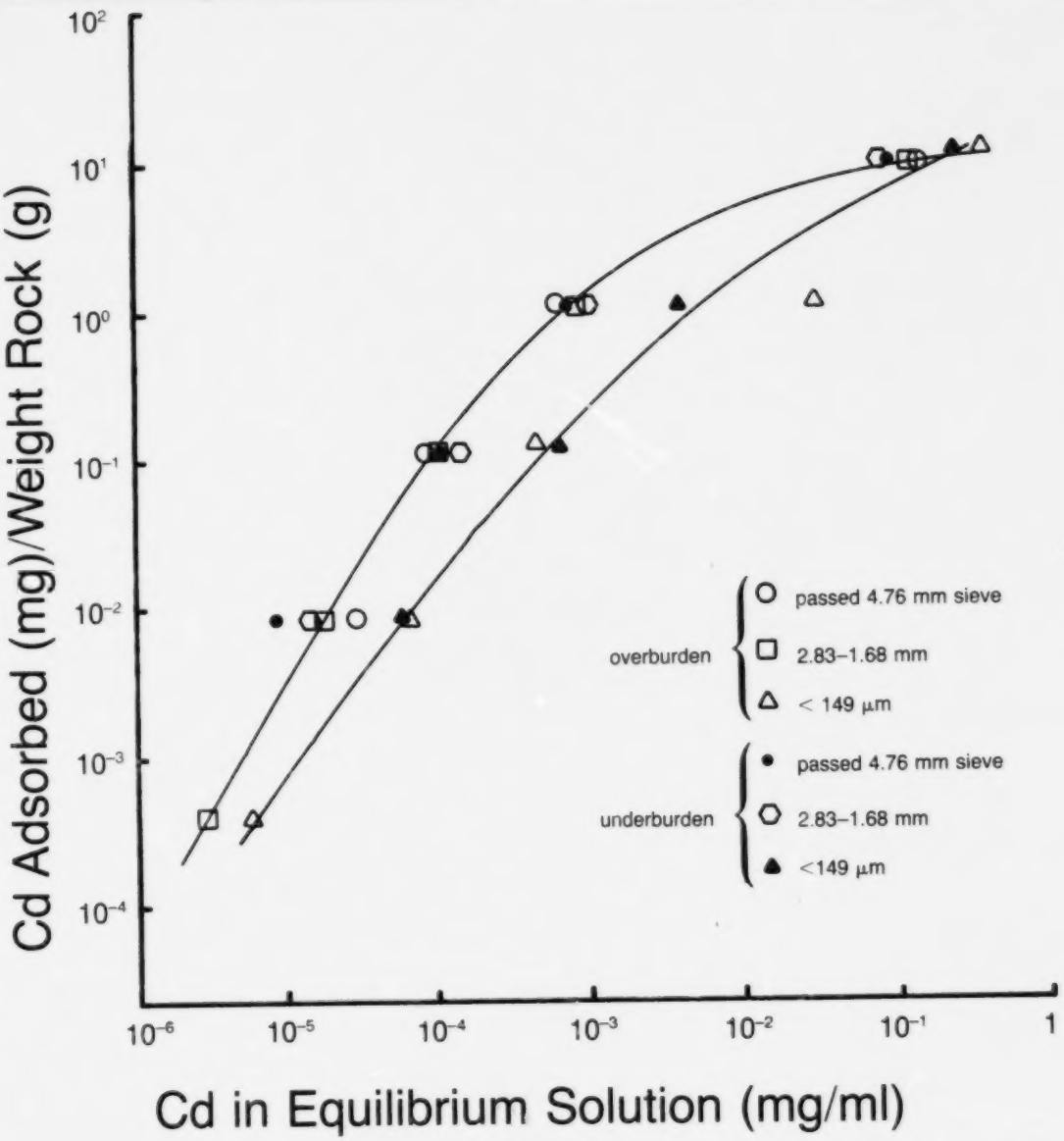

Figure 10. The amount of Cd^{+2} adsorbed per gram of rock as a function of the concentration of Cd^{+2} remaining in solution.

cadmium ion exchange capacity of 16-20 meq/100 g rock. This value is in reasonable agreement with that obtained by the conventional ion exchange method.

An alternative treatment of the data is the isotherm approach. In Figure 11 the quantity of Cd^{+2} adsorbed per gram of rock is plotted as a function of the initial concentration of Cd^{+2}. This plot is linear on a log-log scale. Behavior of this sort is known as a Freundlich isotherm; it is commonly observed for adsorption of solutes on a solid phase. The Freundlich isotherm is an empirical relationship, so the slope and intercept cannot be ascribed any particular physical significance, though this behavior is generally regarded as indicative of a heterogeneous surface. The slope and intercept are frequently associated with the adsorption capacity and adsorption strength of the system. It is interesting that the results for both Kirtland shale and Pictured Cliffs sandstone lie on the same line; this may merely indicate that the Freundlich isotherm is not a very sensitive way to display adsorption data.

The effect of particle size on adsorption is shown in Table 10 and Figures 8 and 9. The K_d's for the smallest size range studied were smaller than the K_d's for the other size ranges.

A plot of K_d (Mg^{+2}) vs. pH is shown in Figure 12. Under this set of conditions K_d increases sharply with increasing pH. This increase occurs in the vicinity of a pK value in the carbonate ion equilibrium scheme, so it is likely that the decrease in Mg^{+2} in solution is related to the reaction

$$Mg^{+2} + CO_3^{=} \rightarrow MgCO_3$$

in which $MgCO_3$ is only slightly soluble.

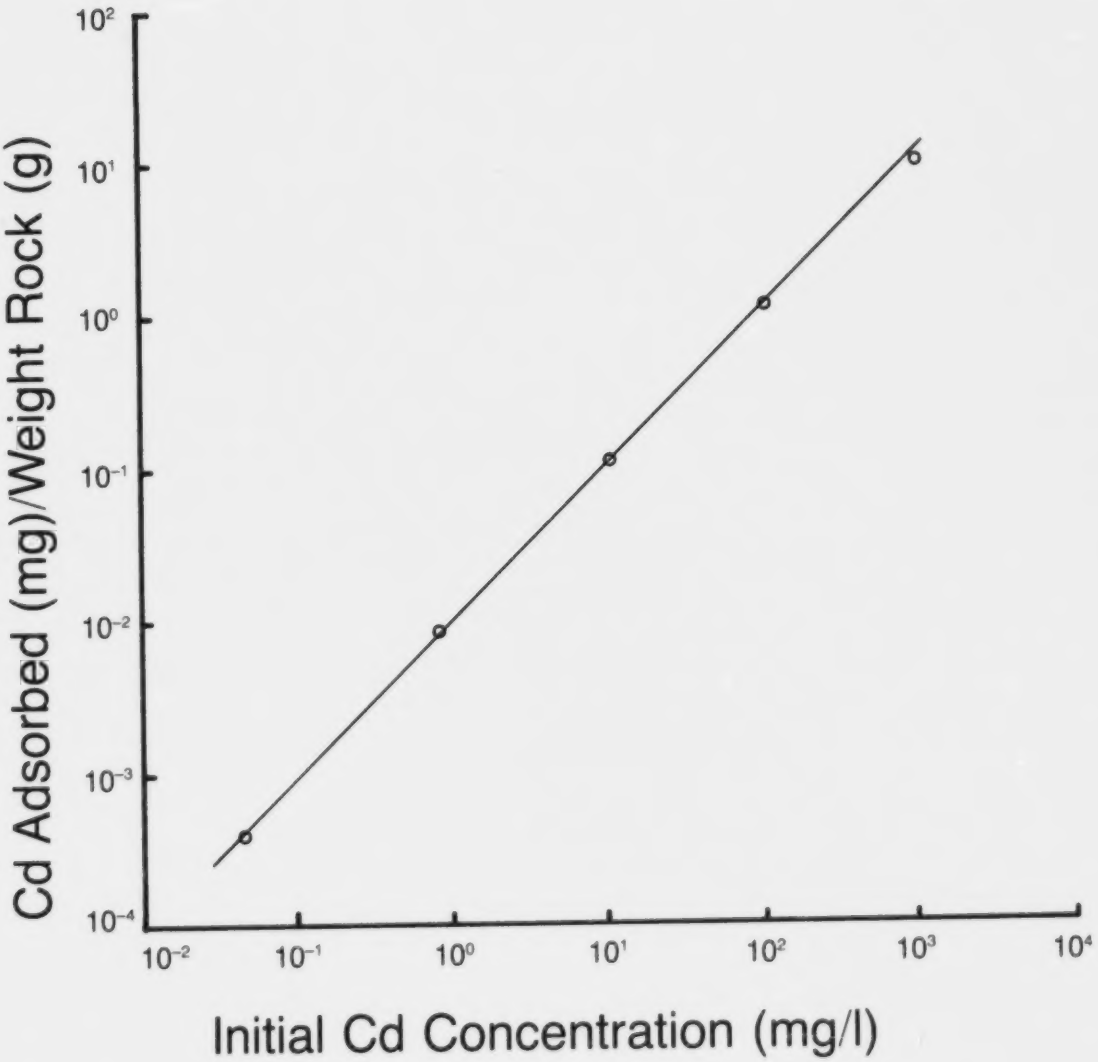

Figure 11. The amount of Cd^{+2} adsorbed per gram of rock as a function of initial concentration (all particle sizes, for both underburden and overburden, lie very close together. Thus each represents 6 points).

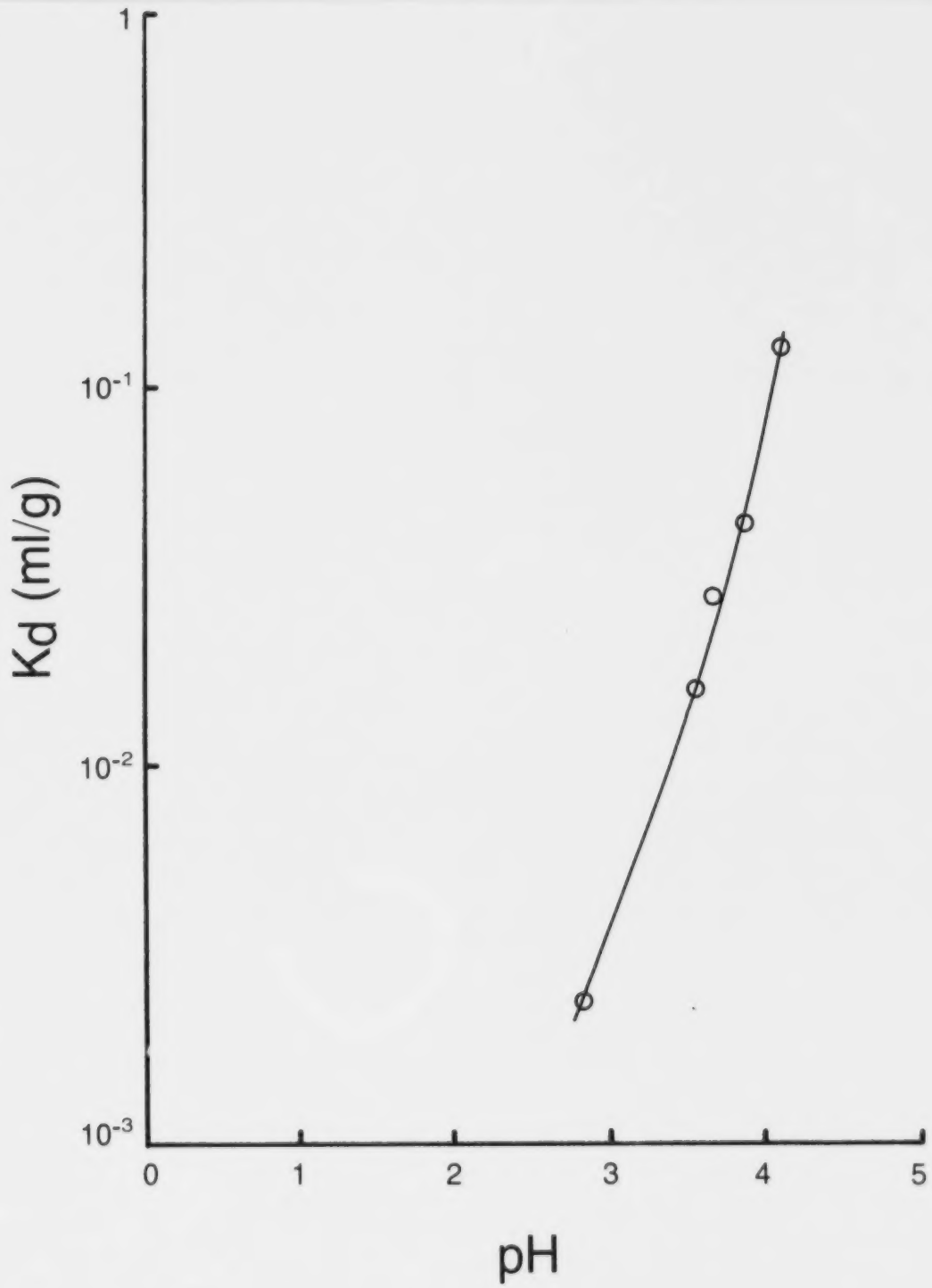

Figure 12. K_d for Mg^{+2} on Kirtland shale as a function of pH.

SECTION 7

SORPTION STUDIES ON COAL

SORPTION CAPACITIES

Sorption refers to the removal of chemical species from a liquid or gas phase onto a solid phase without specifying a mechanism. Sorption may be a physical process, a chemical process or an intermediate combination of both phenomena (17). Soils, clays, and coals all possess sorptive properties and both the organic matter (18) and the inorganic matter in coal, especially the clay minerals (19), are responsible for sorption. Trace elements are adsorbed onto coal and mineral matter primarily by means of ion-exchange, but this process is often accompanied by simple adsorption or desorption. Wang (20) suggests that metathesis is another sorption mechanism; it is however indistinguishable from ion exchange, though he maintains that when one ion is exchanged for another and the K_d values differ by two or more orders of magnitude the proper term to use in describing the phenomenon is metathesis. In addition to displacing the hydrogen of exposed hydroxyls, Grim (21) claims that cationic species are adsorbed on the edges of silica-alumina clay-mineral structural units, where broken bonds lead to unsatisfied charges, and on the basal plane surfaces, where lattice substitution can occur. Analogously, anionic species may replace hydroxyl groups or be adsorbed onto particle edges as a result of geometrical considerations, or on basal plane surfaces as a consequence of unbalanced charges within the lattice.

In an effort to determine the extent to which the mineral matter of Fruitland Formation coal contributes to sorption, an adsorption capacity experiment was conducted. The experiment was designed in such a way as to distinguish between ion-exchange and simple sorption.

Preparation of Demineralized Coal

Coal was cleaned or demineralized by digestion in a series of acids following the procedure of Garten and Weiss (22). Approximately 1 kg of pulverized Fruitland Formation coal was boiled for 6 hr with 6 N hydrochloric acid, cooled and filtered. The residue was boiled again with 6 N hydrochloric acid, cooled and filtered. The solid was then digested with 45% hydrofluoric acid by heating on a steam bath for three hours. This was followed by digestion with 12 N hydrochloric acid on the steam bath for three hours. The hydrofluoric acid-hydrochloric acid treatments were repeated twice after which the final acids were removed by evaporation to dryness. This also removes silicon as SiF_4. The remaining solid was boiled with 6 N hydrochloric acid, filtered and boiled again with 3 N hydrochloric acid. It was then washed several times with distilled water and placed in a

Soxhlet extractor where it was washed with 0.1 N acetic acid for 4 days. The extraction liquid was then changed to distilled water and extraction was continued for 2 days. The cleaned or acid-washed coal was dried in an oven for 8 hours at 90°C. Coal prepared by this method typically contained 0.5% ash.

Sorption Capacity Determination

The exchangeable ion sites on coal were loaded with Na^+ by adding coal, either raw or acid-washed, to a 1 N NaCl solution, allowing it to stand for 3 days, filtering the solution and repeating the process. Sorption capacities were determined by equilibrating the sodium-loaded coals with a solution of 1 N ferrous ammonium sulfate.

Ferrous ion was chosen as the adsorbate as being typical of the anticipated trace metal pollutants with respect to both charge and size. Furthermore, large quantities of iron are expected to be released into the groundwater following UCG. To ensure equilibrium, samples were agitated twice daily for a period of five days after which they were gravity filtered.

Following filtration the solutions were analyzed for Fe^{+2} and Na^+ content by atomic absorption flame spectroscopy. The solutions were also analyzed for the presence of Ca^{+2} that may have been displaced by Fe^{+2}. Appreciable amounts of aluminum are present in Fruitland coal and, even though Na^+-loading solutions were concentrated, a significant number of aluminum ions may not have been replaced. Because of the high retention of Al^{+3} by coal (23,24) the slight amounts displaced by Fe^{+2} are likely to have escaped detection by atomic absorption spectroscopy. Silicon present in Fruitland coal in appreciable quantities as silica or silicates, is at the center of a tetrahedral array of oxygen atoms. While trivalent Al^{+3} may be substituted for Si^{+4} to a very limited degree (19), incorporation of monovalent Na^+ or divalent Fe^{+2} into this lattice is highly unlikely, so the silica tetrahedra were assumed to be unaffected throughout the experiment.

After blank correction for leachable Na^+, ion-exchange and sorption capacities were calculated for both raw and acid-washed coal. The total amount of Na^+ and Ca^{+2} released into solution was interpreted as the ion-exchange capacity of the coal, while the total sorptive capacity was taken to be the amount of Fe^{+2} adsorbed by the coal, calculated by subtracting the final iron concentration from the initial concentration. The difference between total sorption and sorption due to ion-exchange is simply called adsorption. Data from this experiment, based on replicate analyses, are presented in Table 12.

The data of Table 12 show that inorganic matter accounts for approximately 95% of the sorptive capacity of Fruitland Formation coal while the carbonaceous material of coal itself contributes only about 5% to the adsorption of trace metals. It can also be seen that from one-third (for acid-washed coal) to perhaps as high as one-half (for raw coal) of the sorptive capacity of Fruitland coal may be directly attributed to ion-exchange. This should be regarded with some caution, however, in light of the warning by Grim (19) that "the determination of cation-exchange capacity is at best a

TABLE 12. SORPTION CAPACITIES OF RAW AND ACID-WASHED FRUITLAND COAL

	Raw Coal	Acid-Washed Coal
Total Sorption Capacity	155±15 meq Fe^{+2}/kg	8.1±0.8 meq Fe^{+2}/kg
Ion-Exchange Capacity*	55±5 meq Na^{+}/kg	2.2±0.2 meq Na^{+}/kg
	10±1 meq Ca^{+2}/kg	0.5±0.1 meq Ca^{+2}/kg
	65±4 meq/kg	2.7±0.2 meq/kg
Adsorption Capacity (by diff.)	90±11 meq Fe^{+2}/kg	5.4±0.6 meq Fe^{+2}/kg

*Small amounts of trace elements, such as K^{+} or Mg^{+2}, not replaced by Na^{+} may have been displaced by Fe^{+2}. Therefore, reported ion-exchange capacities are considered to be minimum values.

more or less arbitrary matter and no high degree of accuracy can be claimed". It is known that different experimental methods yield widely different values for exchange capacities, so the figures reported in Table 12 must be considered accordingly, that is, they should be compared directly only with sorption capacities determined by Fe^{+2} sorption

DISTRIBUTION COEFFICIENTS

Although certain sorbed ions may become nonexchangeable, as in the case of potassium fixation by illite (19), the sorption process is for the most part an equilibrium one. Therefore, natural adsorbents like coal tend only to retard the movement of pollutants rather than remove them permanently from solution. Because adsorption is an equilibrium process the distribution coefficient, K_d, the ratio of the concentration of the ion in the solid phase to the concentration in the liquid phase, is a very useful parameter. It is inversely proportional to the pollutant transport rate and directly proportional to both the exchange capacity and selectivity of the exchanger (25).

The extent to which an ion replaces or is replaced by other ions varies greatly with the nature of the ion, particularly the charge and size of the ion compared to the site it must occupy. The resulting affinity for adsorption is called the replaceability of the ion and the adsorbent is said to exhibit a certain affinity for that ion. Preference in sorption is an important phenomenon since an adsorbent which possesses a high affinity for certain contaminants may retard these ions even though the exchange capacity may be small.

Distribution coefficients are dependent upon the specific experimental conditions for which the values are obtained. Some of the factors which influence them include the composition of the liquid phase, the chemical nature and particle size of the solid phase, temperature and pH. Since a change in any of these variables may cause K_d values to vary considerably, Borg suggests that distribution coefficients be determined under conditions which simulate actual situations or are at least close enough to allow for extrapolation to field conditions (25).

In an effort to approximate actual field conditions, it was decided that the K_d of an ion be determined in the presence of all other ions selected for study, that the background ionic strength be adjusted to a constant value with the predominant cationic and anionic constituents of the local groundwater, and that realistic concentration ranges be employed. When estimating the distribution coefficient of an ion in the presence of competing ions it is assumed that the ion is in simultaneous equilibrium with all other chemical species for the available sites. These include the ions used as ionic strength adjusters and the remaining elements of environmental concern. We take the number of sorption sites to be fixed so each of these equilibria may be described by a simple mass action equation. This approach is substantiated by Kaufman's finding that K_d is inversely proportional to the concentration of competing ions (26).

It would be desirable to adjust the solution pH to a value comparable to that found for San Juan Basin groundwater (Section 4). Acidities much different from this may cause complications. For example, lowering the acidity may cause some cations to hydrolyze, while raising the acidity may cause certain anions to hydrolyze, thus changing the nature of the chemical equilibria under observation. Also, carbonate minerals will decompose in solutions of low pH. San Juan Basin groundwater is quite alkaline (Section 4), and dissolution of metal oxides in the UCG ash may be expected to raise the groundwater pH above the original baseline value of 9.4. Some qualitative experiments with solutions adjusted to pH 10 with NaOH confirmed the expectation that Fe^{+3}, Al^{+3}, Cr^{+3}, Zn^{+2}, and Mn^{+2} formed insoluble hydroxides so that very low concentrations of these metal ions remained in solution. The concentrations were much lower than found in the actual groundwater samples. A possible explanation for the difference is the formation of soluble chelates of the metal ions.

Humic substances are ubiquitous constituents of soil, peat, coal, and natural water. Humic material includes humic acid, that fraction of soil organic matter soluble in dilute base but insoluble in mineral acid and alcohol, and the similar but simpler fulvic acids, soluble in dilute base and mineral acid (27). Although there exists no simple, unique structure for these macromolecules, it is believed that the humic acid core is partially aromatic in nature with structural elements derived from lignin, phenols and resorcinol phenols of woody plants (28). The principal functional groups present in humic acid are phenolic and alcoholic hydroxyl, carboxyl, carbonyl and quinoid moieties. The carboxyl and phenolic groups are most responsible for the large cation exchange capacity (4000-6000 meq/kg as measured by $Ca(OAc)_2$) and for the metal complexing ability of humic materials (28,29). Humic substances also possess amino groups, which may or may not contribute to chelation but are important in exchange reactions (28).

Humic substances are the main constituents of river water organic matter (30), and apparent excesses of nickel, copper, zinc, cobalt, aluminum, iron and manganese in natural waters have at times been attributed to the formation of stable metal-organic matter complexes(28,31,32). Because humic material exerts such a strong influence on the distribution of aqueous metal ions via chemical complexation, it was decided that all distribution coefficients be determined in the presence and absence of humic acid.

Selection of Experimental Conditions

The local groundwater movement in the San Juan Basin is known to be very low, approximately 1-2 feet per year. Because of this low flow rate the experiments reported here are based on the assumption that equilibrium will be established between the ions in solution and the coal surfaces. Consequently, all distribution coefficients reported here were determined by the standard batch, or static method. In the batch method a known amount of contaminant solution is added to a measured quantity of solid material and the mixture is agitated until equilibrium is reached. The distribution between the solid and liquid phase is then calculated by comparing the initial pollutant concentration with the final concentration (25).

As discussed above, a number of metal ions are present in San Juan Basin groundwater at considerably higher concentrations than would be expected from the tabulated solubility products of the corresponding metal hyroxides at pH values between 9 to 10. This is a well-known phenomenon in ground- and surface-water problems and it is attributed to chelation by any number of multidentate ligands that may be found in natural water systems. The problem and its complexities have been reviewed by Stumm and Morgan (33). For example, the concentration of Fe^{+3} in solution in the presence of excess of the hexadentate ligand EDTA at pH 9 is about 4 orders of magnitude greater than the concentration of Fe^{+3} above $Fe(OH)_3$ at the same pH. There are many organics in the groundwater that pass through the Fruitland Formation coal seam, but their nature is unknown. Some of them are undoubtedly the natural chelating agents of humic and fulvic acid, but others are equally likely. The result is that an adequate reconstruction or synthesis of groundwater with the properties that would be required is very difficult. Since a complete description of the groundwater is unavailable, we decided that artificial construction of simulated groundwater with sufficient EDTA to support a concentration of Fe^{+3} of up to 2 mg ℓ^{-1} at pH 10 would be completely unrealistic. Noncomplexing buffers such as cis-2,6-dimethylpiperdine (34) were tried, but, as expected, did not stabilize Fe^{+3} or Al^{+3} solutions at high pH. Consequently the results reported below were all obtained with distilled-deionized water with no pH adjustment; this results in K_d values at attained equilibrium with pH's lying between 6 and 7.

Distribution coefficients for all cations were determined with the background ionic strength adjusted to a constant value with Na^+, Ca^{+2}, K^+, and Mg^{+2}, the principal cations released as a result of UCG. Chloride ions were employed to represent the anionic constituents of the natural water.

Distribution coefficients for the anions were determined with the ionic strength adjusted to a constant value with chloride and sulfate ions. The question of an appropriate cationic matrix must be addressed. Calcium ions may not be used due to precipitation of $CaSO_4$, and Na^+ strongly interferes with the atomic absorption analysis for selenium. (Since Na^+ also interferes with the AA analysis of Be, adsorption coefficients for this element were determined with the anionic samples rather than with the other cations.) For these reasons, it was decided that K^+ would best represent the cationic species in the water, therefore potassium salts were used to prepare the solutions for the anionic K_d determinations. Details of the adjustment of sample ionic strength are summarized in Table 13.

Optimum values for other conditions important to the sorption process, also determined as a result of preliminary adsorption experiments, are listed in Table 14. The particle size of the coal samples corresponds to the standard size suggested for such determination, that is, coal which passes a 0.25-1.40 mm sieve (35). The concentration of humic acid (Aldrich -- Na^+ salt, technical grade) chosen for this study is representative of the humic content of natural waters (36). These experimental conditions were used for the determination of all distribution coefficients.

TABLE 13. BACKGROUND IONIC STRENGTH OF SORPTION EXPERIMENT SAMPLES

Experiment Set	Ionic Strength Adjuster	Salt Used	Ion Concentration (mg/ℓ)
Cations	Na^{+}	NaCl	1000
	Mg^{+2}	$MgCl_2 \cdot 6H_2O$	100
	K^{+}	KCl	100
	Ca^{+2}	$CaCl_2 \cdot 2H_2O$	500
Anions	Cl^{-}	KCl	2000
	SO_4^{-2}	K_2SO_4	1000

TABLE 14. EXPERIMENTAL VALUES OF SORPTION VARIABLES

Variable	Value	Variable	Value
Weight of coal	50.0 g	pH	Unadjusted
Particle size	0.25-1.40 mm (no. 60 sieve)	temperature	Room temp
Sample volume	200 ml	equilibration time	5 days
Humic acid concn	5.00 mg/ℓ	agitation	2x daily

Experimental Procedure

Since K_d is a function of ion concentration, distribution coefficients were determined over a wide range of concentrations. With respect to the cations of environmental concern, the amount of a particular trace metal expected to be present in the groundwater following UCG was estimated and an appropriate concentration range bracketing this point was selected.

Coal samples of approximately 50 g were first weighed into clean 250 ml Nalgene polyethylene screw-cap bottles. Solutions were prepared by

dissolving chloride salts of the metal ions of interest (Fe^{+2}, Al^{+3}, Mn^{+2}, Zn^{+2}, Hg^{+2}, Cr^{+3}, Co^{+2}, Ni^{+2}, Cu^{+2}, and Pb^{+2}) in doubly distilled deionized water. To determine K_d for a particular metal ion, solutions were prepared in which the concentration of that ion was varied while the concentrations of all other ions were held fixed. Samples were prepared from these stock solutions by adding to a coal sample 100 ml of the stock solutions, the necessary amount of ionic strength adjuster, 50 ml of either distilled water or humic acid solution, and finally enough distilled water to give a final volume of 200 ml. A summary of the salts used and their initial concentrations is given in Table 15. The samples were sealed inside the plastic bottles and allowed to stand at room temperature (22±2°C) with regular agitation for 5 days (see Table 14). Following equilibration, solutions were gravity filtered using Whatman #2 filter paper and analyzed by flame atomic absorption spectroscopy on a Varian AA-6 atomic absorption spectrophotometer using the standard methods described in Section 4. Solution blanks containing no coal were used to obtain the initial concentrations of the trace elements while blanks containing no metal ions were used to correct for any trace elements which might be leached from the coal or exchanged by the humic acid.

A similar experiment was performed using solutions with selected anions and Be^{+2} in varying concentrations. The compounds used and the concentration ranges employed are given in Table 16. The potential chelating agent humic acid was also used in these studies.

Results and Discussion

The distribution between the solid and liquid phase for each of these elements and the derived distribution coefficients are collected in Tables 17 and 18. Adsorption isotherms may be deduced from these data; the isotherms are shown in Figures 13-27.

Low concentration studies with mercury, cobalt, nickel, copper and lead were not possible by flame AAS due to the fact that the concentrations were at or below the detection limit of the method. Furnace methods are unreliable because of the unknown interferences arising from the complex matrix these samples present. Consequently K_d values are reported only at higher concentrations for these elements. As with the cations, the amount of anionic contaminant expected to be present in the groundwater following gasification was estimated and an appropriate concentration range was chosen. Actual postburn values of Be, cyanide and fluoride ions are expected to lie within the realistic concentration ranges selected for these elements. However, the distribution coefficients of selenite, molybdate, and arsenate ions were determined at higher concentrations due to the low sensitivity and high detection limits of atomic absorption spectroscopy for Se, Mo, and As. Since the K_d for cyanide was found to be infinite and the K_d for arsenate determined to be approximately zero over all concentrations studied, no sorption isotherms are presented for these ions.

Since previous research involving the adsorption of trace elements by coal is extremely limited, few sorption plots of this nature are available for comparison with the results of this study. Nandi and Walker have found that

TABLE 15. INITIAL CATION CONCENTRATION RANGES

Trace Element	Salt Used	Init. Conc. Range (mg/ℓ)
Fe	$FeCl_2 \cdot 4H_2O$	1-100
Al	$AlCl_3 \cdot 6H_2O$	0.2-160
Mn	$MnCl_2 \cdot 4H_2O$	0.2-20
Zn	$ZnCl_2$	0.2-20
Hg	$HgCl_2$	12-100
Cr	$CrCl_3 \cdot 6H_2O$	0.2-16
Co	$CoCl_2 \cdot 6H_2O$	2-16
Ni	$NiCl_2 \cdot 6H_2O$	1.6-14
Cu	$CuCl_2 \cdot 2H_2O$	2-16
Cd	$CdCl_2 \cdot 2.5H_2O$	0.03-0.50
Pb	$PbCl_2$	5-40

TABLE 16. INITIAL ANION AND Be^{+2} CONCENTRATION RANGES

Ion	Salt Used	Init. Conc. Range (mg/ℓ)
Be	$BeSO_4$	1-8
CN^-	KCN	1-12
F	$KF \cdot 2H_2O$	20-160
Se	H_2SeO_3	17-176
Mo	$(NH_4)_6Mo_7O_{24} \cdot 4H_2O$	21-182
As	K_3AsO_4	21-164

TABLE 17. THE ADSORPTION OF SELECTED CATIONS ON FRUITLAND FORMATION COAL

Trace Element	No Humic Acid				Humic Acid, 5 ppm			
	C_o (mg/ℓ)	Amt in Soln (mg/ℓ)	Amt Ads (mg/kg)	K_d	C_o (mg/ℓ)	Amt in Soln (mg/ℓ)	Amt Ads (mg/kg)	K_d
Mn	0.186	0.093	0.372	4.0±0.22	0.187	0.093	0.376	4.0±0.22
	0.963	0.560	1.61	2.9±0.22	0.963	0.590	1.49	2.5±0.22
	5.00	2.24	11.04	4.9±0.22	5.03	2.24	11.2	5.0±0.22
	21.1	11.4	38.8	3.4±0.22	21.4	12.0	37.6	3.1±0.22
Fe	1.08	0.015	4.26	280±23	1.18	0.015	4.66	310±23
	5.72	0.080	22.6	280±23	5.67	0.080	22.4	280±23
	27.3	0.520	107	210±23	26.3	0.520	103	200±23
	103	3.68	397	110±23	106	5.67	401	70±23
Zn	0.210	<0.02[a]	0.840	∞	0.210	<0.02[a]	0.840	∞
	1.07	<0.02[a]	4.28	∞	1.07	<0.02[a]	4.28	∞
	4.74	0.305	17.7	58±3.7	4.75	0.282	17.9	63±3.7
	20.6	4.36	65.0	15±3.7	20.8	4.48	65.3	15±3.7
Cd	0.032	$<7\times10^{-4}$[a]	0.128	∞	0.032	$<7\times10^{-4}$[a]	0.128	∞
	0.063	0.006	0.228	38±3	0.063	0.019	0.176	9±3
	0.123	0.045	0.312	7±3	0.123	0.071	0.208	3±3
	0.490	0.134	1.42	11±3	0.490	0.142	1.39	10±3

a) The symbol < indicates the concentrations were below the given detection limit. (Continued)

TABLE 17. (Continued)

Trace Element	No Humic Acid				Humic Acid, 5 ppm			
	C_o (mg/ℓ)	Amt in Soln (mg/ℓ)	Amt Ads (mg/kg)	K_d	C_o (mg/ℓ)	Amt in Soln (mg/ℓ)	Amt Ads (mg/kg)	K_d
Al	20.2	<0.04	80.8	∞	20.2	<0.04	80.8	∞
	39.3	<0.04	157	∞	39.3	<0.04	157	∞
	75.3	5.48	279	51±3	69.3	4.85	258	53±3
	154	34.6	479	14±3	153	28.6	498	17±3
Cr	2.52	0.127	9.57	75±4.4	2.36	0.127	8.83	70±5.5
	4.48	0.339	16.6	49±4.4	4.42	0.324	16.4	50±4.4
	9.10	0.981	32.5	33±4.4	4.94	0.876	32.3	37±4.4
	17.35	3.88	53.9	14±4.4	17.6	2.93	58.7	20±4.4
Co	2.16	0.363	7.19	20±5.9	2.08	0.248	7.33	30±5.9
	4.21	1.00	12.8	13±5.9	4.22	0.722	14.0	19±5.9
	8.15	3.16	20.8	6.3±0.37	8.10	2.93	20.7	7.1±0.37
	16.45	9.75	26.8	2.8±0.48	16.9	8.77	32.5	3.7±0.48
Ni	1.60	0.247	5.41	22±5.8	1.50	0.101	5.60	55±5.8
	3.10	0.902	8.79	10±3.9	3.06	0.611	9.80	16±3.9
	6.36	2.83	14.1	5.0±0.96	6.40	2.58	15.3	5.9±0.96
	13.6	8.26	21.4	2.6±0.89	13.8	7.47	25.3	3.4±0.89

(Continued)

TABLE 17. (Continued)

Trace Element	No Humic Acid				Humic Acid, 5 ppm			
	C_o (mg/ℓ)	Amt in Soln (mg/ℓ)	Amt Ads (mg/kg)	K_d	C_o (mg/ℓ)	Amt in Soln (mg/ℓ)	Amt Ads (mg/kg)	K_d
Cu	2.02	<0.003	4.08	∞	2.03	<0.003	8.12	∞
	4.08	0.071	16.0	230±17	4.11	0.084	16.1	190±17
	8.12	0.179	31.8	120±11	8.03	0.178	31.4	180±11
	16.5	1.08	61.7	60±11	16.6	0.908	62.8	70±11
Hg	11.7	<0.2	46.8	∞	11.4	<0.2	45.6	∞
	23.5	0.60	91.6	153±4.3	23.1	0.6	90.0	150±4.3
	49.4	2.60	187	72±4.3	48.9	2.4	186	78±4.3
	97.7	13.3	338	25±4.3	95.8	11.5	337	29±4.3
Pb	6.85	1.98	19.5	10±2.4	6.85	1.75	20.4	12±2.4
	11.9	2.43	37.9	16±2.4	11.9	2.21	38.8	18±2.4
	21.6	2.87	74.9	26±2.4	21.8	2.87	75.7	26±2.4
	40.8	3.76	148	39±2.4	41.4	4.19	149	36±2.4
Be	0.64	<0.002	2.46	∞	0.64	<0.002	2.56	∞
	1.12	0.14	3.92	28±2.5	1.18	0.17	4.04	24±2.5
	2.31	0.81	6.00	7.4±0.4	2.38	0.78	6.40	8.2±0.4
	4.31	2.33	7.92	3.4±0.1	4.18	2.30	7.52	3.3±0.1

TABLE 18. THE ADSORPTION OF SELECTED ANIONS ON FRUITLAND FORMATION COAL

Trace Element	No Humic Acid				Humic Acid, 5 ppm			
	C_o (mg/ℓ)	Amt in Soln (mg/ℓ)	Amt Ads (mg/kg)	K_d	C_o (mg/ℓ)	Amt in Soln (mg/ℓ)	Amt Ads (mg/kg)	K_d
CN^-	1.25	<0.03[a]	4.96	>1500	1.20	<0.03[a]	4.80	>1500
	2.58	<0.03[a]	10.3	>1500	2.48	<0.03[a]	9.92	>1500
	5.63	<0.03[a]	22.5	>1500	5.25	<0.03[a]	21.0	>1500
	11.2	<0.03[a]	44.8	>1500	10.7	<0.03[a]	42.8	>1500
F	48.4	24.0	97.6	4.1±0.23	47.6	22.6	100	4.4±0.23
	75.4	41.0	138	3.4±0.23	74.6	41.0	134	3.3±0.23
	121	67.0	216	3.2±0.23	120	68.0	208	3.1±0.23
	203	90.0	452	5.0±0.23	202	92.0	440	4.8±0.23
Se	16.9	12.8	12.8	0.93±0.02	16.9	13.7	12.8	0.93±0.02
	42.1	38.0	16.4	0.43±0.02	42.5	38.4	16.4	0.43±0.02
	77.2	72.8	17.6	0.24±0.02	76.4	71.7	19.2	0.27±0.02
	176	155	84.0	0.52±0.02	172	151	84.0	0.56±0.02
Mo	21.4	16.4	20.0	1.2±0.60	22.0	18.4	14.4	0.78±0.06
	44.3	29.5	59.2	2.0±0.60	43.6	33.9	38.8	1.1±0.60
	95.4	51.4	176	3.4±0.60	90.6	52.9	151	2.8±0.60
	182	145	150	1.0±0.60	180	149	125	0.8±0.60

(Continued)

TABLE 18. (Continued)

Trace Element	No Humic Acid				Humic Acid, 5 ppm			
	C_o (mg/ℓ)	Amt in Soln (mg/ℓ)	Amt Ads (mg/kg)	K_d	C_o (mg/ℓ)	Amt in Sol (mg/ℓ)	Amt Ads (mg/kg)	K_d
As	21	19	≃0	≃0	21	21	≃0	≃0
	45	46	≃0	≃0	45	48	≃0	≃0
	86	86	≃0	≃0	91	88	≃0	≃0
	164	164	≃0	≃0	163	160	≃0	≃0

a) Below the detection limit.

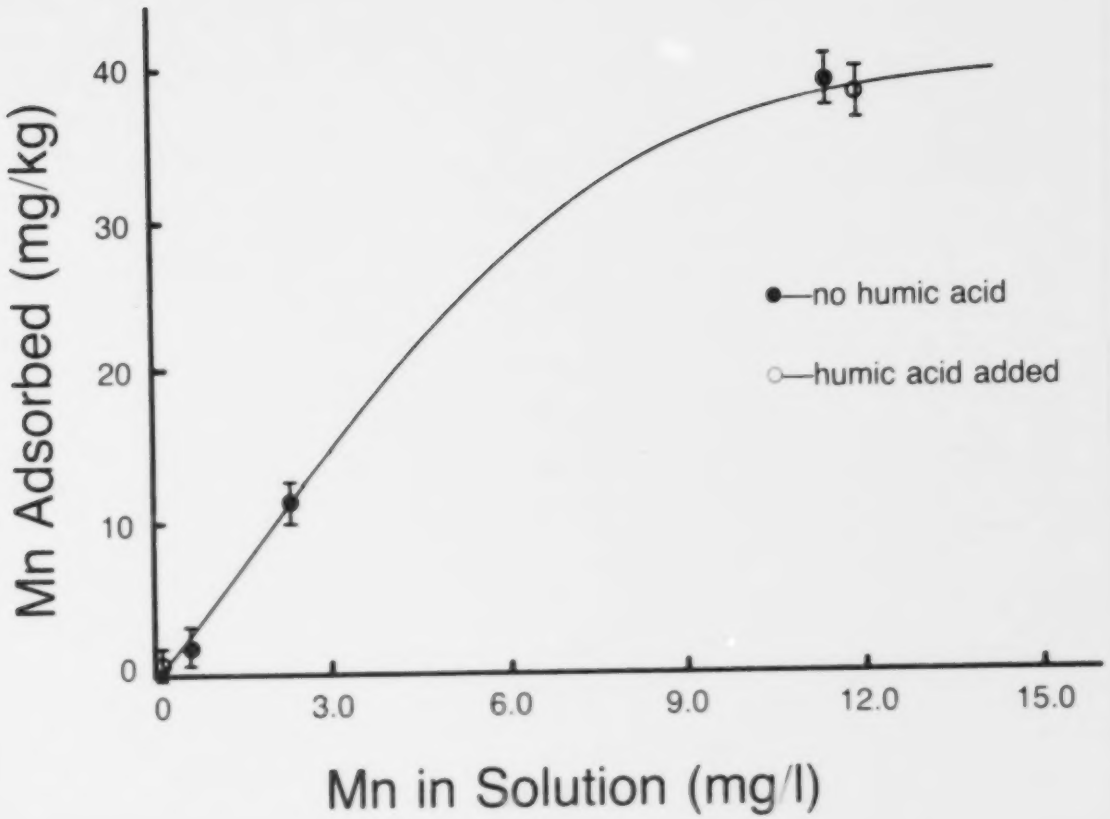

Figure 13. Sorption isotherm of manganese.

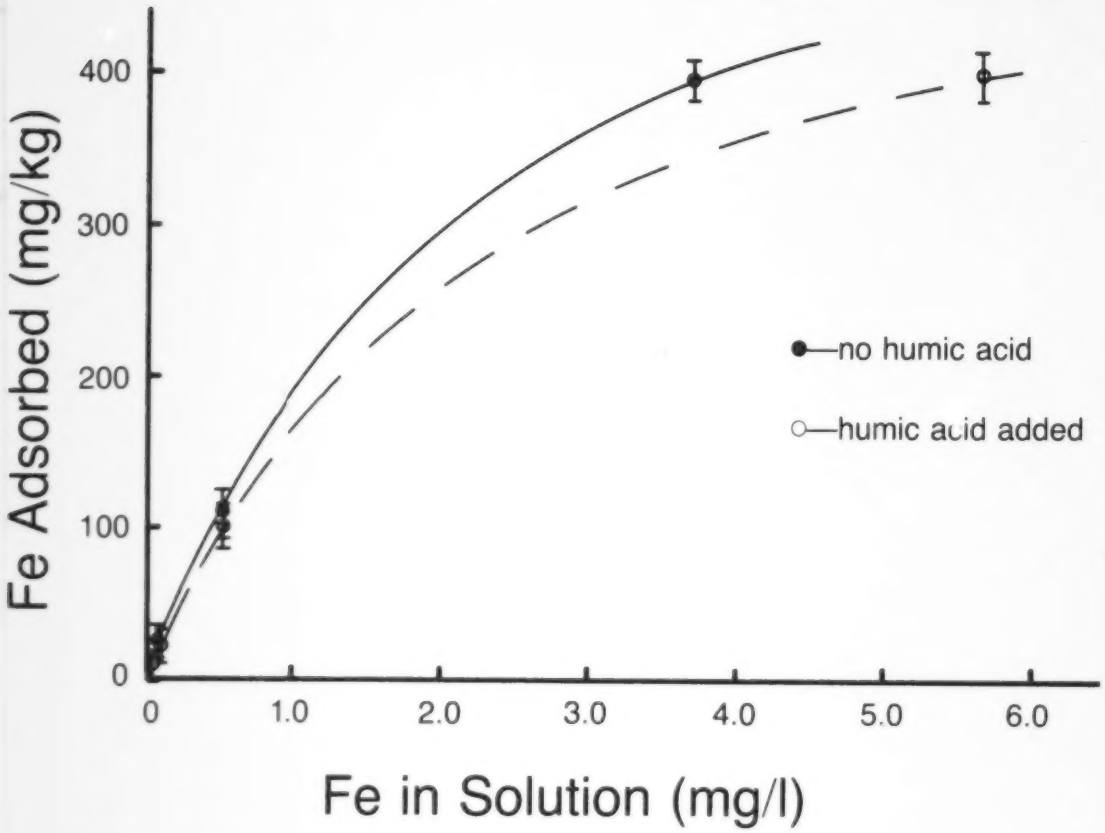

Figure 14. Sorption isotherm of iron.

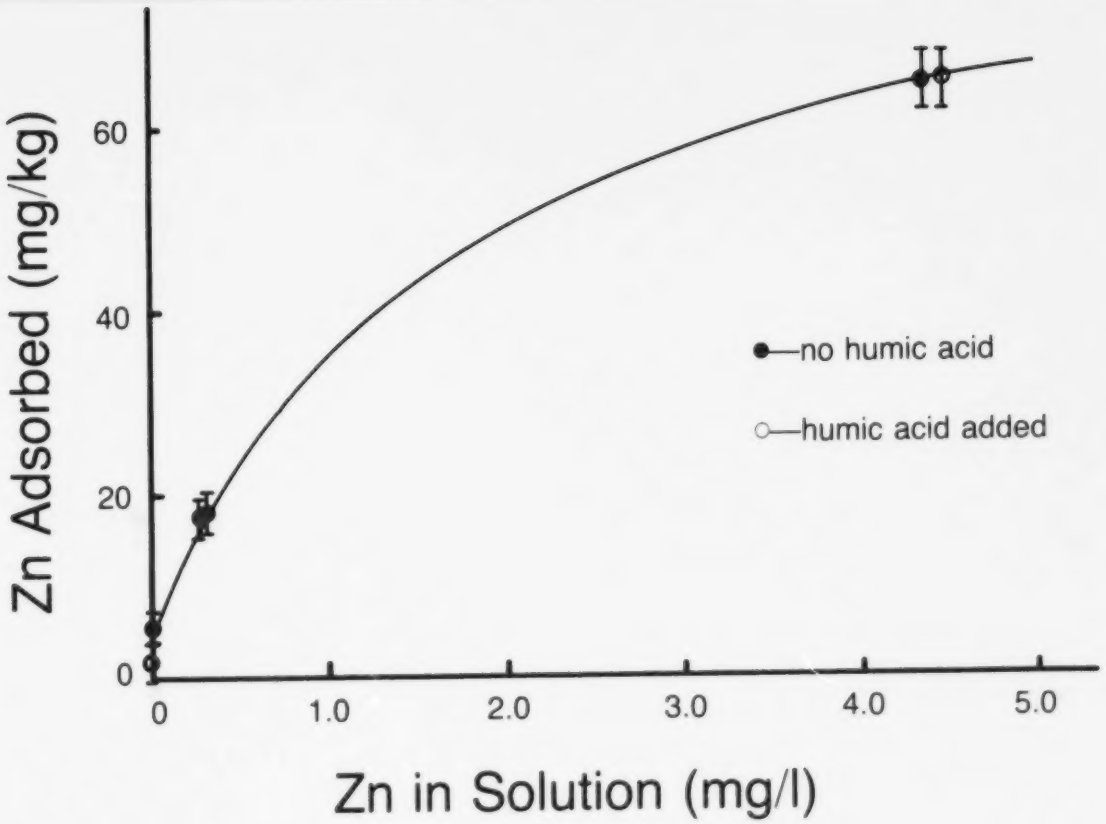

Figure 15. Sorption isotherm of zinc.

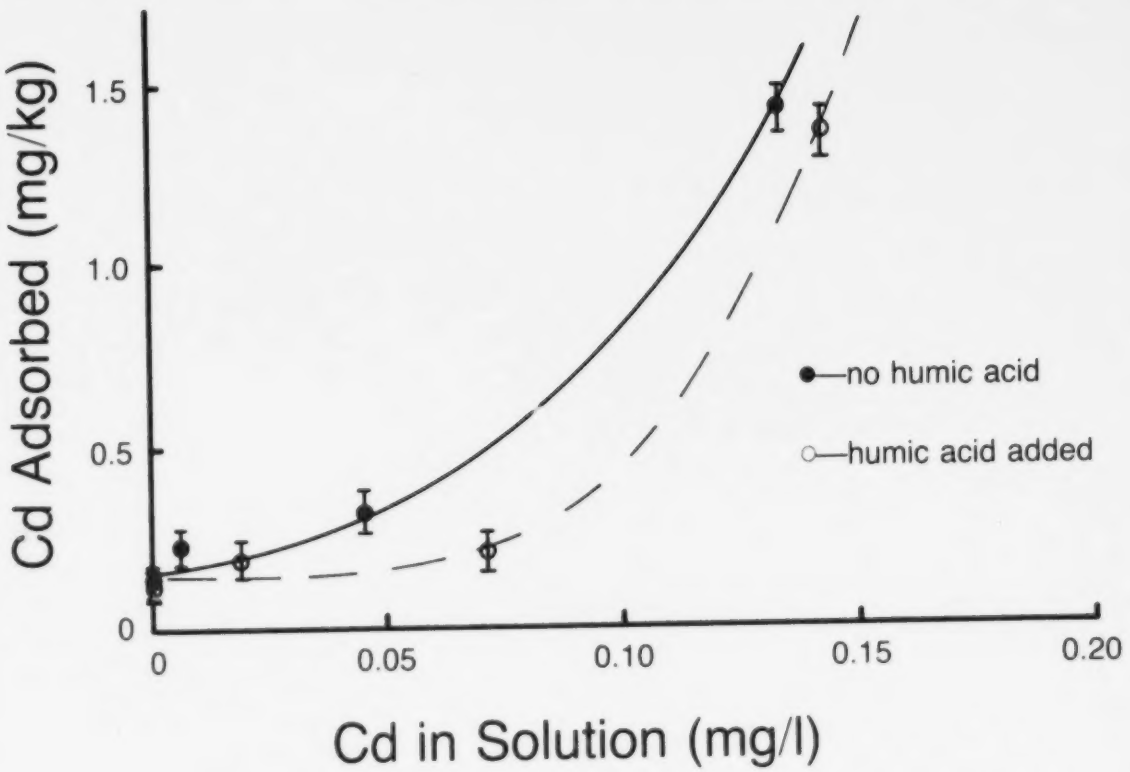

Figure 16. Sorption isotherm of cadmium.

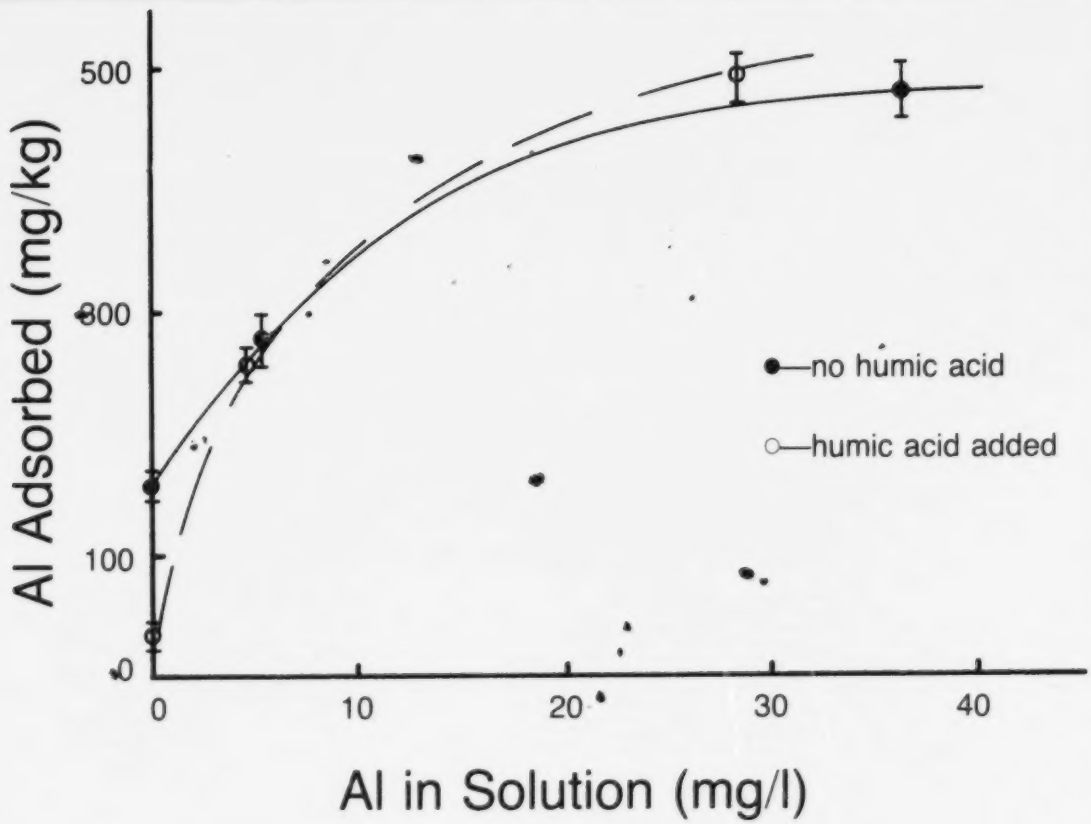

Figure 17. Sorption isotherm of aluminum.

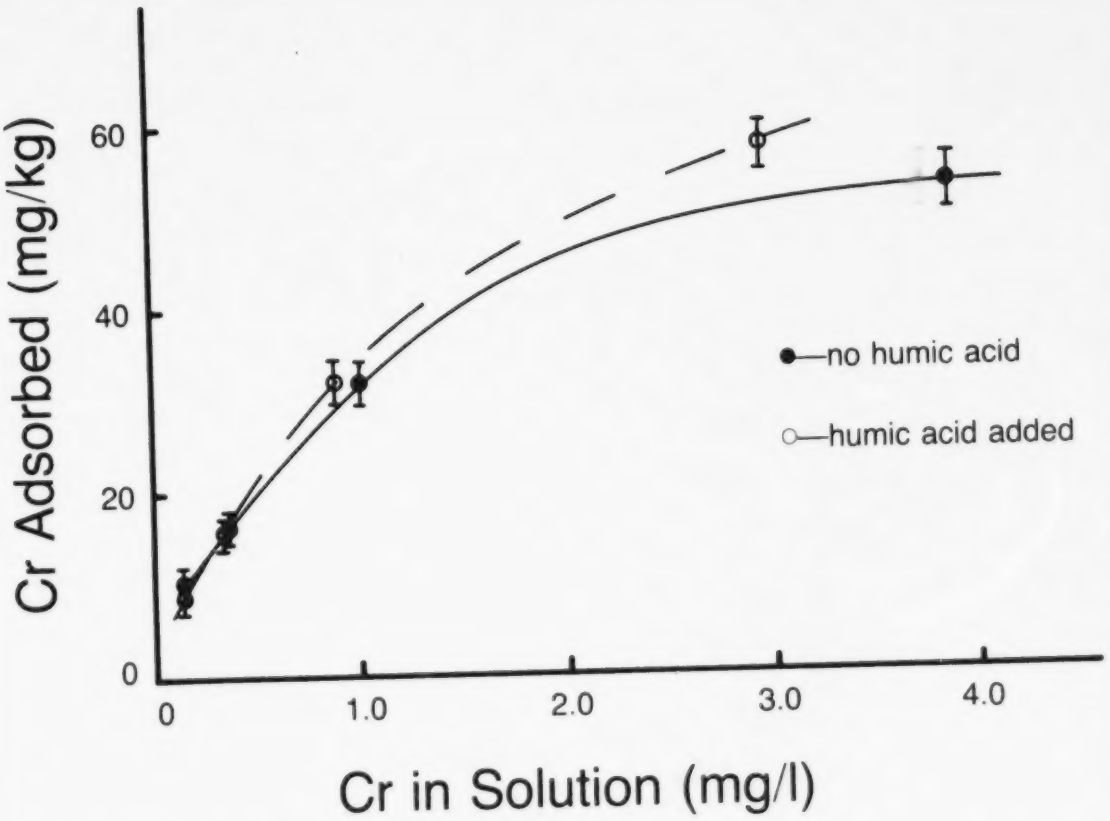

Figure 18. Sorption isotherm of chromium.

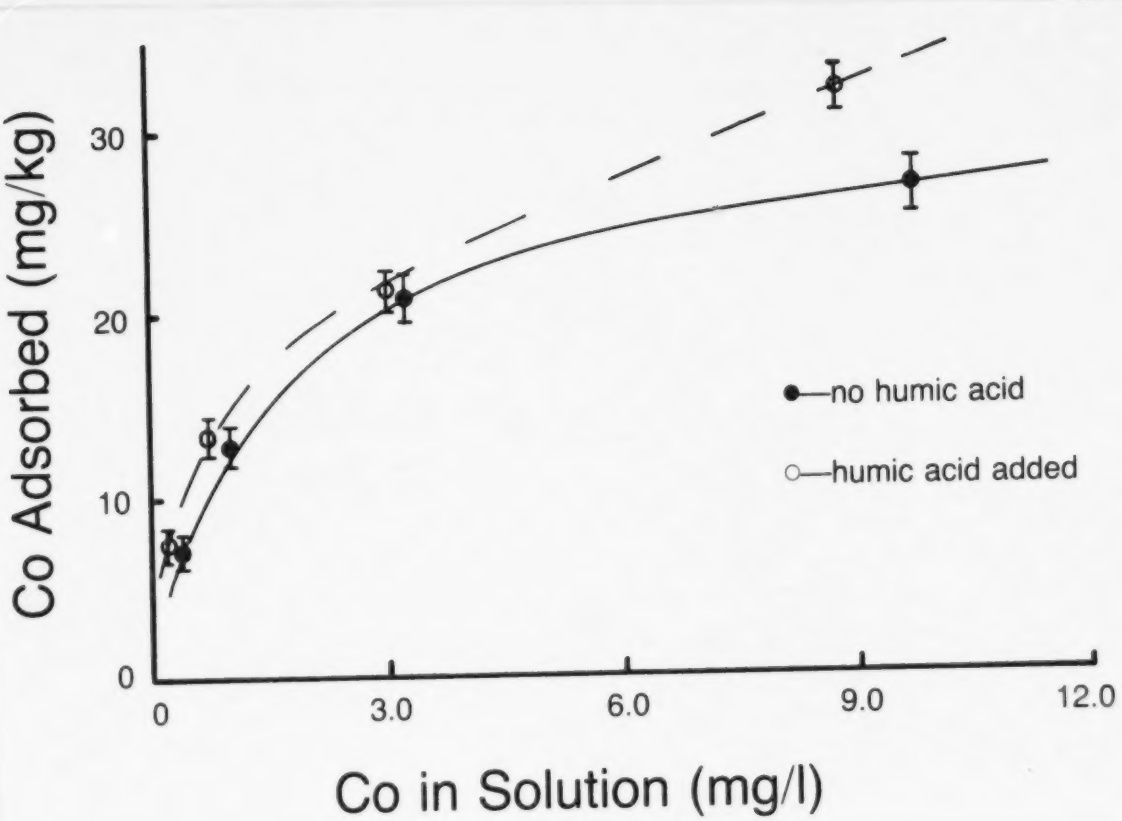

Figure 19. Sorption isotherm of cobalt.

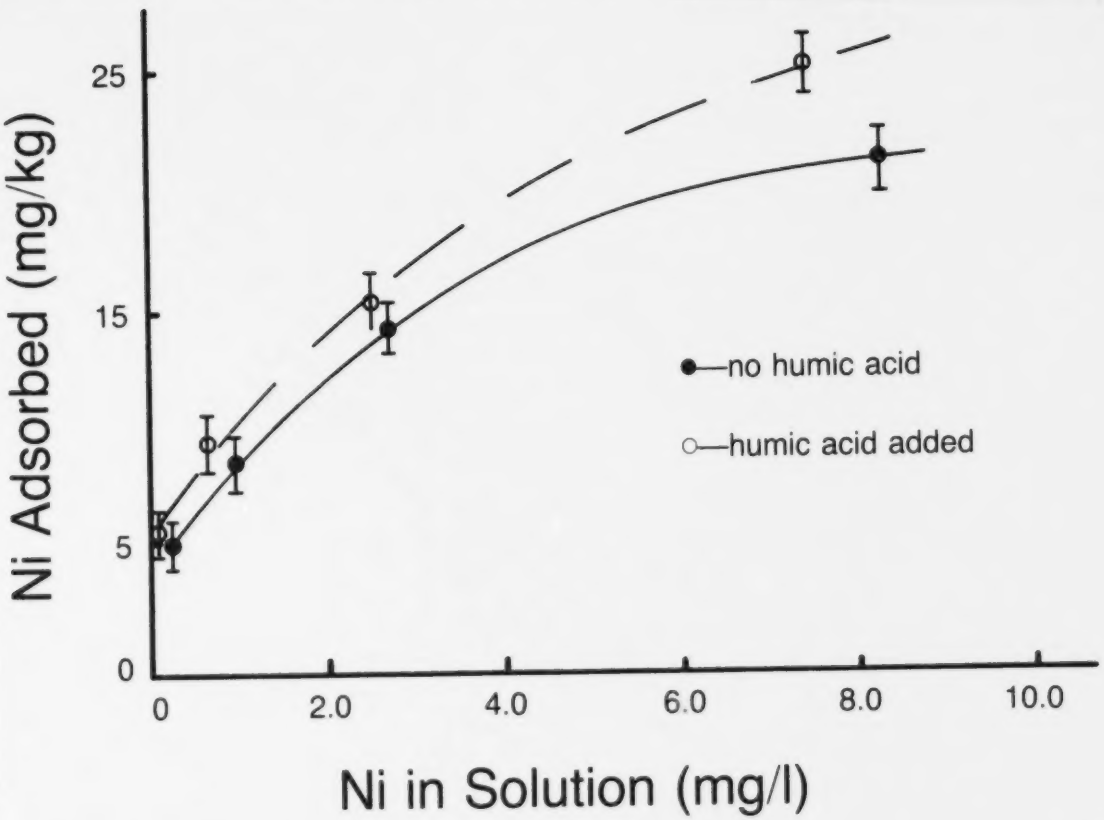

Figure 20. Sorption isotherm of nickel.

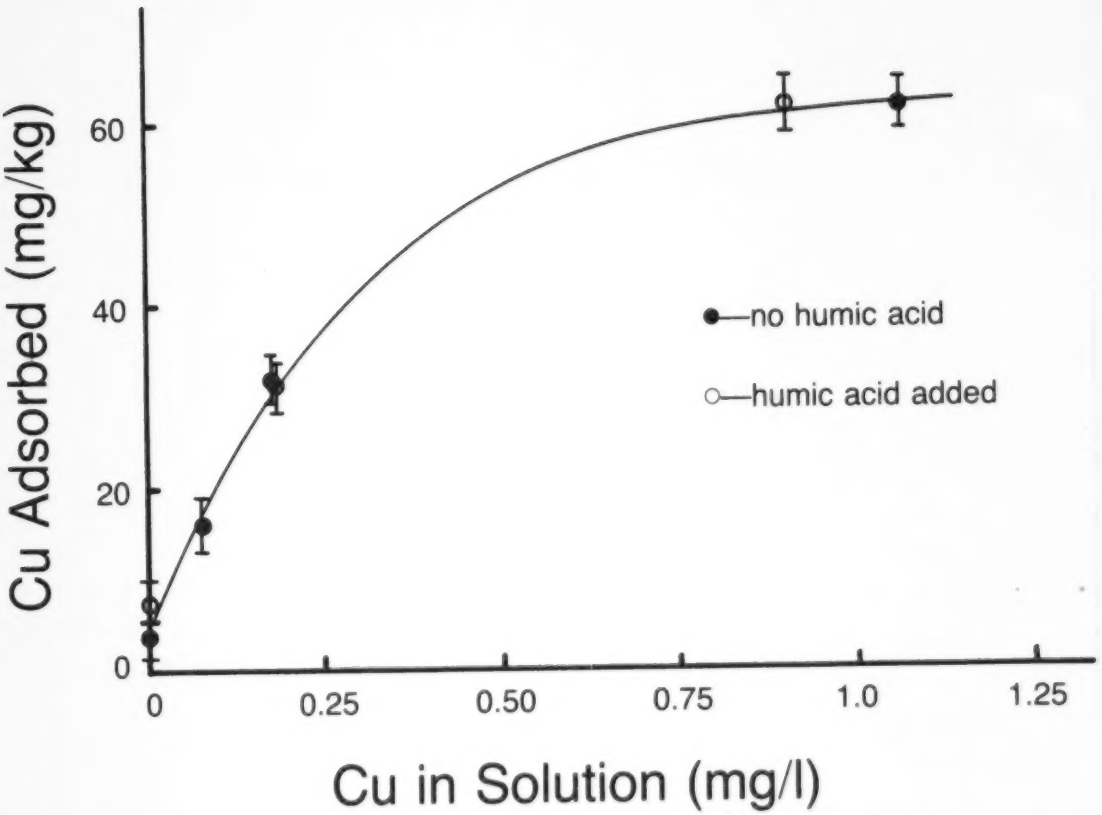

Figure 21. Sorption isotherm of copper.

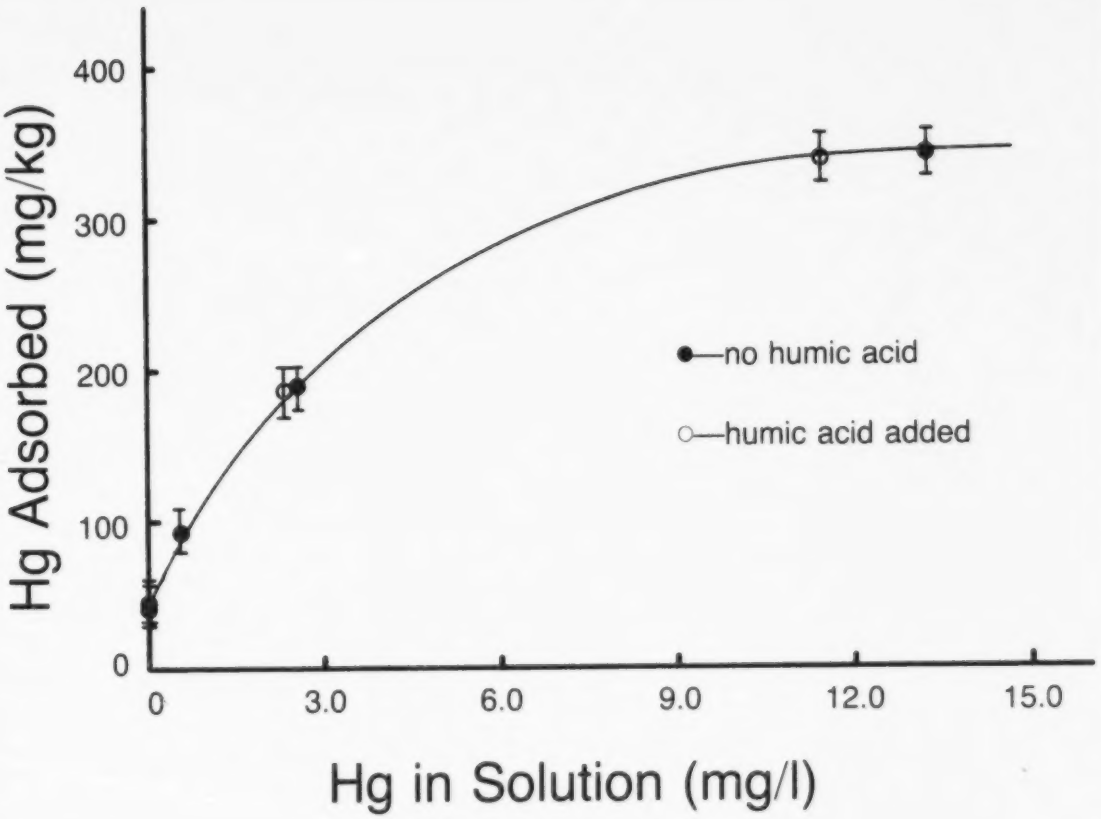

Figure 22. Sorption isotherm of mercury.

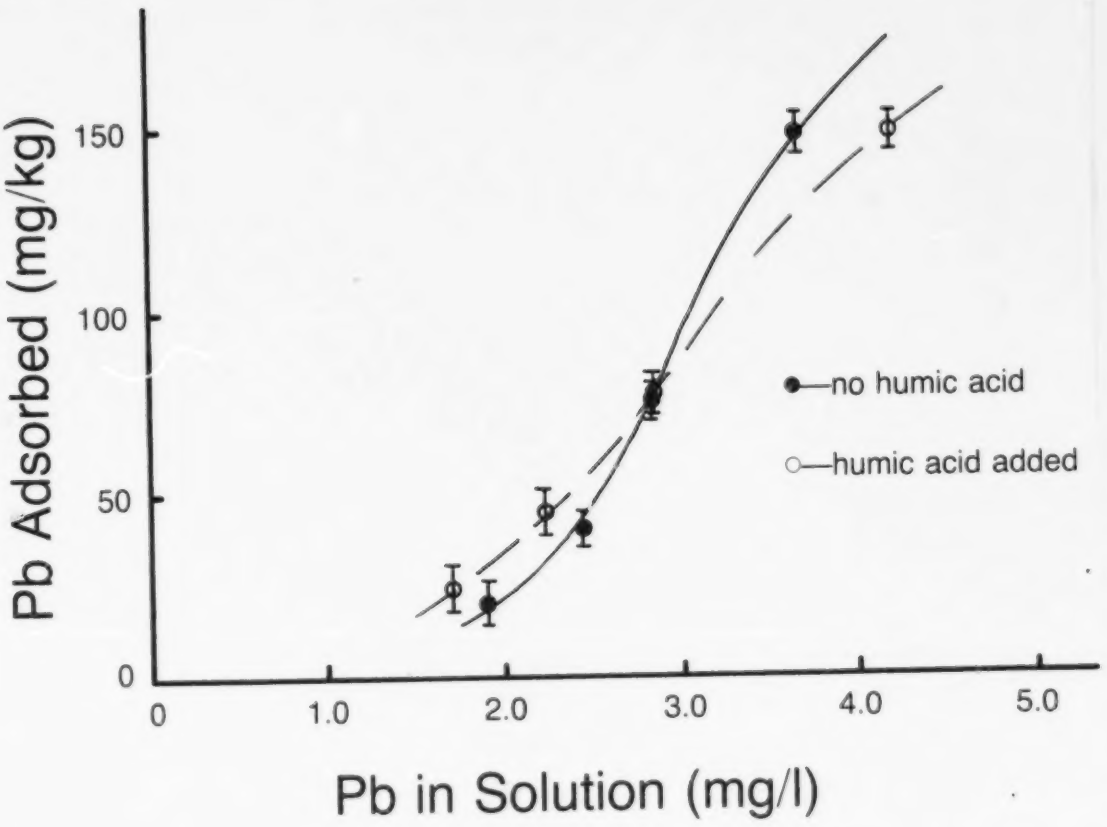

Figure 23. Sorption isotherm of lead.

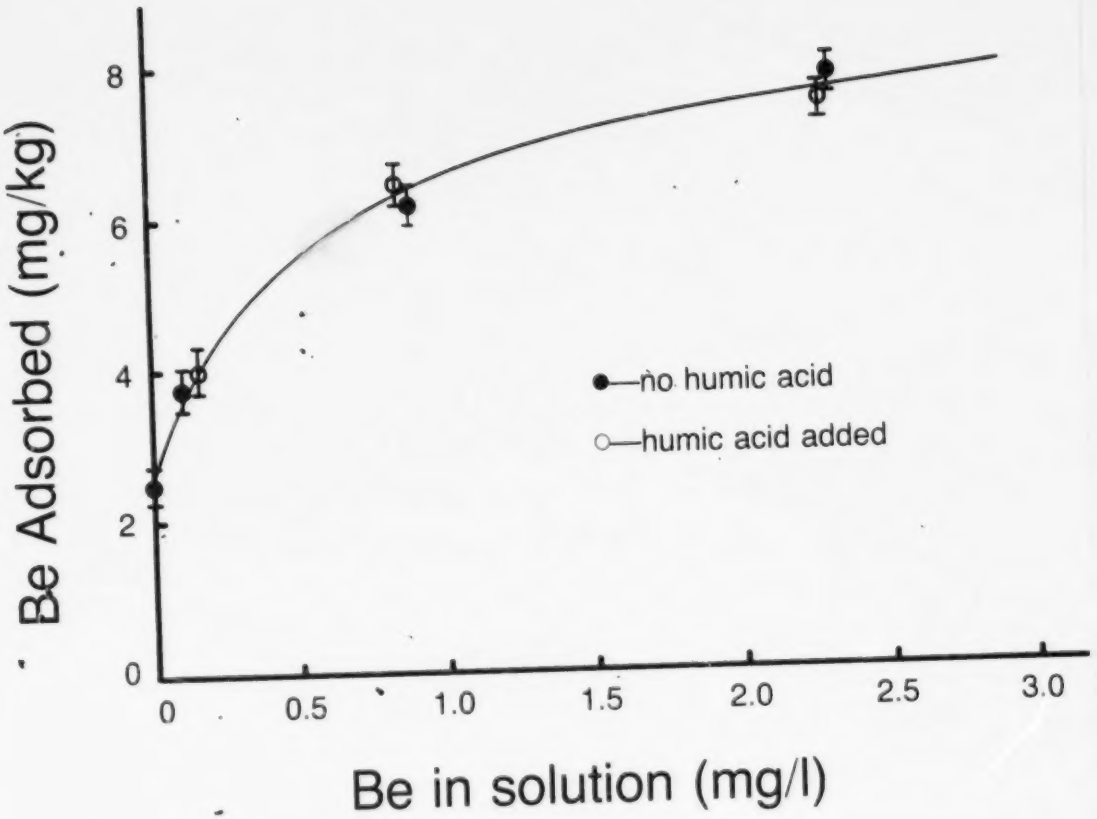

Figure 24. Sorption isotherm of beryllium.

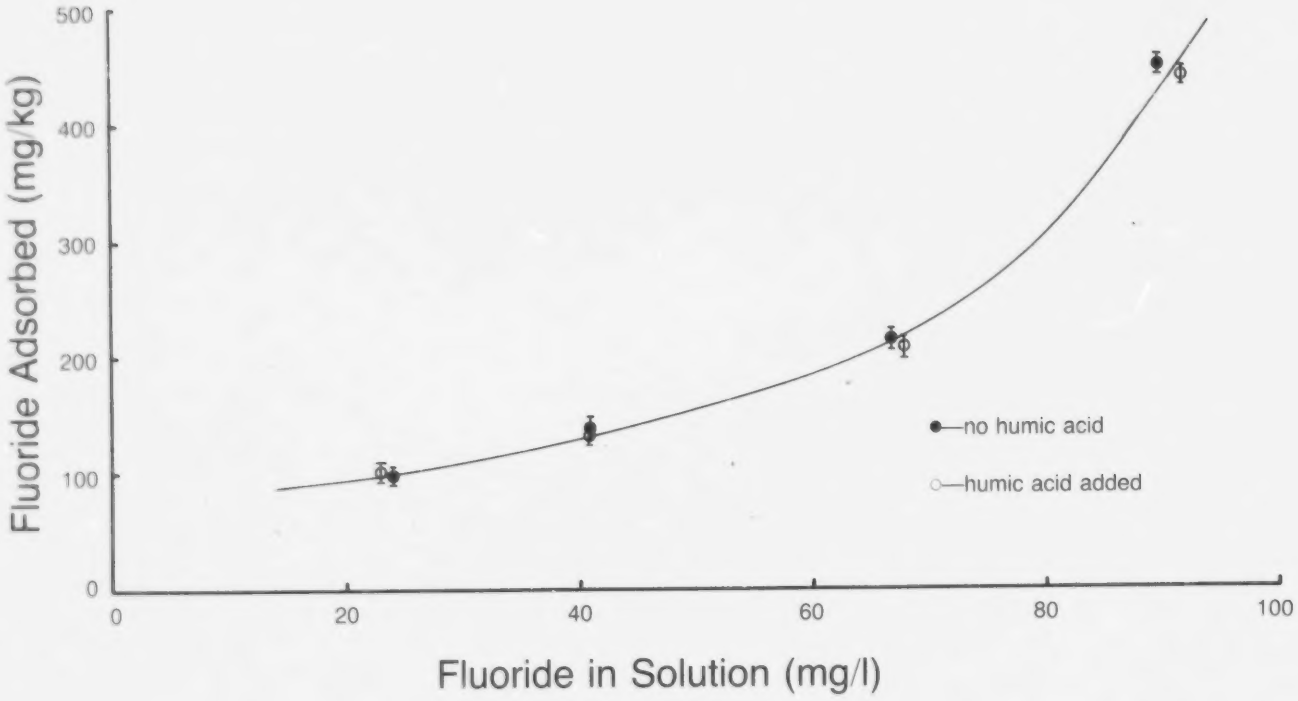

Figure 25. Sorption isotherm of fluoride.

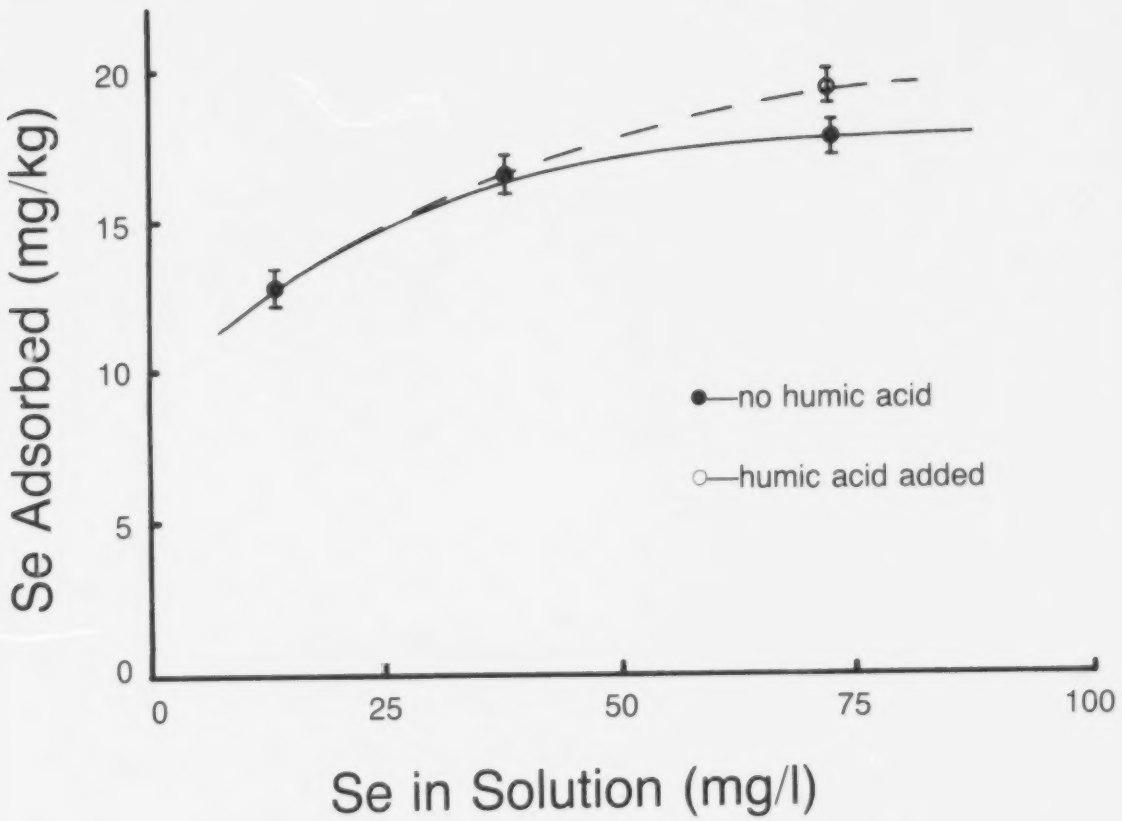

Figure 26. Sorption isotherm of selenite.

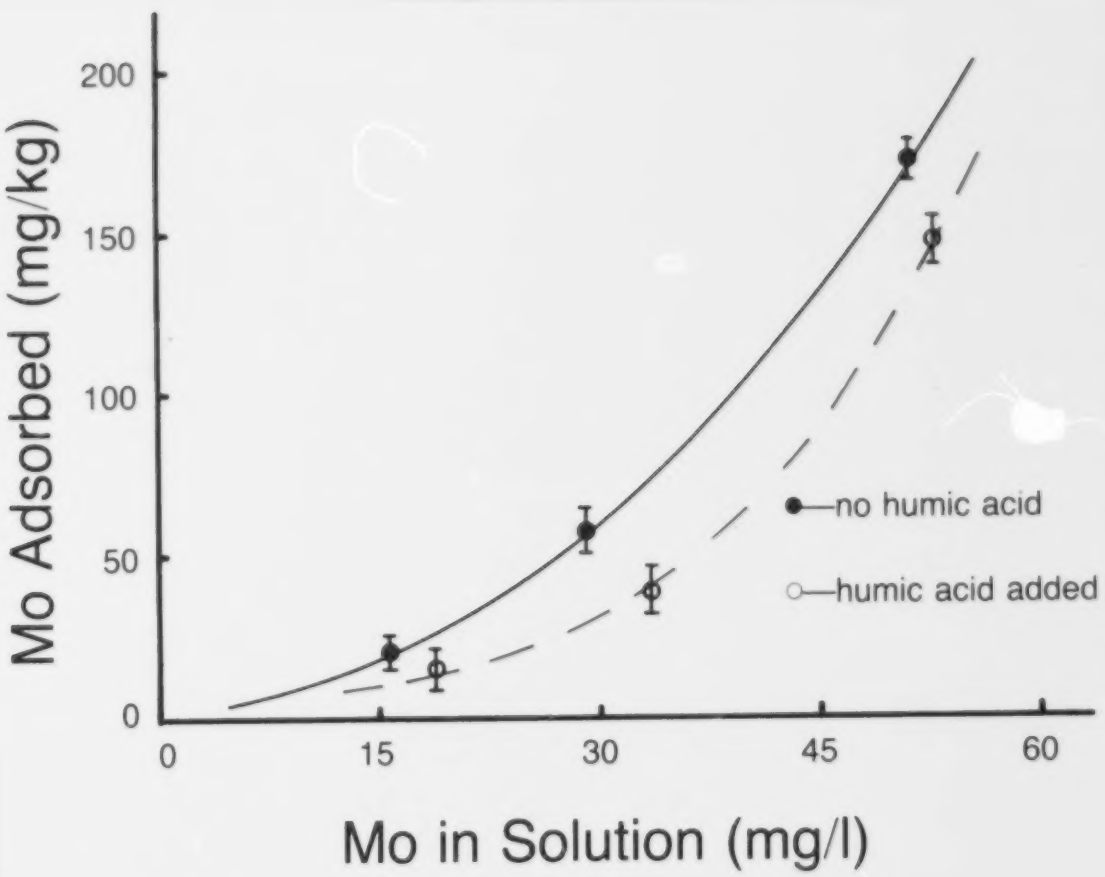

Figure 27. Sorption isotherm of molybdate.

compared to other coals, high volatile (HV) bituminous coals, such as Fruitland Formation coal, have the largest adsorption capacities for organic dye molecules (18). Shapes of the sorption isotherms determined by Nandi and Walker are quite similar to the curves in Figures 13-27. According to Brunauer's classification of isotherms, Cd, F, and Mo resemble Type III isotherms, Pb, Cu, and Mn resemble Type V isotherms (based on the sigmoid curve shapes) which are extensions of Type III, while the remainder of the trace elements have sorption plots similar to Type I isotherms (37). (The shape of Type I isotherms is thought to result from monolayer adsorption while it is believed that multilayer adsorption is responsible for the shapes of Type III and Type V isotherms (37). However, Brunauer's classification concerns the physical adsorption of gases and similar inferences of this nature cannot necessarily be drawn regarding the chemisorption of aqueous ions.)

Sorption isotherms can also yield valuable information on the affinity of an adsorbent for specific trace elements. Examination of Figures 13-27 and Table 18 shows that the amounts of Be, Al, Cu, Zn, Hg, and CN^- expected to be dissolved by groundwater following gasification should be quickly and completely adsorbed by the coal. However, quantitative replaceability series for the cation studied here cannot be formulated because replacability is a function of concentration. The sorption data were obtained from several independent sets of experiments and all cation concentration ranges were not the same. Moreover, the interpretation of the Pb and Cd isotherms present added difficulty as these plots fail to give an indication of the saturation point of the coal for these metal ions over the limited concentration ranges studied. Nevertheless, it may be qualitatively stated that Fruitland Formation coal demonstrates a high affinity for Al^{+3}, Hg^{+2}, Fe^{+3}, and Cu^{+2}; a moderate affinity for Pb^{+2}, Zn^{+2}, and Cr^{+3}; and a lower affinity for Cd^{+2}, Mn^{+2}, and Co^{+2}, Ni^{+2}, and Be^{+2}. The replacement power of the anions has been found to be: $CN^- > F^- > MoO_4^{-2} > SeO_3^{-2} > AsO_4^{-3}$. Since affinity depends on experimental conditions, the nature of the adsorbent, and the ions themselves, there is no universal replaceability series. However, some general trends have been noticed regarding the nature of the adsorbates. The most important factor governing selectivity is valence, that is, highly-charged cations exhibit the greatest adsorptivity (17,19). For cations of the same valence, it is believed that replacing power increases with increasing ionic size (19). The cation exchangeabilities determined as a result of this study are in good agreement with these general selectivity rules. Although little information is available concerning the replaceability of anions, it appears that, in this case, affinity tends to decrease as the anionic charge increases.

Chelation of a trace element by humic material decreases the amount of free ion available for adsorption. Since a greater quantity of trace element remains in solution, K_d values will decrease when chelation by humic substances occurs. The data presented here generally show small increases in the solubility of the metal ions in the presence of humic acid. Over the rather limited range of conditions explored the effect is not large. In the cases of Cd^{+2} and Pb^{+2} there may even be a slight increase in K_d with addition of humic acid.

In addition to dissolved metal-humic complexes present in natural waters, some metal-organic associations appear to be colloidal (29). We saw evidence that humic substances may cluster about ions to the point where these macromolecules become insoluble and precipitate at high ion concentration. This is consistent with earlier observations that coagulation and precipitation of metal-humic complexes are a function of metal ion concentration (29).

The highest concentrations of both transition and heavy metal ions used in this work were considerably higher than those found in natural water systems. At these high concentrations humates form insoluble metal complexes with the result that the metal humates precipitates were removed by filtration. Thus, the measured equilibrium concentration of the ion is lower than the actual concentration and the amount of trace element adsorbed is overestimated so the calculated value of the distribution coefficient is larger than the true K_d. Hence, distribution coefficients determined in the presence of humic acid must be considered maximum values.

It can be seen from the figures that the sorption isotherms of Al, Cr, Co, and Ni are affected in the same way by humic acid, but those of Be, Cu, Zn, Mn, and Hg are not altered in the presence of humic acid. The isotherms of Pb, Cd, and Fe also fall into another category, that is, one in which the amount of ion adsorbed decreases with increasing metal ion concentration. These data can be interpreted by assuming that all or most of the complexed Al, Cr, Co, and Ni precipitates from solution while only a fraction of the complexed Cu, Zn, Mn, and Hg precipitates. These assumptions appear to be sound since:

a) humates of Al are insoluble while humates of Zn are only partically insoluble (38).

b) humic acid has a large exchange capacity for Co and Ni, which eventually leads to precipitation (28), and a large capacity for Cu, Hg, and Pb which, although complexed, remain soluble due to the high stability constants of these metal-humic complexes (38-40).

In this light, the affinity of humic acid for the specific trace metal ions investigated is: $Fe^{+2} > Al^{+3} > Pb^{+2} > Cr^{+3} > Co^{+2} > Ni^{+2} > Mn^{+2} > Cd^{+2} > Be^{+2}$. Since the solid-liquid phase distribution of complexed Cu^{+2}, Zn^{+2}, and Hg^{+2}, could not be determined, these metal ions were omitted from the replaceability series. The affinity of humic acid presented here is in good agreement with previous literature results which indicate that Fe^{+2}, Al^{+3}, and Pb^{+2} are strongly complexed by humic material, whereas Cd^{+2} is only loosely complexed (29,38).

The affinity of humic acid for the anionic constituents studied may also be cast in the form of a replaceability series: $MoO_4^{-2} > F^- > SeO_3^{-2} > AsO_4^{-3} \simeq CN^-$. According to the sorption isotherm of selenite, Se adsorption increases in the presence of humic acid. Whether this is due to the partial precipitation of complexed Se, as in the case of the cations, or to some systematic error in the AAS analysis of Se remains unclear.

A final comment regarding the influence of organic chelation on the sorption process concerns pH. While it has been shown that in slightly acidic solutions, chemical complexation by humic acid has a pronounced effect on the adsorption of trace metals (17,27,38), on the basis of literature this effect is expected to be enhanced in the highly alkaline groundwater of the San Juan Basin.

Several attempts to describe quantitatively ion-exchange and adsorption based on thermodynamic, kinetic and electrostatic considerations have met with moderate success, but all equations suffer, to varying degrees, from theoretical deficiencies and cannot be universally applied (41). Wiegner and Jenny (42), and Vageler and Woltersdorf (43) derived empirical adsorption equations based on the Fruendlich isotherm,

$$\frac{n_2^s}{n^s} = a\, C_2^{1/n}$$

where n_2^s = mg of solute adsorbed per gram of absorbent

n^s = adsorption capacity of adsorbent in mg g^{-1}

C_2 = equilibrium solute concentration

a,n = empirical constants

Since this equation has previously proven successful in describing adsorption from solution (44), the data presented in Tables 17 and 18 were fit to the logarithmic form of the Freundlich isotherm,

$$\log \frac{n_2^s}{n^s} = \frac{1}{n} \log C_2 + \log a$$

The method of linear least squares was applied to this equation to obtain the parameters a and n. Correlation coefficients were very high ($R > 0.95$) for all trace metal ions analyzed here.

The sorption isotherms reported here are similar to Brunauer Type I isotherms (37), which are accurately described by the linearized Langmuir isotherm. The sorption data were fit to this equation expressed in a form appropriate for adsorption from solution.

$$\frac{C_2}{n_2^s} = \frac{C_2}{n^s} + \frac{1}{n^s b}$$

where

C_2 = equilibrium solute concentration

n_2^s = mg of solute adsorbed per gram of adsorbent

n^s = adsorption capacity of adsorbent in mg g^{-1} of substrate

b = intensity of adsorption, related to Q the heat of absorption through the equation

$$b = b' \, e^{Q/RT}$$

As expected, correlation was good for all elements possessing Type I-like sorption isotherms, but was poor for Mn^{+2} and those ions (Cd^{+2}, Pb^{+2}, F^-, MoO_4^{-2}) for which the coal failed to exhibit a clear saturation effect.

The actual adsorption of trace elements following UCG may reach completion only after a period of several years (24). Since it would be more convenient and more useful to determine phase distributions of the ions as a function of initial concentration rather than equilibrium concentration, the Freundlich and Langmuir equations were slightly modified to yield

$$\log\left(\frac{n_2^s}{n^s}\right) = \frac{1}{n} \log C_o + \log a$$

and

$$\frac{C_o}{n_2^s} = \frac{C_o}{n^s} + \frac{1}{n^s b}$$

where C_o = initial concentration (g/ℓ). As a result of this alteration, linear correlation improved for all ions investigated. Results of this data treatment are presented in Tables 19 and 20.

Whereas the Fruendlich isotherm is purely an empirical equation, the derivation of the Langmuir isotherm is based on a firm theoretical foundation. Although originally derived for the monomolecular adsorption of gases, the modified Langmuir equation may be applied here to adsorption from solution. It provides an alternate way to determine adsorption capacity. Assuming that a limited number of surface sites are available on coal for sorptive purposes, the fraction of surface covered, θ, is defined as (45).

$$\theta = \frac{n_2^s}{n^s}$$

As more ions are adsorbed, θ increases. When the coal surface becomes saturated ($\theta = 1$), the sorption capacity of the coal is attained and

$$n^s = n_2^s$$

TABLE 19. FRUENDLICH AND LANGMUIR CONSTANTS FOR CATIONS

Trace Elements	$K_d = \infty$ for $C_o \leq$	Humic Acid[a]	Freundlich Constants			Langmuir Constants		
			R^b	Slope (1/n)	Intercept (log a)	R	Slope ($1/n^s$)	Intercept ($1/n^s b$)
Mn		-	0.998	1.00	-2.71			
		+	0.997	0.988	-2.73			
Fe		-	1.000	0.995	-2.42	0.999	57.5	3.32
		+	1.000	0.991	-2.43	0.997	106	2.82
Zn	1.1 mg/ℓ	-	1.000	0.949	-2.57	0.998	3,330	-1.11
Cd	0.03 mg/ℓ	-	0.990	0.874	-2.99			
	0.03 mg/ℓ	+	0.953	0.882	-3.04			
Al	40 mg/ℓ	-	0.998	0.875	-2.59	0.986	567	-18.1
Cr		-	0.999	0.901	-2.67	0.985	3,930	1.15
Co		-	0.988	0.649	-3.38	0.996	22,400	-10.6
Ni		-	0.997	0.642	-3.46	0.998	27,950	11.5
Cu	2.0 mg/ℓ	-	1.000	0.970	-2.48	0.981	1,150	-1.91
Hg	12 mg/ℓ	-	1.000	0.934	-2.52	0.994	449	-5.52
Pb		-	0.999	1.14	-2.24			
		+	1.000	1.10	-2.29			
Be	0.64 mg/ℓ	-	0.994	0.590	-3.69	1.000	80,500	-52.5
	0.64 mg/ℓ	+	0.986	0.586	-3.70	0.995	85,900	-62.4

[a] - means results in the absence of added humic acid, + means results with 5 mg of humic acid added per liter.

[b] R = correlation coefficient.

TABLE 20. FRUENDLICH AND LANGMUIR CONSTANTS FOR ANIONS

Trace Elements	$K_d = \infty$ for $C_o \leq$	Humic Acid	Freundlich Constants			Langmuir Constants		
			R	Slope (1/n)	Intercept (log a)	R	Slope ($1/n^S$)	Intercept ($1/n^S b$)
F		-	0.999	0.868	-2.87			
		+	0.996	0.793	-2.96			
Se		-	0.981	0.215	-4.51	1.000	50,900	197
Mo		-	1.000	1.455	-2.27			
		+	0.997	1.66	-2.11			

The sorption capacity of the coal then simply becomes the reciprocal of the Langmuir slope. The sorption capacity of Fruitland Formation coal for both cationic and anionic constituents was determined in this manner and the results appear in Table 21. The replacing power of Na, Mg, K, and Ca is

TABLE 21. SORPTION CAPACITY OF FRUITLAND FORMATION COAL DERIVED FROM THE LANGMUIR ISOTHERM

Chemical Species	Langmuir Slope, $\frac{\text{g, adsorbent}}{\text{g, adsorbate}}$	Sorption Capacity, g/kg
all cations	709.9	1.4
all anions	364.5	2.7

very low compared to those of the transition and heavy metals. Nevertheless, these ionic strength adjusters were present in high concentrations and some of these ions were, more than likely, adsorbed by the coal due to stoichiometric considerations. Since the summations do not take this additional adsorption data account, calculated sorption capacities would consequently yield slightly lower values than sorption capacities obtained by specific ion adsorption. Thus, the calculated cation adsorption capacity of 1.4 g/kg coal is in good agreement with the experimentally determined values of 2.5 g Fe^{+2}/kg coal (Table 12).

Particle Size Effects

The effect of coal particle size on the adsorption of trace metal ions was also investigated. An experiment was performed to determine K_d as a function of particle size at constant solute mixture concentration. It was conducted in a similar manner to those experiments in which K_d was determined as a function of concentration using only one standard size of coal.

A simulated contaminant solution consisting of Fe^{+2}, Al^{+3}, Mn^{+2}, and Zn^{+2} ions was prepared with the background ionic strength adjusted to 880 ppm using Ca^{+2}, and Na^{+}. Coal was separated into four particle size ranges by the use of standard sieves. Approximately 50 g. coal samples were weighed into clean plastic containers and a 200 ml aliquot of the simulated groundwater was added to the bottle. Samples were agitated twice daily for five days after which they were filtered and analyzed by AAS as described earlier. Results of the experiment, based on replicate analyses, are presented in Table 22 and histograms of the distribution coefficient as a function of coal particle size appear in Figures 28-32. Mean particle size for each range is used in the figures.

Particle size effects are believed to be predominantly surface area phenomena (46). This however is something of an oversimplification. For example, in the case of clays much adsorption occurs with species between

TABLE 22. EFFECT OF PARTICLE SIZE ON ADSORPTION

Trace Element	C_o (mg/ℓ)	Particle size range, mm	K_d
Al	50	<0.250	∞
		0.250-1.397	∞
		1.397-3.327	10±1.5
		3.327-6.680	8±1.5
Mn	13	<0.250	2.3±0.22
		0.250-1.397	0.9±0.22
		1.397-3.327	0.5±0.22
		3.327-6.680	0.4±0.22
Fe	120	<0.250	160±23
		0.250-1.397	36±5.2
		1.397-3.327	1.4±0.20
		3.327-6.680	1.0±0.14
Zn	10	<0.250	32±3.7
		0.250-1.397	10±1.2
		1.397-3.327	1.5±0.17
		3.327-6.680	1.2±0.13
Σ	193	<0.250	56±13.4
		0.250-1.397	24±3.1
		1.397-3.327	2.3±0.76
		3.327-6.680	1.8±0.76

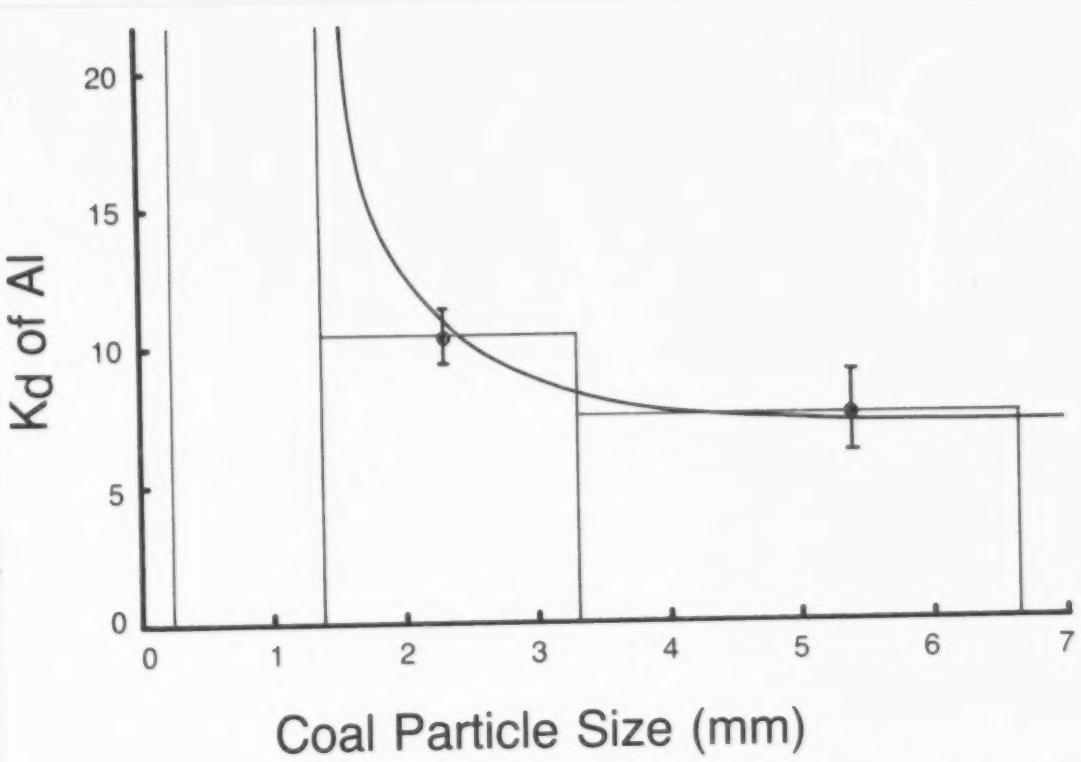

Figure 28. K_d of aluminum vs. coal particle size.

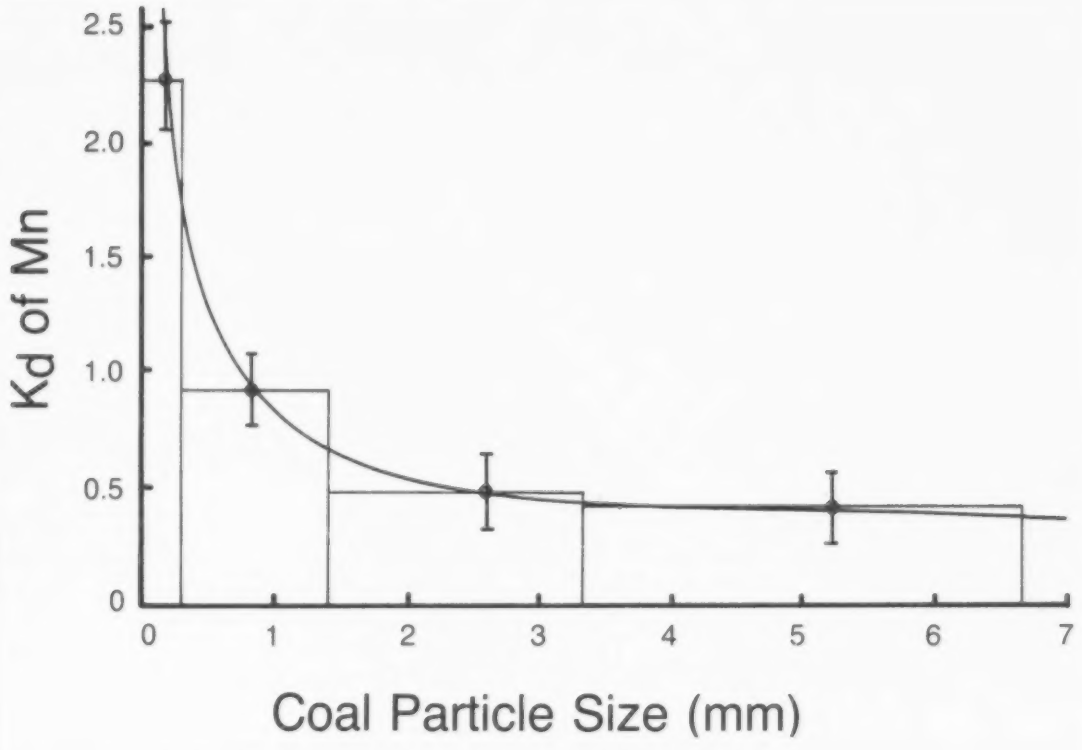

Figure 29. K_d of manganese vs. coal particle size.

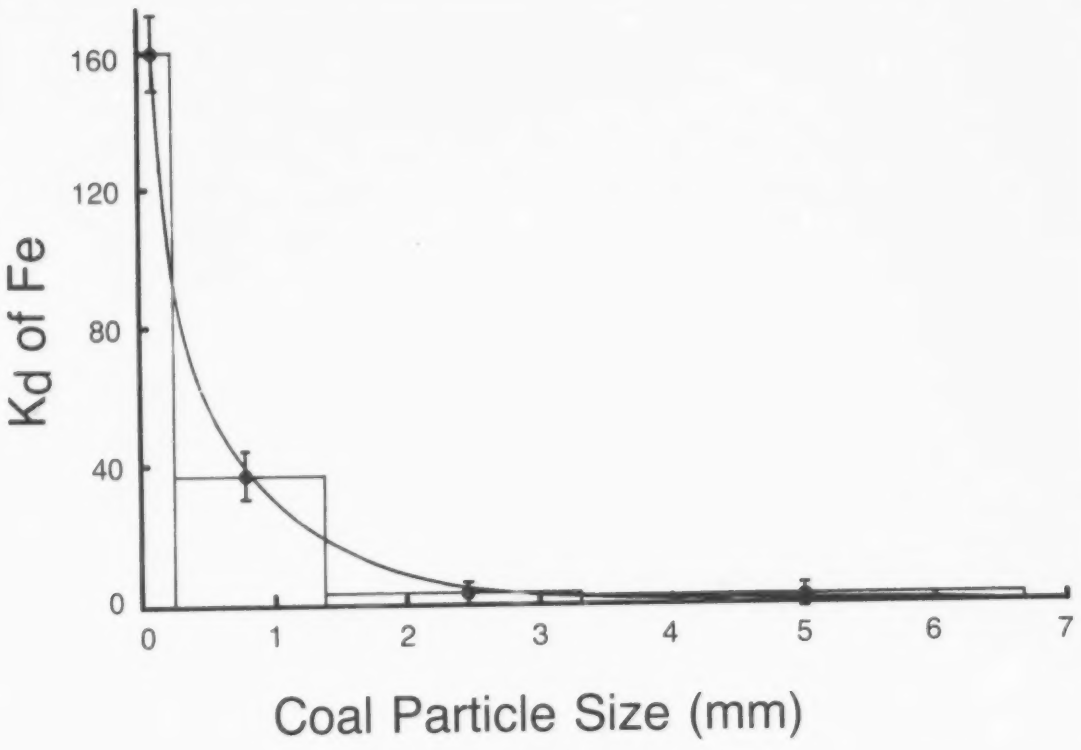

Figure 30. K_d of iron vs. coal particle size.

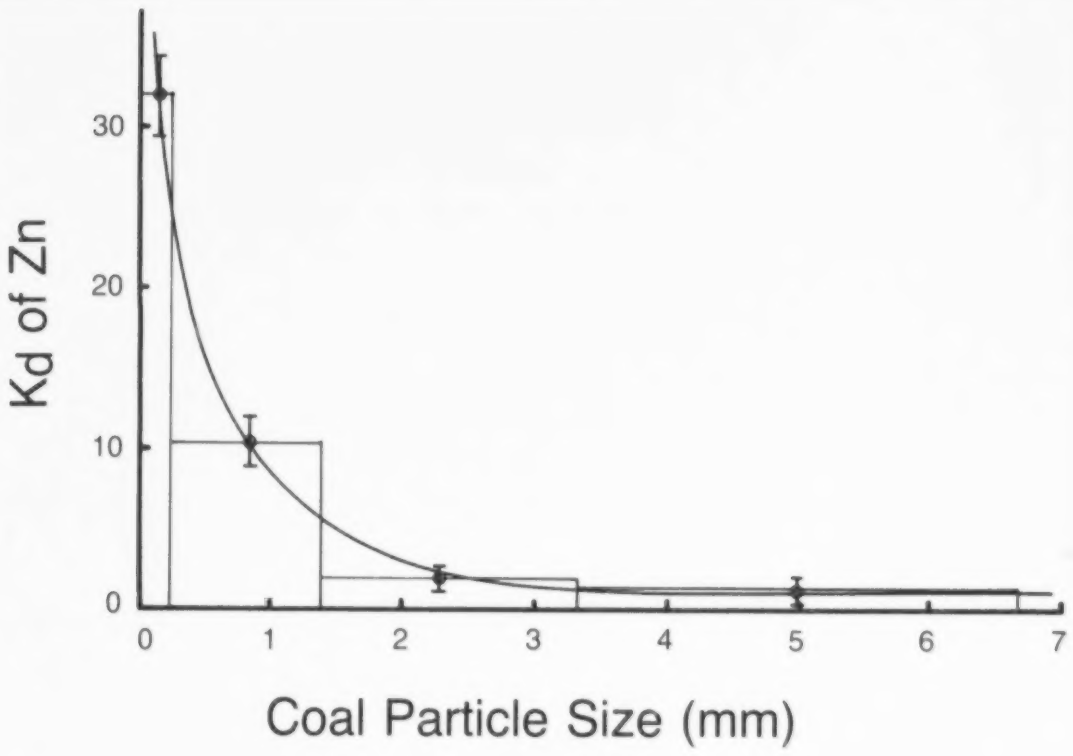

Figure 31. K_d of zinc vs. coal particle size.

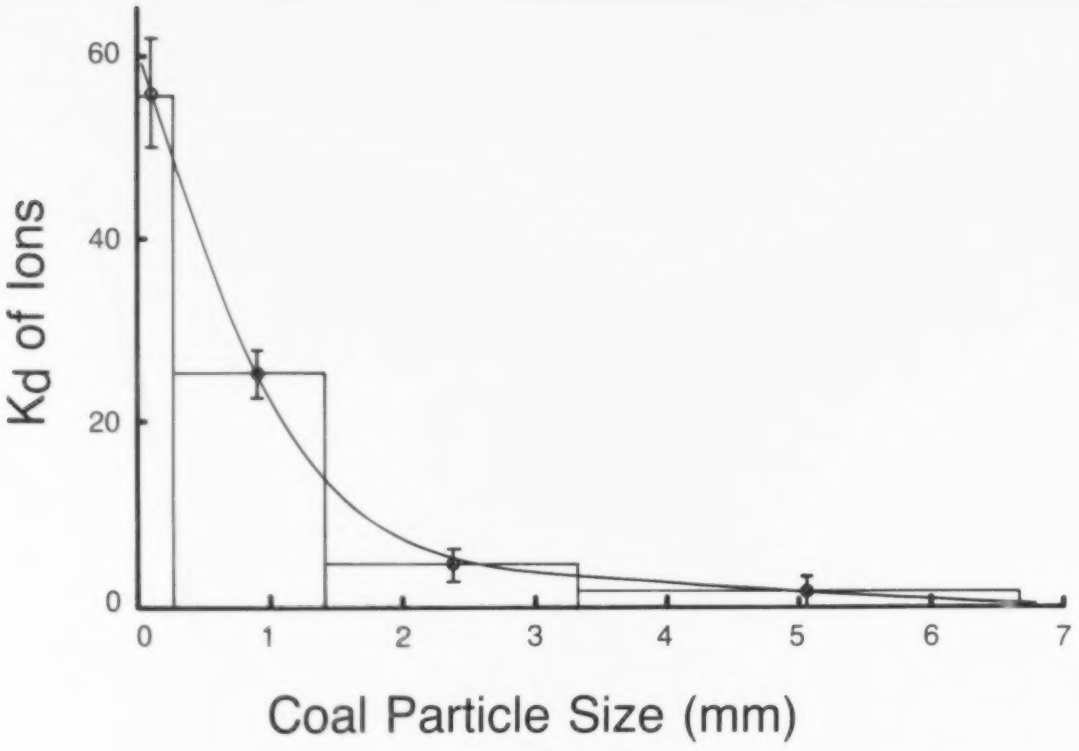

Figure 32. K_d of the sum of ions vs. coal particle size.

the basal planes of the silicate structure of clay. Consequently, effects of swelling, degree of hydration and ionic radius are also important. In fact, cycles of adsorption-desorption of substances on montmorillonite are known to exhibit pronounced hysteresis loops (47). Simple K_d-surface area relationships may therefore be expected only when the adsorbent behaves as if adsorption occurs only at the surface. The particle size effects reported here bears a close resemblance to exponential functions, that is, K_d appears to decrease exponentially with increasing mean particle size. The data could not be made to fit any function which was proportional to r^2 where r is the mean particle radius. (r^2 will be directly proportional to surface area whether the particle is a sphere or other irregular figure.) We conclude therefore that some of the adsorption occurs at surface sites and that there are additional sites inside the coal molecular network that become more accessible as the particle size decreases.

SECTION 8

ADSORPTION OF ORGANICS

It has been recognized that the potential for release of large quantities of both inorganic and organic contaminants is one of the principal environmental concerns associated with UCG. A large number of organics are generated during the pyrolysis stage of UCG; those are transported in the vapor phase to the region surrounding the burn where they then enter the groundwater (48-53). Phenolic compounds are a major constituent of the organics produced. Comparison with waste water effluents from surface coal processing plants has produced the estimate that concentrations of phenolic compounds alone could reach levels of 1000-3000 mg/ℓ (48). On this basis, we have chosen to use phenol as a model organic, and perform a detailed study of the interaction of phenol with the UCG surroundings.

Studies performed to date have involved the adsorption of phenol on standard clay, overburden, raw coal and clean coal. The standard clay was Na-Montmorillonite (CMS-SWy-1 from Source Clay Repository, Department of Geology, University of Missouri, Columbia, Missouri 65211). It was used without further treatment. Coal samples were taken from Fruitland Formation coal either from the coal of one of the two wells drilled into the seam at the site described earlier (54), or from the exposed seam in the San Juan Mine operated by Western Coal Company about two miles from the site. Differences between the two samples were no greater than sample variations within a single core. Overburden samples were taken from the core of well GT-1.

Clean coal was prepared by a standard acid washing technique of the raw Fruitland Formation coal (27). Less than 0.5% ash remained after this washing procedure. Solutions of phenol in distilled, deionized water were prepared by dilution of a gravimetrically prepared stock solution. A 50 ml aliquot of phenol solution of the desired initial concentration was pipetted into a polyethylene bottle containing 1 g of the sample. The bottles were all washed with dilute nitric acid and rinsed repeatedly with distilled water prior to use. The sample mixture was allowed to stand at room temperature with frequent vigorous agitation for a period of five days. The supernatant liquid was then centrifuged to settle most of the suspended matter, decanted and filtered through 0.45 μm Millipore filter paper. The phenol concentration in the liquid was determined spectrophotometrically using the standard technique (9) of addition of aminoantipyrene and potassium ferricyanide to develop a colored solution whose absorbance is proportional to the concentration of phenol remaining in solution.

The results of the absorption studies performed will now be presented and discussed. Much of the current data involves clay minerals that would be

expected to interact strongly with inorganics due to ionic exchange capabilities. There is, however, interaction with organics as well. These interactions will be contrasted with those involving coal.

The adsorption data acquired in this experiment were observed to fit a Langmuir adsorption isotherm discussed in Section 7.

$$\frac{C_2}{n_2^s} = \frac{C_2}{n^s} + \frac{1}{n^s b}$$

Again, C_2 is the equilibrium concentration of phenol in solution, b is related to the heat of adsorption ($b = b'e^{Q/RT}$), n^s is the adsorption capacity of the sample in mg g^{-1}, and n_2^s is the mg adsorbed per gram of sample at concentration C_2. Results of all the phenol adsorption experiments reported here conformed to the same isotherm. The results are given in Table 23 for adsorption of phenol on a variety of substrates. The correlation coefficient R is a measure of the goodness of fit to a linear function.

TABLE 23. ADSORPTION OF PHENOL ON COAL AND MINERALS

Sample	Conc. Range, ppm	R*	n^s, mg g^{-1}
Na-Montmorillonite	50-1000	0.9799	3.52
	1000	nonlinear	--
Overburden	50-1000	0.937	4.82
Raw coal	20-400	0.9999	4.69
	500-4500	0.9995	20.2
Clean coal	50-400	0.9945	8.33
	500-4500	0.9945	108

*R = correlation coefficient

Montmorillonite makes up approximately half of the clay minerals found in the overburden and the San Juan Basin groundwater contains a large concentration of monovalent cations (Section 4), so the adsorption characteristic of phenol on Na-Montmorillonite will provide a reasonable model for phenol adsorption on overburden. Adsorption on Na-Montmorillonite conforms to the Langmuir isotherm over the equilibrium phenol concentration range of

50-1000 ppm. The observed adsorption capacity is 3.52 mg phenol per gram of clay (3.74 mmol per 100 g). This value is approximately the same as the total cation exchange capacity of the overburden which was earlier found to be 2.5 meq per 100 g (54). At concentrations of greater than 1000 ppm the amount of phenol adsorbed increases substantially, the amount adsorbed accelerating for some magnitude beyond this concentration. This behavior is characteristic of physical adsorption described by the Brunauer-Emmett-Teller (BET) equation which takes into account multiple layer formation of physically adsorbed molecules (44).

An alternative explanation for the increase in phenol adsorption is that there are two kinds of sites on the clay and the second is occupied only after a concentration of 1000 ppm phenol is reached. Although we cannot eliminate this alternative rigorously, it is generally believed that physical adsorption is an unactivated process so that all-physical adsorption reactions occur at the same diffusion controlled rate. This militates in favor of a multilayer interpretation of the high concentration data.

Phenol adsorption on Kirtland shale overburden is quite similar to adsorption on Na-Montmorillonite. Adsorption follows the Langmuir equation up to about 1000 ppm phenol solution with an adsorption capacity only slightly larger than that of the standard clay. This implies that sorption sites on the overburden are likely of the same nature as those in clays; in fact, sorption on the Kirtland shale is probably due to sorption on the clay components of the shale. Again, as in all cases reported here, sorption appears to be physical adsorption with multilayer effects showing up at high phenol concentration.

For adsorption on coal there are two linear segments to the Langmuir isotherm followed by the rapid increase in adsorption at equilibrium phenol concentrations in excess of 4500 ppm. In the case of raw coal the overall adsorption data may be interpreted as a sum of contributions from overburden clay minerals in the coal plus that from the organic matter of coal. The adsorption capacity of the organic component seems to have a substantially higher value than the clay minerals based on the data for the raw and clean coal. The significance of this is that a large quantity of phenol can be adsorbed on coal so that the coal remaining in the aquifer down-dip from the burn site will retard phenol migration quite effectively.

SECTION 9

ANALYTICAL METHODS DEVELOPMENT

Initially only standard procedures for the analysis and storage of samples were used as has been previously discussed in the baseline studies section. Almost all of the standard procedures have proved to be adequate and efficient for the needed analysis. The trace metal analyses were performed by standard flame AAS, however, in some cases the increased sensitivity obtainable by using furnace AAS has been desirable. Thus, we have spent some effort in an attempt to apply furnace AAS to the water samples obtained for this study. Following is a report of three areas where progress has been made in the development of accurate and precise furnace AAS techniques.

LEAD ANALYSIS

One metal for which increased sensitivity was sought was lead. It has been shown, however, that the groundwater matrix greatly affects the analysis of lead by furnace AAS. This is due to the high chloride content of the groundwater taken from the wells at the UCG site (Section 4). Therefore, a careful study was made of the Cl^- interferences on the analysis of Pb in a graphite furnace. From the results obtained in our laboratory it can be concluded that the reaction

$$PbO(s) + C(S) \rightarrow Pb(g) + CO(g)$$

is responsible for the atomization of Pb. Thus, the availability of carbon is important and we obtained superior results using nonpyrolytic graphite rather than the standard pyrolytic graphite. Also, our results indicate that occlusion is the dominant physical interaction and the use of the nonpyrolytic graphite also helps reduce this problem. These results and conclusions are discussed in much more detail elsewhere (55).

SILICON DETERMINATION

Silicon has proved to be a difficult element to determine using atomic absorption spectroscopy. This is especially true when it is to be determined in a matrix as severe as the brine solutions encountered in the samples taken from the test wells at our field site. In the presence of this matrix the silicon signal all but disappeared.

Our initial assumption was that the silicon was being removed from the tube as the chloride, or SiC was forming on the furnace surface. This seemed plausible due to the high chloride content, the thermal stability of $SiCl_2$ and a high volatility of $SiCl_2$. Further studies indicated that a matrix consisting of chloride alone had relatively little effect on the silicon signal. A series of experiments revealed that the sulfate in the matrix is the problem. At this time the nature of the sulfate interference is not known. Experiments to better define this interference are currently planned. The possibility of carbide formation interfering when performing silicon analysis is real even when no matrix is present. Other workers have encountered this problem and have suggested the use of furnace tubes made of something besides carbon (56,57). On this suggestion, we decided to try the analysis using tubes with carbide, in particular tungsten carbide, coatings. The results of some initial experiments have been very encouraging.

Both pyrolytic graphite (PG) and nonpyrolytic graphite (NPG) surfaces were tested for use in the determination of silicon. The nonpyrolytic graphite was examined because of the good results achieved for lead analysis in the presence of a heavy matrix. The effect of treating a pyrolytic tube with a tungsten carbide coating is shown in Figure 33. This figure shows the absorbance as a function of time during the furnace atomization cycle. Presumably the active sites on the surface are blocked by the formation of tungsten carbide thus enhancing the atomization efficiency of silicon. The fact that an enhancement is observed indicates silicon indeed does form carbides on the tube surface. Similar results were obtained for treatment of an NPG tube in the same manner.

Assuming silicon does form carbides on the graphite surface, comparison of the absorbance signals should yield some information concerning the chemical differences in these surfaces. The absorbance vs. time profiles for silicon when atomized from PG and NPG are presented in Figure 34. The absorbance pulse generated from the NPG surface has a much lower peak height and is much broader than the one from the PG surface. This behavior is characteristic of NPG surfaces and attributed to a decrease in the rate of atomization as discussed earlier. If the amount of carbide formation is deduced from the peak height measurements, one would mistakenly conclude that carbide formation is much more severe on the NPG surface. The working curves from peak height measurement demonstrate the slower atomization rate from the NPG surface as evidenced by the reduced sensitivity when this surface is used (Figure 35).

The working curves derived from the integrated absorbance measurements are shown in Figure 36. The results show that the tungstate treated surfaces yield the greatest sensitivity, however, there is no difference in the untreated surfaces.

These results, summarized in Table 24, suggest that there is little chemical difference between PG and NPG. This is somewhat surprising due to the great difference in surface areas. The data also show that the best results were obtained using the tungsten carbide coated PG surface. These results are very encouraging and have allowed Si analysis to become fairly

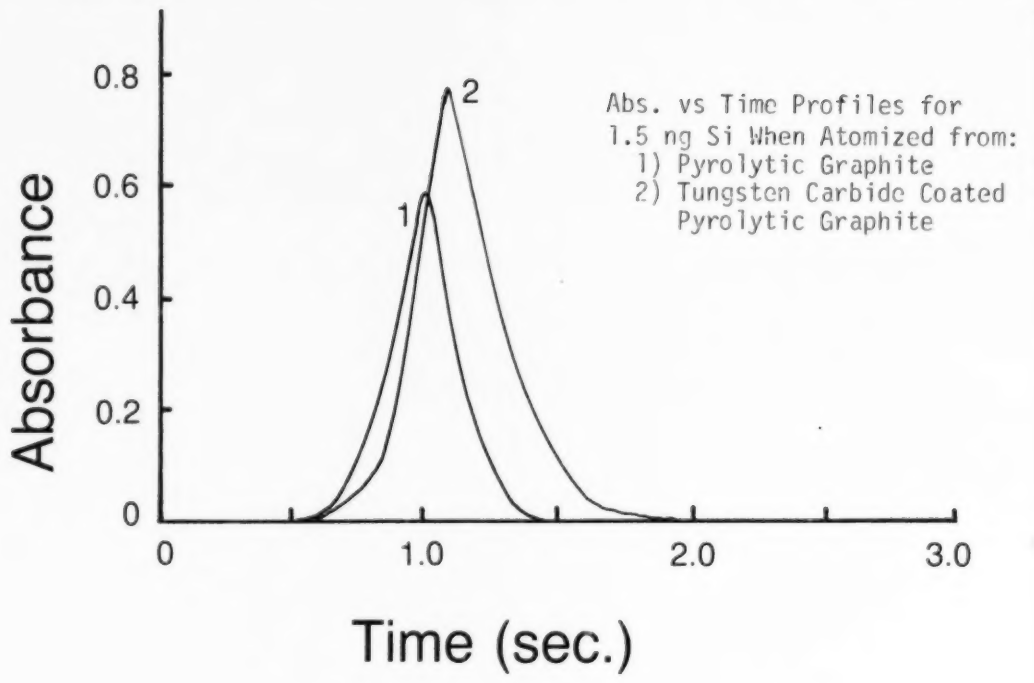

Figure 33. Effect of tungstate treated tube on the measured absorbance for Si.

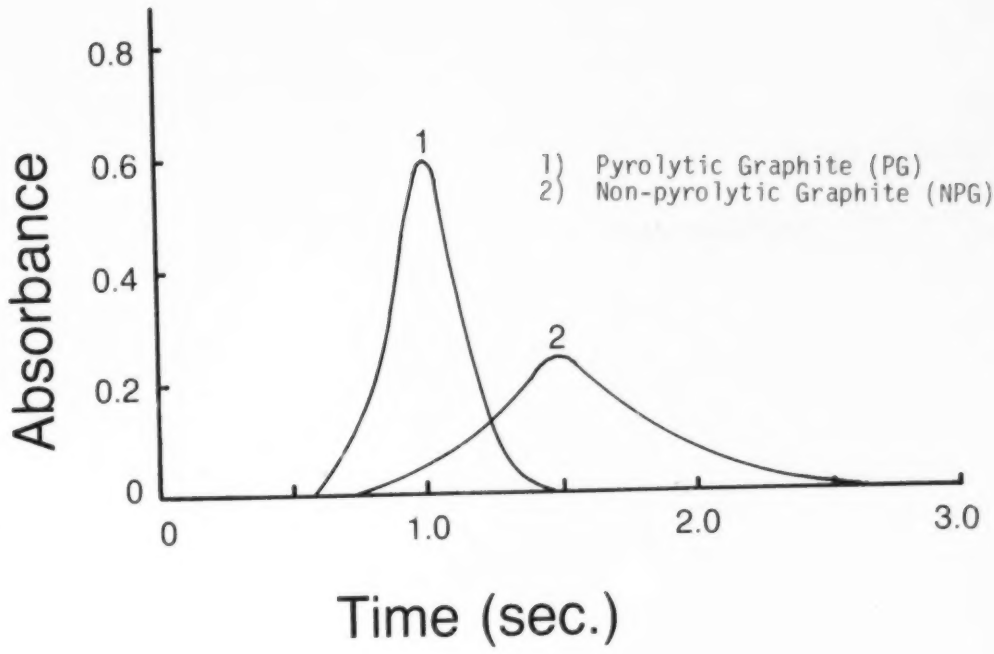

Figure 34. Absorbance vs. time profiles for Si when atomized from PG and NPG surfaces.

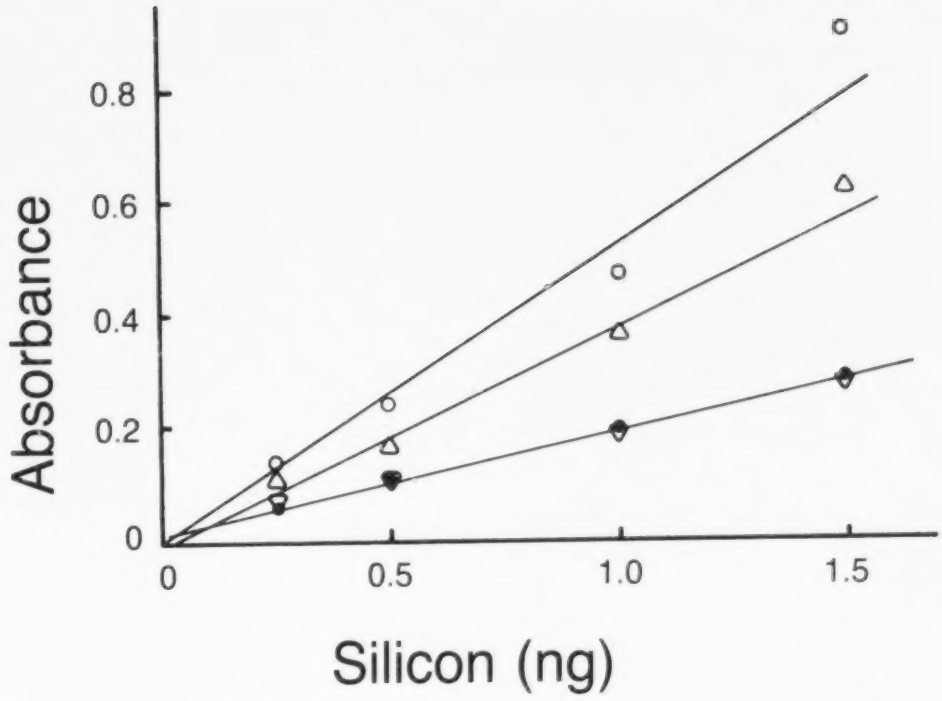

Figure 35. Working curve for Si from peak height measurements.

○ Tungsten Carbide Coated Pyrolytic Graphite
△ Pyrolytic Graphite
▽ Non-pyrolytic Graphite
● Tungsten Carbide Coated Non-pyrolytic Graphite

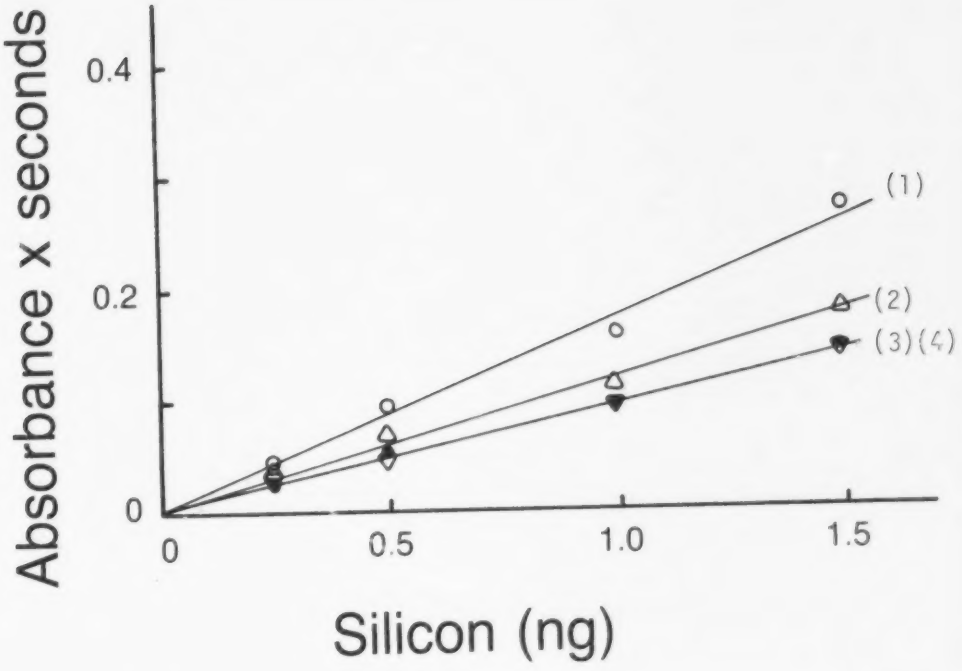

Figure 36. Working curve for Si from integrated absorbance.

(1) Tungstate treated PG
(2) Tungstate treated NPG
(3) PG
(4) NPG

routine. Further experiments designed to explore the application of carbide coated tubes have been planned.

TABLE 24. SENSITIVITIES OBTAINED FOR Si WHEN ATOMIZED FROM VARIOUS SURFACES.

Surface	Sensitivities* (pg) Peak Height	Integrated Absorbance
PG	10	44
Tungsten coated PG	7.3	25
Graphite (NPG)	27	48
Tungsten coated NPG	26	40

*Sensitivity is defined as that amount of Si which will produce a 1% absorption.

TEMPERATURE EFFECTS IN NONFLAME AAS

Flameless AAS has proven to be an extremely powerful tool in the analysis of trace metals. The work performed to date in our laboratory has shown, however, that matrix effects can be significant. Another problem is the fact that the temperatures produced in the furnace are not necessarily reproducible from day to day. Indeed, the instrument in use in our laboratory, a Varian CRA-90, is typical of most commercial furnace atomizers in that there is no way of obtaining accurate temperature data. This includes both the temperature ramps and the absolute temperatures reached during the three heating stages used when a sample is atomized. As discussed previously (55), the heating rate of the furnace during the atomization cycle can affect the precision of the results, so a knowledge of the temperature variables is important.

In flameless atomic absorption spectroscopy high temperatures are used to produce an atomic vapor in the optical path for analysis. The solution containing the element of interest is introduced into the tube and the solvent is driven off during a drying cycle. The furnace is then heated to a set ashing temperature to remove matrix materials such as organic compounds. In the atomization step the temperature is increased very rapidly at a set rate until it reaches the preset atomization hold temperature. The temperatures required for atomization can range from 1000° to as high as 3000°C depending on the element to be determined.

The temperatures utilized in the drying and ashing cycles can be effectively measured using thermocouples. In this manner we have been able to calibrate the furnace temperatures for these cycles. The main problem is, however, that thermocouple measurements are not fast enough to follow the rapid temperature changes during the atomization cycle. Ramp rates of 200°C/sec to 800°C/sec are used with the maximum temperature sometimes as high as 3000°C. We have concluded that optical methods must be employed to make the necessary temperature measurements and thus have explored various techniques that could be utilized.

Radiation pyrometry is actually the basis of the international temperature scale above the gold point (1064.4°C). Most commercially available pyrometers measure either a wide or narrow band of radiation in the infrared region of the spectrum. For accurate temperature determination by these methods the emissivity of the hot object must be accurately known; this is further complicated by the fact that the shape of an object influences the emissivity. Also the response times of pyrometers using conventional infrared detectors is on the order of 0.1 to 10 seconds, too slow to follow the rapidly changing temperatures encountered in flameless atomic absorption.

The basis of temperature determination by optical means is the wavelength distribution of intensity as a function of temperature. This radiation intensity is a function of temperature and wavelength and is described by the Planck equation

$$L_\lambda = E_\lambda \frac{2c^2h}{\lambda^5} \left[\exp\left(\frac{hc}{\lambda kT}\right)-1\right]^{-1}$$

where L is the intensity at wavelength λ, c is the speed of light, h is Planck's constant, k is the Boltzman constant, and T is the temperature in degrees Kelvin. E_λ is the emissivity of the object at wavelength λ. For grey bodies ($E_\lambda > .7$) the emissivity remains essentially constant over reasonable wavelength ranges. For two closely spaced wavelengths we can ratio the intensities and eliminate the need to know the emissivity or the geometrical aspects of the object.

$$R = \frac{L\lambda_1}{L\lambda_2} = \left(\frac{\lambda_2}{\lambda_1}\right)^5 \left[\frac{\exp\left(\frac{hc}{\lambda_1 kT}\right)-1}{\exp\left(\frac{hc}{\lambda_2 kT}\right)-1}\right]^{-1}$$

This may be further simplified by Wien's approximation:

$$R = \left(\frac{\lambda_2}{\lambda_1}\right)^5 \exp\left[\frac{C_2}{T}\left(\frac{1}{\lambda_2} - \frac{1}{\lambda_1}\right)\right]$$

and for fixed values of λ_1 and λ_2 this can be expressed as

$$R = c_3 e^{c_4/T}$$

From this we can see that by plotting ℓnR versus $1/T$ a straight line is obtained.

The pyrometer developed in this lab makes use of this ratio method as well as other unique features which improve the speed, reliability and measurement range. A schematic of the pyrometer is shown in Figure 37. The radiation from the graphite furnace is randomly split and carried to the interference filter-photodiode combination whose response curves are shown in Figure 38. The output from two of these photodiodes is selected by a comparator circuit through a differential multiplexer and the ratio is taken. By using relatively fast electronics and no moving parts, a response time of less than 10 msec is achieved, which is fast enough to follow the fast temperature ramp rates within the resolution of the pyrometer. Figure 39 shows the calibration curve for the output of the pyrometer for the lower temperature (longer wavelength) pair of photodiodes. It is because of this leveling off of response that a third shorter wavelength is measured and selected as a ratio, extending the dynamic range and sensitivity.

Further experiments are being carried out to calibrate the pyrometer and determine the optimum wavelength to be measured. This pyrometer is not only faster than commercial instruments but can be constructed for substantially less than the price of a commercially available pyrometer. In all experiments performed to date this pyrometer has proven to be very useful and should contribute to improved precision when performing trace metal analyses.

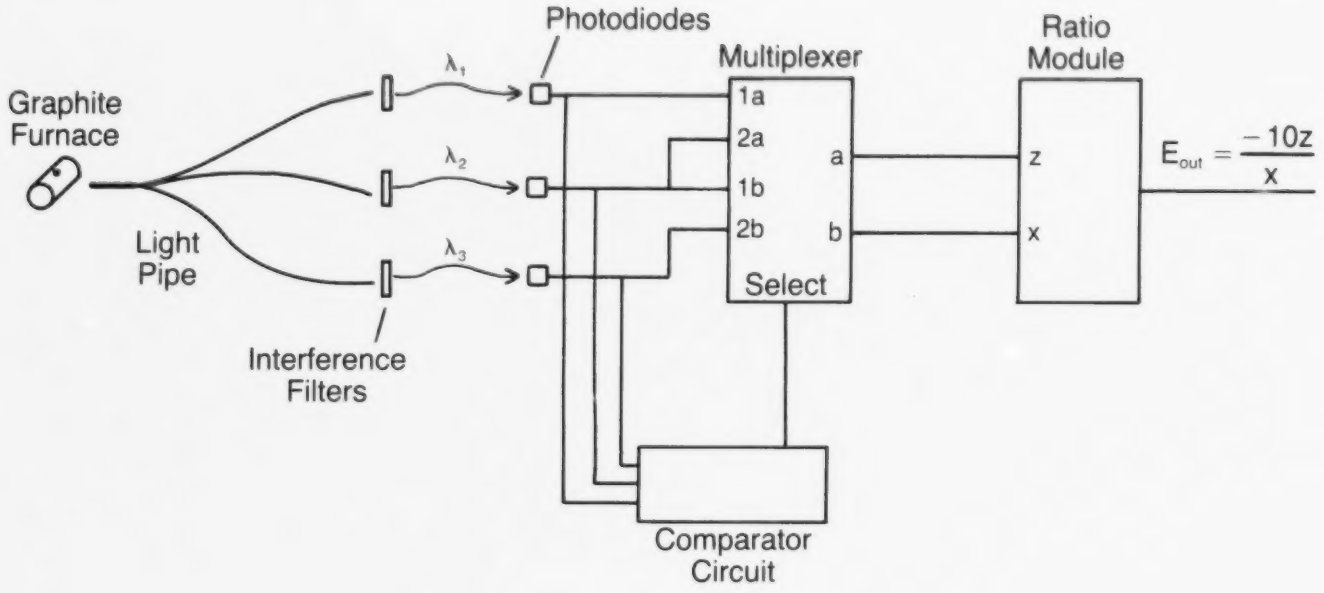

Figure 37. Schematic diagram of the optical pyrometer.

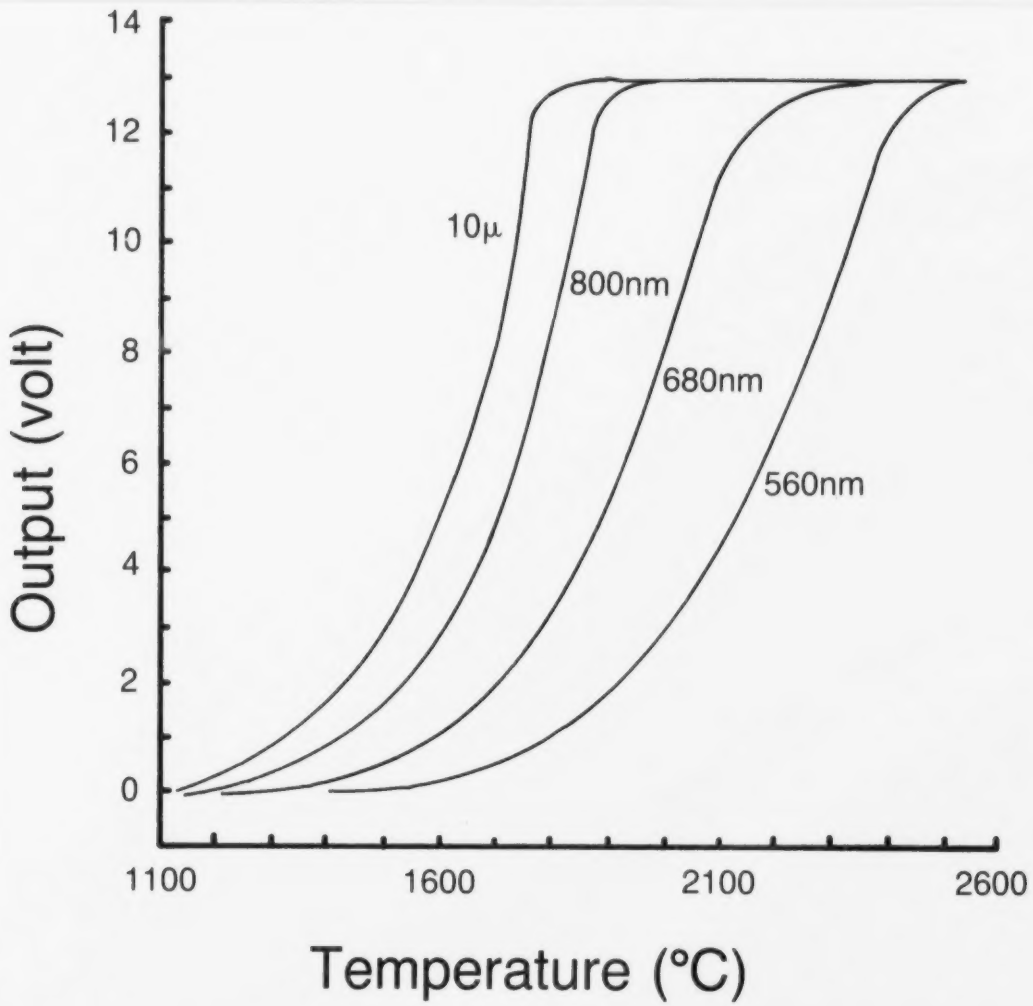

Figure 38. Pyrometer response for various filters.

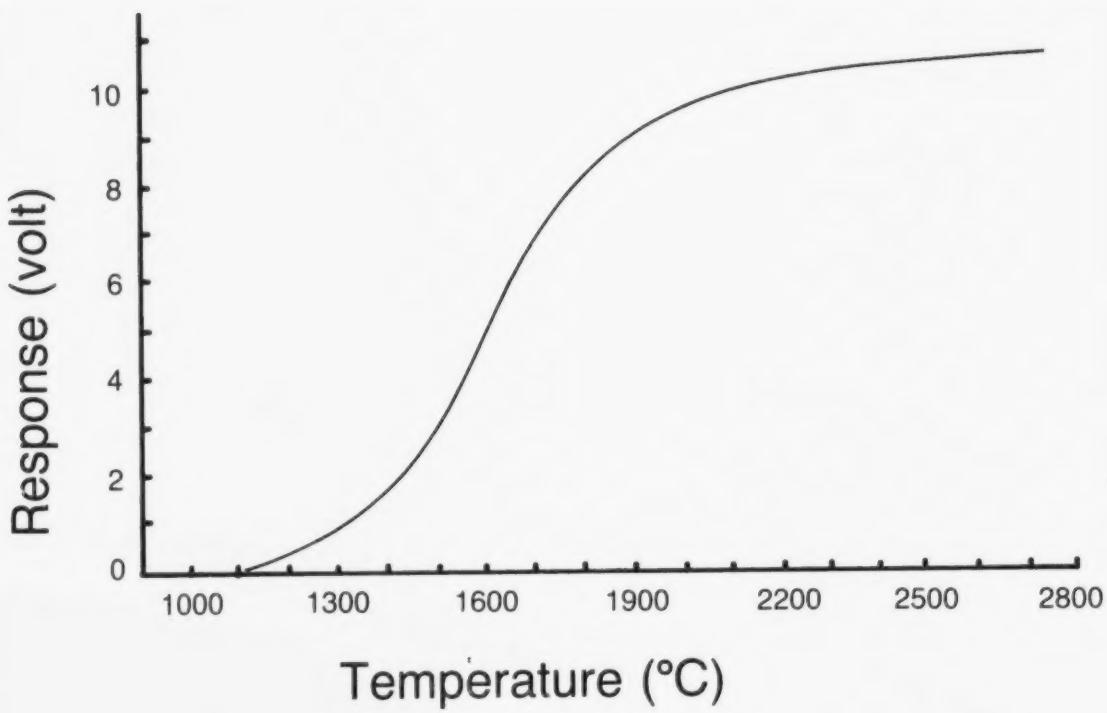

Figure 39. Pyrometer response for the low temperature pair of diodes.

SECTION 13

REFERENCES

1. K. Ong, U.S. Geological Survey, Albuquerque, NM, personal communication.

2. a) R.J.M. DeWiest, "Geohydrology," John Wiley & Sons, Inc., NY, 1965, Chapter 6; b) S. N. Davis and R.J.M. DeWiest, "Hydrology," John Wiley & Sons, Inc., NY, 1966, Chapter 7.

3. F. L. Williams, H. E. Nuttall, C. E. Tyner and R. D. Jacobson, Proceedings of the 6th Underground Coal Conversion Symposium, Shangri-La, near Afton, OK, July 13-17, 1980.

4. H. E. Nuttall and A. Ray, 15th Intersociety Energy Conversion Engineering Conference, Seattle, WA, Aug. 18-22, 1980, p. 1321.

5. K. Ong, U.S. Geological Survey, Albuquerque, NM, unpublished results.

6. S. N. Davis and R.J.M. DeWiest, "Hydrology," John Wiley & Sons, Inc., NY, 1966, p.431.

7. R. F. Spalding, M. E. Exner, and J. R. Gormly, Water Resour. Res., 12, 1319 (1976).

8. Standard Methods for the Examination of Water and Wastewater, 14th Edition; American Public Health Association, American Water Works Association, Water Pollution Control Federation, 1975.

9. "Methods for Chemical Analysis of Water and Wastes," Environmental Protection Agency, U.S. Government Printing Office (EPA-600/4-79-020), Washington, DC 1977.

10. "Varian AA-6 Operation Manual," Varian Techtron Ltd., Melbourne, Australia, 1972.

11. R. B. Barrett and C. S. Wickham, Clays and Clay Minerals, 26, 372 (1978).

12. N. H. Suhr and C. O. Ingamells, Anal. Chem., 38, 730 (1966).

13. C. H. Chu and L. J. Johnson, Clays and Clay Minerals, 27, 87 (1979).

14. "Standard Methods of Laboratory Sampling and Analysis of Coal and Coke," D-271, Amer. Soc. for Testing and Materials, 1976; W. J. Montgomery, Analytical Methods for Coal and Coal Products, C. Karr, Jr., Ed., Vol. I, Academic Press, New York, 1978, p. 203.

15. V. A. Dalton and J. H. Campbell, In-situ, 2, 295 (1978).

16. J. H. Campbell, E. Pellizzari, and S. Santor, UCRL-52405, Lawrence Livermore National Laboratory, 1978.

17. K. Rankama and T. G. Sahama, Geochemistry, University of Chicago Press, 1950.

18. S. P. Nandi and P. L. Walker, Jr., R&D Rep. 61, Int. Rep. 1, U.S. Dept. Int., Off. Coal Res., 1972.

19. R. E. Grim, Clay Mineralogy, McGraw-Hill, 1968.

20. S. W. Mead, F. T. Wang, H. C. Ganow and D. H. Stuermer, Proceedings of the 5th Underground Coal Conversion Symposium, Alexandria, VA, June 19-21, 1979.

21. R. E. Grim, Clay Mineralogy, McGraw-Hill, 1968, p. 193.

22. V. A. Garten and D. E. Weiss, Aust. J. Chem., 8, 68 (1955).

23. W. R. Curtis, Pap. Symp. Coal Mine Drainage Res., 4th, 19 (1972).

24. J. H. Campbell and H. Washington, UCRL-78303, Lawrence Livermore National Laboratory, 1976.

25. Y. Borg, R. Stone, H. B. Levy, and L. D. Ramspott, UCRL-52078, Lawrence Livermore National Laboratory, 1976.

26. W. K. Kaufman, Rep. HNS-1229-21, Hazelton-Nuclear Science Corp., 1963.

27. C. Steelink, J. Chem. Ed., 40, 379 (1963).

28. M. A. Rashid, Soil Sci., 111, 298 (1971).

29. K. C. Beck, J. H. Reuter, and E. M. Perdue, Geochim. Cosmochim. Acta, 38, 341 (1974).

30. W. L. Lamar, USGS Prof. Pap. 600-D, D24-D29 (1968).

31. H. F. Massey, Soil Sci., 114, 217 (1972).

32. J. L. Means, D. Crerar, J. O. Duguid, Science, 200, 1477 (1978).

33. W. Stumm and J. J. Morgan, Aquatic Chemistry, Wiley-Interscience, New York, NY, 1970, pp. 275-295.

34. J. G. Pritchard and F. A. Long, J. Amer. Chem. Soc., 79, 2365 (1957).

35. "Standard Methods of Laboratory Sampling and Analysis of Coal and Coke," D-271, Amer. Soc. for Testing and Materials, 1970.

36. J. H. Reuter and E. M. Perdue, Geochim. Cosmochim. Acta, 41, 325 (1977).

37. S. Brunauer, The Adsorption of Gases and Vapors, Vol. 1, Princeton Univ. Press, 1945.

38. J. H. Weber and R. E. Truit, Rep. No. 21, Water Resource Res. Center, Univ. New Hampshire, 1978.

39. M. S. Shuman and G. P. Woodward, Jr., Environ. Sci. Technol., 11, 809 (1977).

40. M. S. Shuman and J. L. Cromer, J. Amer. Chem. Soc., 13, 543 (1979).

41. W. P. Kelley, Cation Exchange in Soils, Reinhold, New York, 1948.

42. G. Wiegner and H. Jenny, Kolloid-Z., 43, 268 (1927).

43. P. Vageler and J. Woltersdorf, Z. Pflanzenernähr. Düng. Bodenk., 15, 329 (1930).

44. A. W. Adamson, Physical Chemistry of Surfaces, 3rd Edn., John Wiley and Sons,New York, 1976, Chapter IX.

45. D. E. Holly, N. L. Guinasso, Jr., and E. H. Essington, Rep. NVO-1229-179, Teledyne Isotopes, Nevada Operations, 1971.

46. A. W. Adamson, Physical Chemistry of Surfaces, 3rd Edn., John Wiley and Sons, New York, 1976, Chapter IX, p. 400.

47. R. E. Grim, Clay Mineralogy, McGraw-Hill, 1968, Chapter 8.

48. J. H. Campbell and H. Washington, "Preliminary Modeling Studies on the Environmental Impact on In-Situ Coal Gasification," Proceedings of the 2nd Annual Underground Coal Conversion Symposium, Morgantown, WV, August, 1976.

49. J. H. Campbell, E. D. Pellizzari, and S. Santor, Results of a Groundwater Quality Study Near an Underground Coal Gasification Experiment (Hoe Creek I), Lawrence Livermore National Laboratory Report No. UCRL-52405, 1978.

50. E. D. Pellizzari,"Identification of Components of Energy-Related Wastes and Effluents," EPA Report, EPA 600-7-78-004, January, 1979.

51. M. J. Humenick and C. F. Mattox, Water Research, 12, 463 (1978).

52. V. A. Dalton and J. H. Campbell, Laboratory Measurements of Groundwater Leaching and Transport of Pollutants Produced During Underground Gasification of Coal, Lawrence Livermore Laboratories Report No. UCRL 80834, 1978.

53. C. F. Mattox and M. J. Humenick,"Organic Groundwater Contaminants from UCG," Proceedings of the 4th Annual Underground Coal Conversion Symposium, Steamboat Springs, CO, July, 1978.

54. H. E. Nuttall, E. A. Walters, and T. M. Niemczyk,"Hydrologic and Environmental Findings: San Juan UCG Site," Proceedings of the 5th Underground Coal Conversion Symposium, Alexandria, VA, July, 1979.

55. J. P. Erspamer and T. M. Niemczyk, Anal. Chem., 54, 538 (1982).

56. H. M. Ortner and E. Kantuscher, Talanta, 22, 581 (1975).

57. W. Schmidt and F. Seitl, Fresenius Z. Anal. Chem., 295, 110 (1979).